Tgifs regulate ciliogenesis and the development of neuroepithelium in mice.

Anoush Emrazian Anderson
Centerville, Utah

B.S., University of Utah, 2006

A Dissertation presented to the Graduate Faculty
of the University of Virginia in Candidacy for the Degree of
Doctor of Philosophy

Biochemistry and Molecular Genetics

University of Virginia
May, 2016

_____

_____

_____

_____

Abstract

Holoprosencephaly (HPE) is a severe developmental defect affecting 1 in 250 conceptions and 1 in 8,000 live births. 18-25% of HPE cases are caused by single gene mutations, most commonly targeting the Sonic Hedgehog (Shh) pathway. Loss of function mutations in the transcriptional corepressor *TGIF* are also associated with HPE. HPE defects can be replicated in a mouse model in which *Tgif1* is conditionally deleted within the epiblast and *Tgif2* is constitutively deleted (cdKO). The severity of HPE can be partially rescued by decreasing the genetic dose of the *Shh*-antagonist, *Gli3*. Decreased Gli3 does not, however, rescue defects cdKO embryos have in addition to those associated with HPE, including disruption of epithelial polarity, failure to establish proper left-right asymmetry, and defective cilia formation. As Tgif inhibits TGFβ signaling, we hypothesized that Nodal, a TGFβ signaling ligand essential for embryonic development, is misregulated in the absence of Tgifs. We demonstrated cdKO embryos lacking one allele of *Nodal* have rescued epithelial polarity, but not left-right asymmetry. We also hypothesized that the disruption of cilia formation is driven by Tgif target gene overexpression. We performed RNA-seq on whole cdKO and control embryos to identify over-expressed genes that might be TGIF targets. After validating expression by qRT-PCR, several cilia-related genes were identified as differentially regulated in cdKO embryos when compared to wild type embryos. The RabGAP Evi5l, whose overexpression inhibits cilia formation, was found to contain a Tgif binding element in its promoter region. Through knock-down and luciferase experiments we showed that *Evi5l* is a direct Tgif target and that knockdown of *Evi5l* in the absence of Tgifs rescues the

defect in cilia formation in a TGFβ-independent manner. The knowledge that Tgif directly affects cilia formation not only elucidates defects in cdKO embryos, but also helps explain how *Tgif* mutations contribute to defects in Shh signaling via defective cilia and produce left-right asymmetry defects due to defective cilia at the posterior notochord.

Dedication

I dedicate this dissertation to my husband, Benjamin Anderson, who has always been the most magnificently supportive human being in my life. I love you forever.

Table of Contents

List of Figures

List of Abbreviations

DV	dorsoventral
A-P	anterior-posterior
aPKC	Atypical PKC
ARPE19	human retinal pigment epithelial cell line
Aurka	Aurora A kinase
AVE	anterior visceral endoderm
cdKO	conditional double knockout
ChIP-seq	chromatin immunoprecipitation-sequencing
ColIV	Collagen type IV
CRBPII-RXRE	cellular retinol-binding protein II- retinoic acid x receptor responsive element
D	disorganized
Dhh	Desert hedgehog
Disp1	Dispatched homolog 1
dpc	days post-coitum
EMT	epithelial-to-mesenchymal transition
EST	human expressed sequence tag
FBN1	F+B26ibrillin 1
GAP	GTPase activating protein
HDAC	histone deacetylase
Hip1	Hedgehog-interacting protein
HPE	holoprosencephaly
IFT	intraflagellar transport
Ihh	Indian hedgehog
IT	isolated tube
LPM	lateral plate mesoderm
L-R	left-right
MEF	mouse embryonic fibroblast
mG	membrane targeted green fluorescent protein
MIH	middle interhemispheric fusion
mT	membrane targeted Tomato
N	normal
NE	neuroepithelium
PCA	principle component analysis
PCP	planarl cell polarity

pHH3	phospho-Histone H3
PKD	polycystic kidney disease
PNC	posterior notochord
Ptch1	Patched
SARA	Smad anchor for receptor activation
SBE	Smad binding element
Shh	Sonic hedgehog
Smo	Smoothened
TALE	three amino acid loop extension
TGFBR1	TGFβ type 1 receptor
TGFß	Transforming growth factor ß
TGIF1	Thymine/Guanine-interacting factor
WISH	whole-mount in situ hybridization

Chapter One

General Introduction

TGFβ Signaling

TGFβ signaling is important in many aspects of embryonic development, especially in regulating proliferation, differentiation, and apoptosis (1–4). These essential functions can also be hijacked in disease contexts such as cancer (5–7). Misregulation of TGFβ signaling can also cause developmental disorders (8,9).

The TGFβ system consists generally of ligands and receptors that signal through downstream effectors to upregulate or inhibit transcription. TGFβ family ligands include two subfamilies: the BMP subfamily and the TGFβ-Activin-Nodal subfamily (10). BMP was discovered as a compound in demineralized bone extracts that was able to induce new bone growth (11). In addition to functioning in the formation of bone and cartilage, gene activation by BMP subfamily ligands results in establishment of the dorsoventral (DV) axis, neurulation and neural plate development, and other aspects of embryonic patterning and development (2,12–14). BMP signaling is inactivated in most cases of sporadic colorectal cancer, commonly due to mutations in *BMPR1A*, *BMPR2* or *SMAD4*, showing its importance in preventing inappropriate transition to mesenchymal or stem-like cell types (15,16). In addition, knockout of *Bmp7* in mice results in perinatal lethality and skull, eye and kidney defects (17,18).

TGFβ ligand was discovered in an effort to determine what autocrine factors enabled cells to transform from normal to malignant (19,20). TGFβ was also shown to be important in wound healing, a process suggested to be connected to tumor formation

(5,21,22). Subsequent experiments determined that TGFβ could also inhibit cell growth, indicating that TGFβ ligand had a complex and context-dependent effect on cells (23). Gene activation by TFGβ subfamily ligands regulates embryogenesis, differentiation, and apoptosis. For example, TGFβ ligand binding can result in the upregulation of the mesenchymal genes *SNAI1* and *SNAI2*, promoting epithelial-to-mesenchymal transition (EMT). This is essential in normal embryonic development but can also aid in the metastasis of cancerous cells (24–27). Many developmental disorders are the result of defective TGFβ signaling. Mutations in the TGFβ receptors *TGFBR1* and *TGFBR2*, *TGFB2* or *SMAD4* can cause Loeys-Dietz Syndrome, a connective tissue disorder resulting in aneurysms of the aorta (28–30). A more well-known developmental disorder with a similar phenotype is Marfan syndrome. Mutations that result in the misfolding of fibrillin 1 (*FBN1*) result in poor binding to TGFβ ligand and excess TGFβ signaling in the lungs and heart (31,32).

Initiation of TGFβ signaling begins when the TGF-β ligand is secreted into the extracellular space. The ligand binds to a Type II receptor homodimer, consisting of two serine-threonine receptor kinases (33,34). Once ligand-bound, the Type II receptor complex recruits and phosphorylates the Type I receptor homodimer, resulting in a heterotetrameric signaling complex that initiates a signaling cascade within the cell to activate transcription of specific target genes (35). Different Smad proteins respond to the activation of the receptor complex. Smad 2 and 3 respond in the context of TGFβ signaling and Smad 1, 5, and 8 respond to BMP-ligand initiated signaling (36). These Smad proteins are known as receptor-Smads or R-Smads. Cytoplasmic R-SMADs can be

held in the cytoplasm by proteins like SARA (Smad anchor for receptor activation). Once the Type I receptor is phosphorylated, it in turn phosphorylates the appropriate R-Smad. Phosphorylated R-Smads lose affinity for SARA and have increased affinity for the co-Smad, Smad4. Loss of binding to SARA exposes the region of the R-Smad responsible for mediating nuclear import and the Smad complex can translocate into the nucleus (37,38). Depending on the presence of cofactors specific to cell type, target genes are either activated or repressed. After activating target genes, R-Smads are transported back into the cytoplasm (39).

As a mechanism to halt signaling, Smads can be ubiquitinated and degraded. TGFβ signaling also activates transcription of the inhibitory Smad, Smad7. Activation of Smad7 antagonizes TGFβ signaling by binding TGFBR1 (TGFβ type 1 receptor), preventing activation of R-Smads or by recruiting E3 ubiquitin ligases, targeting the receptor for degradation (39–42).

During normal cell growth, TGFβ signaling helps regulate a non-malignant state through controlling cell differentiation and apoptosis, as well as the cell microenvironment (7,43). Through mutation or sequestration of TGFβ signaling family members, such as Type I and Type II receptors or *SMAD4*, all TGFβ signaling can be halted, inhibiting apoptosis for example, thus allowing for uncontrolled cell growth. Mutations in further downstream effectors can result in disabling a subset of TGFβ signaling, such as its tumor-suppressive effects, allowing cancers to take advantage of favorable TGFβ effects, such as EMT, which can lead to metastasis (44–46). High levels

of TGFβ can also manipulate the cell microenvironment, enabling such cells to avoid immune response, further promoting a malignant phenotype (47,48).

There are three mammalian isoforms of TGFβ ligand. Knockout of each isoform in mice results in different defects. *Tgfb1*-knockout mice are born, but die within four weeks of autoimmune inflammatory disease (49–51). *Tgfb2*-knockout is perinatal lethal. In addition, *Tgfb2*- knockout mice have heart, lung, limb, spine, eye, ear and craniofacial defects (52). *Tgfb3*-knockout mice are born with cleft palate and die within 24 hours post-birth (53).

Nodal is a TGFβ-family ligand essential for normal embryonic development, specifically for induction of the mesendoderm and the establishment of both the anterior-posterior (A-P) and the left-right (L-R) axes (54–58). The Nodal ligand itself regulates Nodal gene expression in a positive feedback loop and also leads to transcriptional activation of its own inhibitors, such as Lefty2 and Cerberus-like. Cerberus-like is expressed in the anterior endoderm, allowing for anterior neural development and A-P patterning. It directly binds Nodal ligand to suppress signaling (59). Lefty1 acts redundantly with Cerberus-like in the extraembryonic endoderm, restricting Nodal expression to the epiblast (60). Lefty2 is coexpressed with Nodal in the left lateral plate mesoderm (LPM). Later in development, Lefty1 is also expressed in the left midline (61,62). It is unclear how Lefty proteins block Nodal signaling at a molecular level, but they do function as feedback inhibitors and restrict the duration of Nodal signaling. Some studies suggest that Lefty2 competitively binds to Nodal receptors, preventing signal transduction (56,58,63,64). The Nodal coreceptors Cripto and Cryptic form a complex

with Nodal ligand and its receptors. This complex is important in activating downstream signaling (65–67). Cripto expression can be induced in the epiblast, and Cryptic is expressed in the LPM, overlapping with the region in which Nodal is thought to aid in the determination of the L-R axis (68–71).

Nodal expression in the epiblast before gastrulation signals to extraembryonic tissues that lead to patterning of the epiblast. Patterning within the anterior visceral endoderm (AVE) helps establishment of the A-P axis (72). After gastrulation, Nodal expression is restricted to the primitive streak and is expressed asymmetrically in the left LPM to regulate genes involved in L-R patterning (54). Induction of Nodal in the left LPM also requires Nodal expression in the posterior notochord (PNC, commonly referred to as the node) and PNC cilia creating fluid flow. *Nodal*-knockout mice do not form the primitive streak and arrest just after gastrulation, without the formation of mesoderm (54,55,73). Embryos with one null allele and one hypomorphic allele of *Nodal* are able to develop further but do not survive to birth. These mutants exhibited defects in establishment of the A-P axis, anterior and midline patterning, and L-R development of the heart, lungs and stomach (74).

TGFβ signaling is involved in a wide variety of developmental processes. Disruption of these signaling pathways can result in many varied and diverse developmental defects and disorders. TGFβ signaling also plays a role in cancer progression and malignancy. Understanding all components of TGFβ signaling—from ligands and receptors to repressors and activators—will aid in preventing and treating the aforementioned diseases.

TGIF1

Thymine/Guanine-interacting factor (TGIF1) is a transcriptional corepressor belonging to the TALE (three amino acid loop extension) family of transcription factors (75–77). It was discovered due to its ability to bind to the retinoic acid x receptor responsive element within the cellular retinol-binding protein II promoter (CRBPII-RXRE). The TGIF homeodomain interacts with the motif 5' CTGTCAA 3'. This sequence, present in the CRBPII promoter region, overlaps with and antagonizes binding of RXRα, inhibiting activation (75). In addition to directly binding DNA, TGIF can also act as a repressor of TGFβ-related transcription by binding directly to the activated Smad complex within the nucleus. This binding represses activation of target genes by interfering with the binding of coactivators to the Smad complex (78). TGIF1 also recruits corepressors to aid in the repression of transcription. TGIF binds directly to the corepressor CtBP via an N-terminal PLDLS motif (79). TGIF interacts with the corepressor mSin3 at its C-terminal domain, recruiting Sin3 to the activated Smad complex within the nucleus and thus repressing TGFβ signaling (80). TGIF also recruits histone deacetylases (HDACs) via a c-terminal repression domain, resulting in a closed chromatin formation that prevents transcription (79,81).

TGIF2 is a paralog of TGIF1. It was discovered in a search of human expressed sequence tags (ESTs) for a gene similar to TGIF1, with the idea that the low-penetrance of TGIF1 mutations in holoprosencephaly could be explained by a similar protein compensating for loss of TGIF1 function. They share high sequence similarity, specifically in the homeodomain region, the third DNA binding domain, and 2 C-terminal

MAP kinase sites. These conserved regions suggest that TGIF2 has a similar function to TGIF1, especially in relation to DNA binding and interactions via the homeodomain. Due to these similar functions, it is likely that TGIF2 would be able to compensate for lack of TGIF1 in many contexts. Like TGIF1, TGIF2 is able to repress TGFβ transcription by interacting with activated Smads or directly binding to DNA. TGIF2 is also able to recruit HDACs and mSin3. TGIF2, however, is missing the PLDLS motif required to recruit CtBP and is unable to recruit said corepressor (80,82).

TGIF1 is upregulated in several types of cancer, including colon cancer. It has also been implicated in Wnt-driven breast cancer (83). Presumably it plays a role in inhibiting the anti-proliferative effects of TGFβ signaling to allow for uncontrolled cell growth, but this has not yet been shown directly. Mutations in TGIF1 are associated with Holoprosencephaly (HPE). The majority of these mutations involve the deletion of one allele of TGIF1, but there are some partial loss-of-function mutations and some polymorphisms in TGIF1 also associated with the HPE (84). One of these mutations (S28C) results in a disruption of the PLDLS binding motif necessary for TGIF-CtBP interaction. This disruption then interferes with efficient repression of TGFβ signaling (79). Other HPE-associated mutations within the homeodomain of TGIF are unable to bind to DNA and likely produce a misfolded protein, effectively eliminating any TGIF function.(85) Only one of these mutations (P63R) alters a region of TGIF1 that is conserved in TGIF2, although no mutations in TGIF2 associated with HPE have yet been identified (82).

Inactivation or deletion of a single allele of *Tgif1* in mice does not result in HPE, nor are the associated defects serious in most strain backgrounds (86). Most mice with three intact alleles of the four *Tgif1* and *Tgif2* alleles are fairly normal and are able to reproduce and live a normal life-span (87,88). While in a mixed strain background, *Tgif1*-null mice appear normal and are fertile; in a C57/BL/6J background, *Tgif1*-null mutations are associated with decreased vascularization of the placenta. This results in severe growth retardation. The growth defect is less severe when the mother is heterozygous null for *Tgif1* and is more severe when the mother is homozygous null for *Tgif1* (89). The deletion of all alleles of *Tgif1* and *Tgif2* is embryonic lethal. When embryos were analyzed, it was determined that the double null embryos had failed to gastrulate. When examined more closely, the cellular structure of double null embryos was disorganized; it was characterized by decreased epithelialization of the epiblast and decreased proliferation with no consistent change in apoptosis. With one allele of *Tgif1* present within the extraembryonic tissue, embryos gastrulate, only to stall later in development after developing holoprosencephaly (90,91).

Holoprosencephaly

Holoprosencephaly (HPE) is a brain development disorder in which the developing forebrain fails to divide into the left and right hemispheres of the brain. The phenotype of HPE is diverse, with a range of manifestations and several classifications. The basic diagnostic feature of HPE is established by in examining the anatomy of the brain. Alobar HPE is the most severe manifestation and consists of a complete failure of the

forebrain to divide, resulting in a single ventricle. Semilobar HPE consists of posterior division of brain hemispheres, with fused frontal and parietal lobes of the brain. The least severe form of HPE is lobar HPE, in which cerebral hemispheres and ventricles are mostly separated (92). In addition to brain defects, HPE is also associated with other midline defects, ranging from central maxillary incisor to cyclopia and proboscis (93). More recently an additional subtype of HPE has been described as the, "middle interhemispheric fusion," (MIH) or sytelencephaly. This less-severe variant of HPE is a result of defective dorsal identity, as opposed to the more classical defective ventral identity in the three other forms of HPE (94,95).

HPE occurs in 1 in 250 conceptions and 1 in 8000 live births, illustrating that the most extreme cases of HPE are incompatible with life and result in spontaneous abortion (96,97). Most cases of HPE are sporadic, but 18-25% of HPE cases are caused by a single gene mutation in one of the following genes: sonic hedgehog (*SHH*), *SIX3*, *ZIC2*, *Gli2*, *TGIF* and *PTCH1* (98). 17% of familial HPE cases are due to mutations in *SHH* and 37% of families with dominant transmission of HPE spectrum symptoms have *SHH* mutations (99). Several of the other genes associated with HPE are involved in Shh signaling as well. For example, mutations in *PTCH1* can interfere with SHH ligand binding to the PTCH1 receptor or disrupt the PTCH1-SMO interaction, inhibiting Shh signaling. In regards to those instances of HPE with no known genetic cause, there are several suspected environmental risk factors, mostly derived from case studies, animal models and epidemiologic studies. These include maternal illnesses such as diabetes, respiratory infection during pregnancy, and sexually transmitted infections. Chemical

risk factors include salicylate use, retinoic acid, antibiotics and alkaloids that inhibit hedgehog signaling. Non-therapeutic exposures include alcohol, smoking and illicit drug use. Because of the rarity of HPE, it is difficult to determine causation with confidence (100,101). It has also been suggested that there is a possible genetic-environmental interaction, with some genotypes increasing risk of HPE in the presence of some of the above environmental risk factors. In addition to genetic-environmental interactions, the multiple-hit hypothesis has been applied to HPE, hypothesizing that multiple mutations, possibly in modifier genes in addition to those genes known to be associated with HPE, as well as environmental exposures are required for severe manifestations of the disorder. For example, two HPE patients with mutations in both *SHH* and *TGIF1* have been born to clinically normal mothers with only *SHH* mutations.(102)

Hedgehog Signaling

The hedgehog gene was first discovered in *Drosophila melanogaster* in a screen for embryonic patterning defects (103). There are three homologs of the Drosophila hedgehog in vertebrates: Indian (*IHH*), Desert (*DHH*) and Sonic (*SHH*). Each of these homologs has its own area of functionality within the developing vertebrate. *DHH* is most similar to the *Drosophila hh,* while *IHH* and *SHH* are more similar to each other, suggesting a gene duplication event (104).

In addition to its disruption in HPE, SHH is expressed in the notochord, floor plate and limb bud. Shh signaling is essential for normal brain, neural tube, eye, somite and limb development (105). Once translated, the SHH protein is cleaved and cholesterol

is attached to the amino terminal domain as part of ligand processing (106,107). The processed ligand is then secreted outside the signaling cell, and because of the cholesterol moiety it remains tethered to the cell membrane. This restricts signaling to a very short range. The Patched-related protein DISP1 (Dispatched homolog 1) regulates the release of processed SHH ligand to allow for more long-range signaling (108).

To initiate Shh signaling, the Shh ligand binds to the membrane-bound receptor, Ptch1. Ptch1 normally inhibits Smo, another membrane-bound receptor. Shh binding to Ptch1 allows for the release of inhibition of Smo via phosphorylation. Activated Smo moves into the cilium and interacts with proteins concentrated there, e.g. Gli2/3 complex, activating the transcription factor Gli1. This signaling cascade results in the transcription of Shh-target genes. *Ptch1* is a Shh target gene and transcription of the receptor acts in a negative feedback loop to sequester Shh ligand to the signaling cell (109). *Hip1* (Hedgehog-interacting protein) is another Shh-target gene that acts in negative feedback loop with Shh and is expressed on the surface of cells adjacent to the Shh signaling cell (110). *Gli1* is activated and *Gli3* is repressed by Shh signaling (111). Gli3 negatively regulates both Shh targets and *Shh* itself (112). In the absence of Shh, Gli3 is overexpressed within the cell. This affects patterning of the developing embryo, as Shh-established patterning is initiated via concentration gradient. High Shh is found in the ventral forebrain, and high Gli3 is found in and patterns the dorsal forebrain. Without the gradient between Shh and Gli3 expression, the forebrain and neural tube are unable to properly develop. High Shh is present in the notochord and the floor plate, defining ventral identity of the neural tube. Shh expression decreases gradually toward the dorsal

neural tube in combination with high dorsal expression of Gli3, which in turn decreases gradually toward the ventral neural tube. Shh activates and represses specific genes in a dose-dependent manner, defining distinct neuron classes within the developing neural tube. The expression pattern of each neuron class marker is directly related to its proximity to the source of Shh ligand. For example, the homeodomain transcription factor Nkx2.2 is expressed in a band at the most ventral section of the developing neural tube, requiring a relatively high concentration of SHH ligand. Conversely, Shh represses *Pax7*, a marker of dorsal identity within the neural tube. (113).

HPE Mouse Models

Due to the variability of human mutations associated with HPE, animal models of the disease can help develop understanding regarding the development of HPE, although most models of HPE are much more consistently severe than in human patients. Most models are based on disruptions in two pathways: Shh signaling and Nodal. Both of these pathways are involved in inducing ventral cell fate (114).

Shh-null mouse embryos develop severe HPE due to loss of ventral structures along the neural axis. They exhibit cyclopia and proboscis and die soon after birth (115). Signaling components downstream of SHH ligand have also been used in models of HPE. *Smo*-knockout mice develop HPE and die by 9.5 days post-coitum (dpc), presumably because SMO plays a role in all Hh signaling and not just that of Shh (116). Mutations in *SMO* have not yet been found in human HPE patients. *Nodal*-mutant mice also exhibit HPE. This is likely due the role of NODAL in establishing a rostral domain for SHH

expression in the early embryo (74). Relationship between ZIC2 and Shh signaling is unknown, but as *ZIC2* mutations are associated with HPE in humans, *Zic2*-knockdown mice were developed. They exhibit HPE with fused cerebral hemispheres, although these embryos do have normal ventral neural tube formation. These mice die soon after birth (117).

The Wotton lab has developed a mouse model of HPE in an effort to understand why mutations in TGIF1 are associated with HPE in humans. As stated previously, TGIF function is required in the extraembryonic tissue for gastrulation to occur. SOX2 is expressed in the epiblast, but not in the extraembryonic tissue (118). By deleting both alleles of *Tgif2* and conditionally knocking out a floxed *Tgif1* allele (86) in the epiblast using a *Sox2-Cre*, the developing embryo successfully gastrulates with one unrecombined allele of *Tgif1* remaining in the extraembryonic tissue. These mice are referred to as "conditional double knockout" embryos or "cdKO" (*Tgif1* $^{r/r}$; *Tgif2* $^{-/-}$ *Sox2-Cre* $^{+}$. Within this context, we were able to show that cdKO embryos develop HPE due to disruption of the Shh pathway (91). Most do not survive past 11 dpc. Separation of the eye and nasal fields is incomplete, and embryos lack ventral forebrain morphology. This is caused by decreased SHH and excess GLI3 interfering with proper development. Two embryos that developed past 11 dpc exhibited cyclopia, and one had a proboscis similar to that seen in *Shh*-null embryos (91). Whole-mount in situ hybridization (WISH) analysis of *Shh* expression showed decreased *Shh* expression in several regions of the cdKO including the ventral forebrain. Tgif function appears to be required for normal *Shh* expression in anterior tissues. When *Gli3* is reduced genetically in the context of a cdKO (*Gli3* $^{r/+}$), *Shh*

expression is not rescued, but the ventral forebrain morphology is improved, as is nasal and eye field separation (91). cdKO embryos have other defects in addition to those often seen in HPE including bilateral expression of *Pitx2*, a left-sided gene required for appropriate heart looping (119). This resulted in 3 distinct classes of heart looping in cdKO embryos: appropriate left-to-right looping, reversed right-to-left looping and extended heart tube with no looping to either side (90).

Cilia

Cilia function is important, both in early development and in continued signaling in an organism Cilia are transient organelles that protrude from the cell surface and assist in carrying out various signaling functions. There are two types of cilia: primary cilia and motile cilia. A single primary cilium is present on the apical surface of most cells in the body during the cell's growth phase. Primary cilia are immotile and are important signaling centers for a cell. They receive signals from outside the cell via ion channels and assist in concentrating signaling pathway components within the cilium to help efficiently propagate signals, e.g. Shh signaling (120–122).

Motile cilia are present on cell surfaces in large numbers. These cilia beat in waves, creating fluid flow in the extracellular space of several organ systems including the developed brain and kidneys. Motile cilia are essential in the PNC region of the developing mouse. Counterclockwise rotation coupled with their angle creates a leftward flow of fluid and assists in establishing the L-R axis. If mechanics of these cilia are defective, L-R patterning is randomized (69,70,123–125). Appropriate L-R patterning is

essential for appropriate functioning of all organs. Human visceral organs are asymmetrically organized in relation to the L-R axis. The heart is left sided, with the aorta arching to the left. The liver and gallbladder are on the right, with the stomach and spleen on the left. Defects in this arrangement are associated with cardiovascular defects and are often fatal to newborn humans (126). The appropriate alignment of these organs is referred to as *situs solitus*. Complete reversal of this arrangement is *situs inversus totalis*. There are many intermediate organ arrangements due to randomized or incomplete patterning information referred to by several terms, such as *situs ambiguus* or heterotaxia (126). Midline abnormalities are common in cases of inappropriate L-R patterning, such as cleft palate or HPE. L-R malformations are estimated to take place in 1 in every 5000 births and are divided evenly between *situs inversus* and *situs ambiguous* (127). Our understanding of the molecular mechanisms behind L-R axis establishment comes from vertebrate model systems like mice. For example, mutations in *Lefty1* result in left thoracic isomerism with bilateral expression of normally left-sided genes like *Nodal* and *Pitx2* (128). There are many diseases associated with malformed or absent cilia, including HPE. Cilia are essential for Shh signaling and *Shh*-null mice develop HPE, in addition to SHH and Shh pathway components being found mutated in human HPE patients (115).

The assembly of a cilium is nucleated at the basal body which is made of the centrioles and pericentriolar proteins. These same centrioles establish spindle poles during cell division. During the cell growth phase (G1), post-mitosis basal bodies migrate to the cell surface, collecting membrane vesicles that fuse with the plasma

membrane to help create the ciliary compartment. Basal bodies nucleate microtubule assembly, and the cilium grows within the extended membrane space to protrude from the cell. The plasma membrane is invaginated at the base of the developing cilium, creating a ciliary pocket (122). The base of the cilium within the ciliary pocket is the transition zone. It is through this region that proteins are selectively transported into the cilium after being translated within the cytoplasm. The distinctness of the cilia microenvironment allows for more efficient signal transduction due to an enrichment of signaling components (129). For example, all components of the Hh signaling pathway are enriched in the vertebrate cilium. Transportation into and along the length of the cilium, including transport of acetylated tubulin to the tip of the growing cilium, occurs through intraflagellar transport (IFT) (130). IFT functions through two complexes that transport cargo along the ciliary axoneme. IFT-A complex along with the minus-end directed motor Dynein-2 assist in retrograde transport, while IFT-B complex is essential for anterograde transport. Other cargo transported by the IFT system includes SHH pathway proteins such as the Gli transcription factors (131,132). IFT works in tandem with protein trafficking regulators to specifically concentrate certain proteins within the cilium depending on the signaling context.

Cilia disassemble around the time of mitosis. In order to reposition basal bodies to form appropriate centrioles, the cilium must be removed. Cilia can be cleaved away from the centriole between the basal body and the transition zone (133). Cilia can also be disassembled from the tip and resorbed. This disassembly is in part regulated by Aurora A kinase (Aurka) which is thought to positively regulate *HDAC6*, leading to tubulin

deacetylation and microtubule instability (134). These two mechanisms can occur simultaneously.

The length of cilia varies between cell types and is important for their function; this is especially true for motile cilia where the length will affect the velocity of the resulting fluid flow. The length is controlled in the same manner as assembly, via IFT, and is dependent upon the availability of precursors, such as acetylated tubulin, and the rate of assembly and disassembly at the cilia tip (135).

Many components of cilia are required for appropriate assembly and function including three RabGTPase membrane trafficking regulators involved in the formation of primary cilia. Rab8a interacts with a basal body and microtubule binding proteins required for cilia formation (136). Rab17 is involved in the apical sorting of endosomes in polarized epithelial cells (137,138). Rab23 is involved in retrograde transport from the tip of primary cilia (139). Each RabGTPase has a specific cognate GTPase-activating-protein (GAP). XM_037557 acts on Rab8a, TBC1D7 acts on Rab7 and Evi5L acts on Rab23. When overexpressed, these RabGAPs block the formation of primary cilia by keeping the associated Rabs in their GDP-bound state (140).

Cilia function in many essential ways within a developing embryo and adult organism. They are involved in signaling pathways within the cell (e.g. Hh signaling), and in generating fluid flow outside the cell. Any disruption in the assembly or function of cilia has significant implications in regards to the overall health of an organism.

Polarized Epithelium

The development of polarized epithelial cells was essential for metazoan development and has significant implications on embryonic development and cell signaling. Polarized epithelial cells have distinct apical, lateral, and basal domains. The apical domain faces the lumen of the organ or tube, the lateral domain contacts adjacent cells, and the basal domain contacts the extracellular matrix. These domains have a unique and specific distribution of nutrients and transporters specific to the cell type and function within the plasma membrane. Polarized trafficking machinery is present to establish and maintain the asymmetric distribution of cell components, including sorting signals that help target vesicles to the apical or basal domains (141). Polarized cells can constrict their apical surface when necessary to shape sheets of epithelial cells, such as in gastrulation or during hinge formation in neural tube development (142). Sheets of epithelial cells are maintained by adherens junctions. Tight junctions between epithelial cells seal the apical surface of the epithelial sheet from the basal surface, creating and maintaining a distinct luminal domain that does not interact with the outer environment (143). Polarized epithelial cells are able to undergo EMT, resulting in a transition from apical-basal polarity to front-rear polarity, and allowing for cell migration (144,145).

During epithelial cell mitosis, the spindle is oriented specifically to determine the outcome of that division. Division parallel to the plane of the cell sheet maintains the surface integrity while increasing the surface area. Division perpendicular to the plane of the cell sheet occurs in the selective differentiation of a daughter cell from a stem cell, maintaining a basal stem cell population with an apical population of differentiated cells

(146). The luminal surface of the developing forebrain and neural tube are comprised of pseudostratified polarized epithelium. These cells are organized in a single layer, but to allow for many cells to have access to the luminal space, they are tightly packed with their nuclei traveling to the apical surface for division and traveling back to the basal surface during the growth phase of the cell. This nuclear movement, called interkinetic nuclear migration, allows the cells to be more tightly packed and results in a cell layer that appears to be more than one cell deep, when in reality it is not (147,148).

The current knowledge concerning the establishment and maintenance of polarized epithelial cells was mostly gathered from genetic and biochemical experiments using *C. elegans*, *D. melanogaster*, and 2D and 3D culture of mammalian cells (149–151). From these studies, three protein complexes have emerged that help elucidate polarity in epithelial cells: The PAR complex, the Crumbs complex and the Scribble complex. The PAR complex proteins were discovered first in a screen in *C. elegans* that searched for genes related to defective cytoplasmic partitioning (152). The PAR complex includes kinases (PAR 1 and 4 and aPKC), scaffold and adaptor proteins (PAR 3 and 6), a GTPase (Cdc42), and PAR5, which interacts with phosphorylated proteins. These proteins are expressed throughout the cytoplasm, but function only in specific domains (apical, lateral, and basal). The protein activity in each domain is restricted by the interaction of PAR proteins with each other and other polarity proteins. The Crumbs complex is apically located and consists of a scaffolding protein (CRB), a kinase (PALS1) and a protein interaction mediator (PATJ). CRB is the only membrane-bound

polarity protein. The Scribble complex is laterally located and consists of scaffolding proteins (DLG and SCRIB) and a cytoskeletal protein (LGL) (149,150).

The apical and basal domains are maintained by reciprocal exclusion. Apical-specific components phosphorylate and cause the dissociation of lateral or basal components. This releases them back into the cytoplasm to be appropriately localized. This also happens within the lateral and basal domains. The mechanism by which CRB is positioned apically is unknown, but CRB defines the apical domain and helps to organize tight junctions, which are located apically within the lateral domain. CRB forms a complex with PAR6 and PALS1 to recruit aPKC to the apical domain (153,154). aPKC phosphorylates basolateral proteins, such as PAR1. This phosphorylation attracts PAR5, causes the dissociation of PAR1 from the cortex and releases PAR1 into the cytoplasm to eventually find the basal domain. PAR1 performs a similar function in excluding apical proteins from the basolateral domain. Specifically, it phosphorylates PAR3, which then interacts with PAR5 and is released into the cytoplasm and dephosphorylated (149,155). After cell division, the centriole is also apically targeted, where it nucleates the formation of the primary cilium. aPKC is required for cilia formation and PAR6, PAR3 and CRB3 are all present within the cilium and required for its formation (156,157). PAR3 is associated with tight junctions, and Cdc42 assists in the assembly of adherens junctions along with PAR3-PAR6-aPKC (158).

In addition to the disruption of tissue organization, the disruption of epithelial polarity has severe developmental consequences. An obvious consequence is a lack of primary cilia, thereby interrupting any cilia-dependent signaling, such as Shh signaling.

Disruption of polarity is also the first step in EMT, widely considered to be the process by which cancers metastasize (159–163).

The evolutionary development of epithelial polarity made complex organ systems in multicellular organisms possible. Polarized epithelial cells also play an integral role in signaling within the cell. The distinct regions within a polarized epithelial cell allow for specialized functions within the cytoplasm. It also makes possible the tight separation of luminal organ spaces from outside those organs. The disruption of epithelial polarity can indicate a developmental disorder or the initial stages of EMT and metastasis in cancer.

For my thesis work, I continued the characterization of the cdKO model of HPE. In addition to those defects discussed above, cdKO embryos also have disorganized neuroepithelium and isolated tubes intermittently along the length of and ventral to the developing neural tube. At a cellular level we have also observed defects in polarity in both the forebrain and neural tube. These interesting phenotypes are caused by an unknown mechanism and may yet be important in understanding the pathogenesis of *TGIF1* mutations. In addition to polarity defects, cdKO embryos have defective ciliary assembly. In the cdKO, PNC cilia are either absent or too short to function in creating a leftward flow of fluid. The cdKO forebrain has fewer cilia than in the normal forebrain, and those cilia present are defective, likely due to the disruption in epithelial polarity. Using tissue culture models, we were able to show cilia defects are due to a lack of Tgifs and overexpression of the direct Tgif-target *Evi5l* is a major contributor to cilia defects in the cdKO. These phenotypes give us additional insight into the pathogenesis of *Tgif* mutations.

Chapter Two

Tgif1 and Tgif2 limit both Nodal signaling and *Gli3* expression to maintain normal forebrain development

Kenichiro Taniguchi[1,#], Anoush E. Anderson[1], Tiffany A. Melhuish[1], Annie Carlton[1], Arkadi Manukyan[1], Ann E. Sutherland[2] and David Wotton[1]*

[1] Department of Biochemistry and Molecular Genetics,
and Center for Cell Signaling, University of Virginia, Charlottesville, USA

[2] Department of Cell Biology, University of Virginia, Charlottesville, USA

[#] Present address: Department of Cell and Developmental Biology,
University of Michigan Medical School, Ann Arbor, MI 48109

Ken Taniguchi helped with whole mount in situ hybridization and analysis of the isolated tube phenotype. Tiffany Melhuish helped with ChiIP-qPCR and dissection of 18.5 dpc embryos. Annie Carlton and Arkadi Manukyan helped with qPCR of Gli3 in U87 cells.

Abstract

Holoprosencephaly (HPE) is a craniofacial developmental disorder that has both genetic and environmental causes. The genetics of HPE are relatively complex, and mutations at several loci are associated with HPE in humans. Of these, the Sonic Hedgehog (*SHH*) and TG-interacting factor 1 (*TGIF1*) genes are among those that are routinely screened in HPE patients. Tgif1 is a transcriptional repressor that limits the output of the Transforming Growth Factor ß (TGFß)/Nodal pathway, and can also repress gene expression independent of this pathway. Loss of function mutations in the gene encoding the Shh morphogen result in altered dorsoventral patterning in the forebrain and a failure to properly separate the forebrain into two hemispheres. Although mice lacking both Tgif1 and its paralog Tgif2 have HPE that appears similar to that seen in *Shh* null embryos, how loss of Tgif function causes HPE is not well defined. Here we show that introducing mutations into both the *Nodal* and *Gli3* genes results in improved forebrain structure and neuroepithelial organization, partially rescuing the HPE phenotype in embryos lacking both Tgif1 and Tgif2, consistent with effects on two separate pathways. We show that the *Gli3* gene is a direct target for repression by Tgifs, independent of TGFß/Nodal signaling. In contrast, excess Nodal signaling in the absence of Tgifs results in reduced proliferation and defective cell polarity in the neuroepithelium. Embryos lacking Tgif function do not survive past mid-gestation. However, when a *Nodal* heterozygous mutation ($Nodal^{z/+}$) is combined with loss of Tgif function, a proportion of these embryos survive to late gestation and have a classic HPE phenotype, consistent with this being a Nodal-independent effect of Tgif loss of function. Based on this work,

we propose a model for the function of Tgifs in the Nodal and Shh pathways during forebrain development.

Introduction

Holoprosencephaly (HPE) is a severe developmental disorder affecting the forebrain and facial development. In humans, HPE affects approximately 1 in 8000 live births and up to 1 in 250 conceptions, making it the most frequent forebrain developmental disorder in humans.(96,97) Given the high rate of HPE *in utero* compared to the numbers seen at birth, clearly the majority of HPE cases do not survive to term, and many of the more severely affected individuals die soon after birth. There is considerable phenotypic variability among HPE cases. At its most severe, alobar HPE, there is a single forebrain ventricle with complete lack of midline separation. Less severe forms, termed semi-lobar and lobar, have increasing midline separation of the ventricles.(92) In addition to the forebrain defects, HPE is associated with a spectrum of midline craniofacial defects. These include severe cyclopia and proboscis and microforms, such as hypotelorism and the presence of a single central incisor.(93) This phenotypic variability implies potentially complex underlying mechanisms for the generation of HPE.

HPE can be caused by both genetic and environmental factors, although the clearest evidence for teratogenic causes of HPE comes from mice. The rate of HPE in infants of diabetic mothers is as high as 1-2%, and there is other data implicating in utero exposure to alcohol and some drugs in human HPE.(100,101) 28% of HPE cases may be accounted for by mutations in genes at nine HPE loci. Of the known HPE loci, those that encompass the *SHH*, *ZIC2*, *SIX3* and *TGIF1* genes are most commonly screened as part of routine genetic evaluation of HPE patients. There is no clear correlation between severity and penetrance of the phenotype and the type of mutation.(98,99)

Among the major HPE loci, perhaps the best understood in terms of HPE causation are mutations affecting the *SHH* gene which encodes Sonic Hedgehog, a secreted morphogen. In humans, heterozygous loss of function mutations in the *SHH* gene account for 17% of familial HPE and 3.7% of sporadic cases (99,164,165). Although heterozygous *Shh* mutant mice are normal, homozygous mutants are inviable, and have HPE *in utero* (99,115). SHH binds the Patched transmembrane receptor (Ptch1), thereby relieving inhibition of Smoothened (Smo), which then signals to the Gli transcriptional regulators (Gli1, Gli2 and Gli3) to activate target gene expression (104,166–169). Gli1 and Gli2 are the primary activating transcription factors in response to SHH signaling, whereas Gli3 plays an inhibitory role. During forebrain development in mouse, *Shh* is first expressed in the prechordal plate at approximately 7.75 days post-coitum (dpc), and Shh in this tissue activates the expression of the *Shh* gene in the overlying ventral diencephalon by approximately 9.0 dpc. Expression of Shh in the ventral diencephalon helps specify ventral identity and also limits expression of the *Gli3* gene which is primarily expressed dorsally. Gli3 promotes dorsal fate and also inhibits ventrally acting Shh responses. Thus a balance of mutual inhibition is set up, with Shh favoring ventralization and Gli3 dorsalization. The forebrain of *Gli3* homozygous null embryos has dorsally expanded ventral tissue lacking dorsal identity (170–172). Homozygous *Shh* null embryos have a forebrain ventricle that lacks ventral identity and fails to divide into two hemispheres. In support of the mutual antagonism between Shh and Gli3 in dorsoventral patterning, the introduction of *Gli3* mutations into *Shh* null embryos results in partial rescue of the defective ventral identity.(115) While the Shh-Gli

pathway is one of the major regulators of forebrain dorsoventral patterning, there is evidence suggests other pathways are also required to specify telencephalon development, including FGF signaling via Foxg1.(170,173)

The *TGIF1* gene (Thymine-Guanine Interacting Factor) was identified in the minimal critical region of the HPE4 locus. In addition to the more common heterozygous deletions of this locus that are associated with HPE, several missense and nonsense mutations in *TGIF1* have been identified from HPE patients. Of these, some have been shown to result in at least partial loss of function, but others may also represent non-phenotypic polymorphisms.(79,85) As with *SHH*, it appears *TGIF1* mutations in HPE are heterozygous loss of function mutations.(84) There is no evidence for HPE-associated mutations in the human *TGIF2* gene; however, in mice Tgif1 and Tgif2 share overlapping function during development. Homozygous deletion of either *Tgif1* or *Tgif2* does not cause HPE or other severe phenotypes in mice in a mixed strain background.(82,87,88) Combining both mutations results in a failure of gastrulation in double homozygous null embryos, with defects in the Nodal signaling pathway. However, these embryos do not survive to the point where forebrain development can be observed. Introducing a conditional *Tgif1* allele into a Tgif2 null background allowed embryos to bypass gastrulation defects.(90) Conditional double null (cdKO) embryos, generated using a Sox2Cre transgene to delete *Tgif1* from the embryo proper after about 5.5 dpc, survive to approximately 11.0 dpc and have precursor forms of HPE similar to those seen in *Shh* null embryos. In addition to HPE-like phenotypes, cdKO embryos have decreased forebrain expression of *Shh* and increased *Gli3* expression. The HPE-like phenotypes in

cdKO embryos is partially rescued by introducing a *Gli3* mutation, suggesting that HPE caused by Tgif loss of function may be due at least in part to altered Shh signaling.(91)

In mouse embryos lacking both Tgif1 and Tgif2, gene expression defects, left-right asymmetry defects and HPE can all be partially ameliorated by introducing a heterozygous *Nodal* mutation, consistent with the role of Tgifs in this pathway.(91)

Some candidate HPE genes that have been analyzed functionally are either known components of the SHH signaling pathway (*PTCH1* and *GLI2*), and mutation of *SIX3* has been shown to result in reduced SHH signaling.(114,116,117) However, some of these mutations also appear to fall into the TGFß/Nodal pathway. The *NODAL* gene itself, *FOXH1*, which encodes a forkhead transcription factor that is required for many NODAL responses in the early embryo, and *TDFG1*, that encodes a NODAL co-receptor, have been implicated in HPE.(119,174) Variant *NODAL* and *FOXH1* alleles with reduced function are found in patients with congenital heart disease, laterality defects, and occasionally in HPE patients.(175,176) Additionally, there is evidence from model organisms that mutations in these genes, all of which are expected to reduce the activity of the NODAL signaling pathway, can result in HPE-like phenotypes, including cyclopia and proboscis.(174) In contrast, loss of TGIF function is expected to increase NODAL pathway output. Thus, the mechanisms by which mutations in this pathway cause HPE appear to be quite complex.

Here we show that in cdKO embryos, mutations in both *Gli3* and *Nodal* together improve the partial phenotypic rescue seen with either mutation alone. Reducing Nodal dosage does not prevent the increase in *Gli3* expression in cdKO embryos, and we show

that Tgif1 binds directly to a conserved element in the *Gli3* gene to repress *Gli3* expression. The effects of reducing Nodal signaling appear to be independent of changes in Gli3 expression, and we observe that neuroepithelial cell polarity and proliferation, both defective in cdKO embryos, are rescued by *Nodal* heterozygosity. This leads us to propose a model in which direct repression of *Gli3* by Tgifs regulates dorsoventral forebrain patterning, whereas the effects of Tgifs on Nodal signaling are to maintain neuroepithelial integrity and proliferation. A small proportion of $Nodal^{z/+}$ cdKO embryos survive to 18.5 dpc. Strikingly, those $Nodal^{z/+}$ cdKO embryos present at 18.5 dpc have classic HPE phenotypes, consistent with a failure to rescue the Gli3-Shh balance.

Results

Improved phenotypes in cdKO embryos with Nodal and Gli3 mutations.

We have previously shown that embryos lacking both Tgif1 and Tgif2 have HPE and defects in the Shh signaling pathway. We observed a partial rescue of the HPE phenotype by introducing a heterozygous Nodal mutation (*Nodal*$^{z/+}$). Reducing *Gli3* expression, increased in cdKO embryos compared to controls, also resulted in a partial rescue of the HPE-like phenotypes (91). It is possible that increased signaling from Nodal causes increased *Gli3* expression and decreased *Shh* expression in the ventral region of the forebrain. To test this model, we examined expression of *Gli3* and *Shh* in cdKO embryos with and without mutations in either the *Gli3* or *Nodal* genes. At 9.0 days post coitum (dpc), we observed an increase in dorsal expression of *Gli3* in cdKO embryos, but this increase was not reversed by a heterozygous *Nodal* mutation (Figure 1A). Even in the background of a heterozygous *Gli3* mutation (*Gli3*$^{r/+}$), deletion of *Nodal* had little effect on *Gli3* expression, suggesting that changes in *Gli3* expression are not downstream of altered Nodal signaling. Examination of *Shh* expression revealed a clear decrease in expression in the ventral region of the forebrain in cdKO embryos. At 9.0 dpc, we did not see any obvious restoration of normal expression of *Shh* with mutations in *Gli3*, *Nodal* or both together (Figure 1B). However, when we examined *Shh* expression approximately one half day later, at 9.5 dpc, we observed a partial restoration of expression in the ventral forebrain in *Gli3*$^{r/+}$; *Nodal*$^{z/+}$ cdKO embryos (Figure 1C). In contrast, cdKO

Figure 1. *Shh* expression in cdKO embryos.

Stage matched control and cdKO embryos, cdKO embryos with heterozygous Nodal (*Nodal*$^{z/+}$ cdKO), heterozygous Gli3 (*Gli3*$^{r/+}$ cdKO) mutations, or with both together (*Gli3*$^{r/+}$;*Nodal*$^{z/+}$ cdKO) were analyzed by *in situ* hybridization with anti-sense probes for *Gli3* (A) and *Shh* (B and C), at 9.0 and 9.5 dpc. Side and front views of the same embryos are shown in C. WISH assistance from Ken Taniguchi.

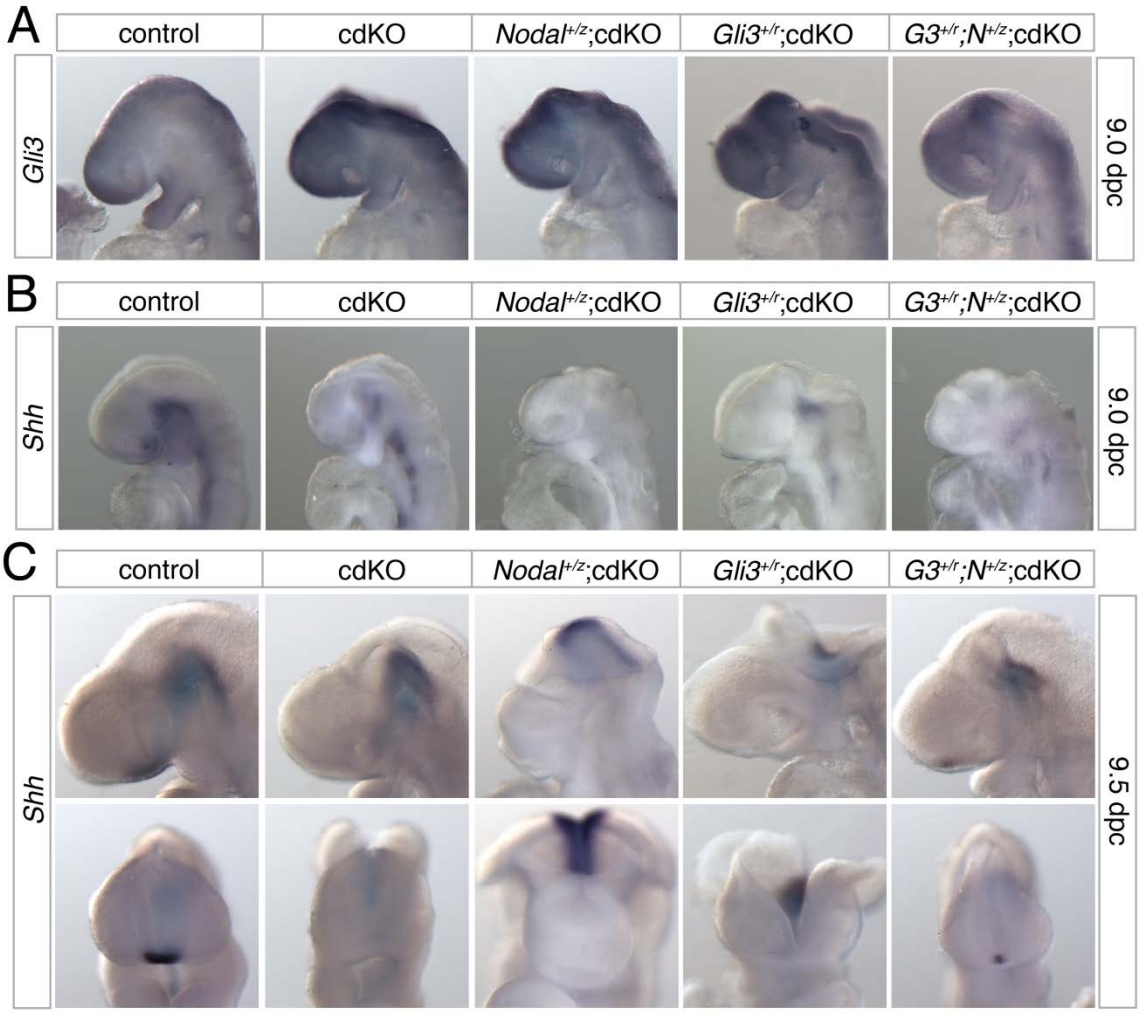
A
control
cdKO
Nodal+/z;cdKO
Gli3+/r;cdKO
G3+/r;N+/z;cdKO
Gli3
9.0 dpc
B
control
cdKO
Nodal+/z;cdKO
Gli3+/r;cdKO
G3+/r;N+/z;cdKO
Shh
9.0 dpc
C
control
cdKO
Nodal+/z;cdKO
Gli3+/r;cdKO
G3+/r;N+/z;cdKO
Shh
9.5 dpc

embryos with mutations in either *Gli3* or *Nodal* alone had no detectable *Shh* expression in the ventral forebrain.

To further test the possibility that reducing both *Nodal* and *Gli3* might result in a better rescue of the HPE phenotype in cdKO embryos, we examined the overall structure of the forebrain ventricle. As shown in Figure 2A, the neuroepithelium (NE) cell layer in control embryos at 9.5 dpc appeared well organized and bisected the underlying neuroectoderm at the midline. In contrast, in stage-matched cdKO embryos the NE appeared to be disorganized and the ventral neuroectoderm layer was much thicker (Figure 2A). Deletion of *Gli3* improved the overall shape of the NE but did not have any effect on the disorganization of the NE at the cellular level. In contrast, the NE appeared to be better organized into a stratified epithelial layer in the $Nodal^{z/+}$ cdKO but still had a very thick ventral neuroectodermal layer. In the double heterozygous ($Gli3^{r/+}$; $Nodal^{z/+}$) cdKO embryos, overall ventral patterning was improved, with the neuroectoderm bisected by the NE. There also appeared to be improved organization of the NE (Figure 2A). To test whether the apparently improved rescue in the $Gli3^{r/+}$; $Nodal^{z/}$ cdKO affected facial patterning, we analyzed expression of the presumptive eye-field marker, *Pax2*. In cdKO embryos, the normal robust expression in the two eye-fields at 9.75 dpc was reduced to a single much weaker band of expression (Figure 2B). In the $Gli3^{r/+}$; $Nodal^{z/+}$ cdKO embryos, expression of *Pax2* was somewhat increased but did not fully separate into two distinct domains, as seen in the control. However, in the $Gli3^{r/+}$; $Nodal^{z/+}$ cdKO expression was stronger and fully separated into two domains, suggesting improved facial pattering in these embryos (Figure 2B). Taken together, these data

Figure 2. Phenotypic rescue by *Nodal* and *Gli3* mutations.

A) Stage matched embryos of the indicated genotypes, at approximately 9.5 dpc, were analyzed by H&E staining. A) section through the forebrain is shown, together with a higher magnification view of the ventral region. B) Embryos of the indicated genotypes were analyzed by *in situ* hybridization with an anti-sense probe for *Pax2*. A side view of the head is shown, with a ventral view shown below. Ken Taniguchi assisted with WISH and H&E.

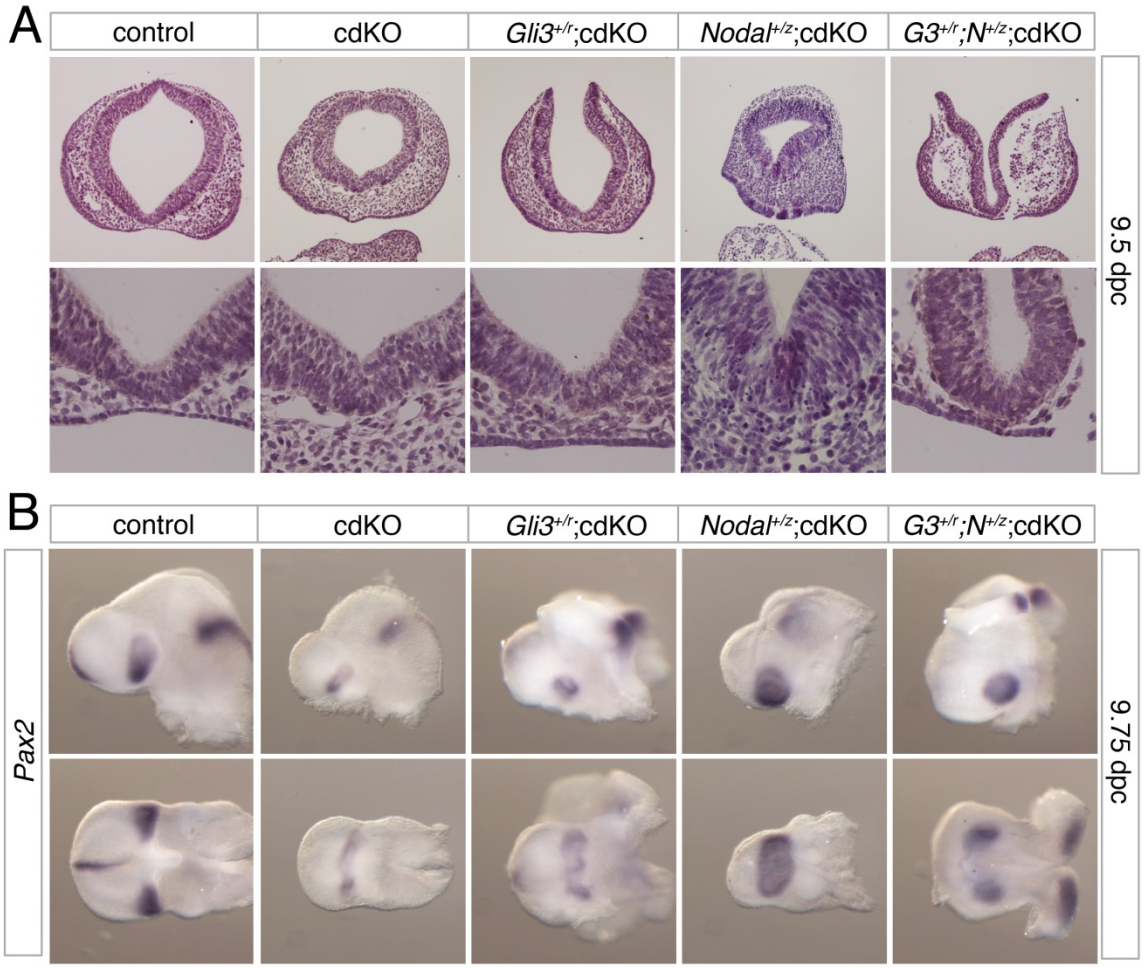
A
control
cdKO
Gli3+/r;cdKO
Nodal+/z;cdKO
G3+/r;N+/z;cdKO
9.5 dpc
B
control
cdKO
Gli3+/r;cdKO
Nodal+/z;cdKO
G3+/r;N+/z;cdKO
Pax2
9.75 dpc

suggest that loss of Tgif function may affect forebrain development by two independent pathways: one via increased *Gli3* expression and one via an increased Nodal response.

Gli3 is a direct Tgif target gene.

Since we observed no effect of *Nodal* mutation on *Gli3* expression and increased *Gli3* expression in the cdKO embryos was consistent with loss of repression, we tested whether *Gli3* could be regulated directly by Tgifs. Several conserved, non-coding elements have been identified within the *Gli3* gene, spanning more than 250kb in both mice and humans (177–180). Additionally, in a chromatin immunoprecipitation-sequencing (ChIP-seq) experiment using antibodies against the coactivator, p300, a number of conserved, forebrain-specific peaks were identified. We scanned each of these conserved regions for consensus Tgif binding sites (CTGTCAA) (75) present in both the mouse and human sequences and identified seven putative Tgif sites in five of these conserved regions (Figure 3A). There were also matches to the minimal Smad binding element (CAGA) in each region, but given there is only a four-base consensus, it is expected at a higher frequency. We first tested binding by performing ChIP-qPCR for each of the Tgif sites using chromatin isolated from 9.0 dpc control embryos. Chromatin was immunoprecipitated with a Tgif1 antiserum, the pre-immune serum or a Smad2/3-specific antiserum. DNA enriched by the ChIP process was made into a cDNA library and analyzed by qPCR for regions with or without the consensus Tgif binding site. As shown in Figure 3A, we observed robust enrichment of the HCNR1 region in the Tgif1 precipitates, whereas none of the other regions tested were bound by Tgif1. No binding of

Smad2/3 was observed in any of the regions tested. To confirm this, we examined binding of Tgif1 to the HCNR1 and to two of the other regions for comparison, in NIH3T3 cells and in primary mouse embryonic fibroblasts (MEFs).). In NIH3T3, Tgif1 again bound the HCNR1 region, and this was not affected by addition of TGFß for one hour prior to isolating the chromatin (data not shown). Smad2/3 binding was not seen to any of the regions tested, and in NIH3T3 cells addition of TGFß did not change expression of the endogenous *Gli3* gene (data not shown).

To ensure that the observed binding was indeed due to Tgifs, we next tested primary MEFs that were either wild type, or lacked both Tgif1 and Tgif2 expression. cdKO MEFs were generated using a Tamoxifen inducible Cre transgene and the *Tgif1* conditional allele, in the background of a *Tgif2* null ($Tgif1^{ff};Tgif2^{-/-};CreER^{+}$). We chose to test cdKO MEFs rather than *Tgif1* single null, as the Tgif1 antiserum may cross-react weakly with Tgif2. In wild type MEFs, the HCNR1 region was highly enriched in Tgif1 precipitates, whereas we observed minimal binding to the other two regions tested and no significant enrichment for any of the three regions tested in chromatin from cdKO MEFs (Figure 3B).

To test whether Tgifs regulate *GLI3* expression in a different system, we used glioblastoma cell lines and tested effects of transient knock-down of *TGIF1* and *TGIF2*. U87 cells express relatively high levels of *TGIF1*, and both *TGIF1* and *TGIF2* are highly expressed in A172. Additionally, both cell lines express endogenous *GLI3*. U87 and A172 cells were transfected with siRNA pools targeting both *TGIF1* and *TGIF2* or with a control pool and RNA was analyzed by qRT-PCR 72 hours later. As shown in Figure 3C,

Figure 3. *Gli3* is a Tgif1 target gene.

A) Binding of TGIF1 to several conserved non-coding regions from the *Gli3* gene was analyzed by ChIP-qPCR in control 9.0 dpc embryos. A truncated version of the Gli3 gene is shown, with exons 1-3 and 14 indicated, together with the conserved regions shown below. Putative TGIF sites and Smad binding elements (SBE) are shown. Chromatin was precipitated with a Tgif1-specific rabbit antiserum, a Smad2/3 specific serum or a control non-immune serum. B) Primary wild type and cdKO MEFs were analyzed in triplicate by ChIP and qRT-PCR using the Tgif1-specific serum or control. C) Tgifs were knocked down in U87 and A172 cells. RNA was extracted, from which a cDNA library was made. qPCR was performed, showing significant increase in Gli3 in the absence of Tgifs. Relative binding compared to pre-immune serum is shown. * $p < 0.001$ by student's T test. Tiffany Melhuish helped with ChIP. Arkadi Manukian provided cDNA and Annie Carlton helped with qPCR.

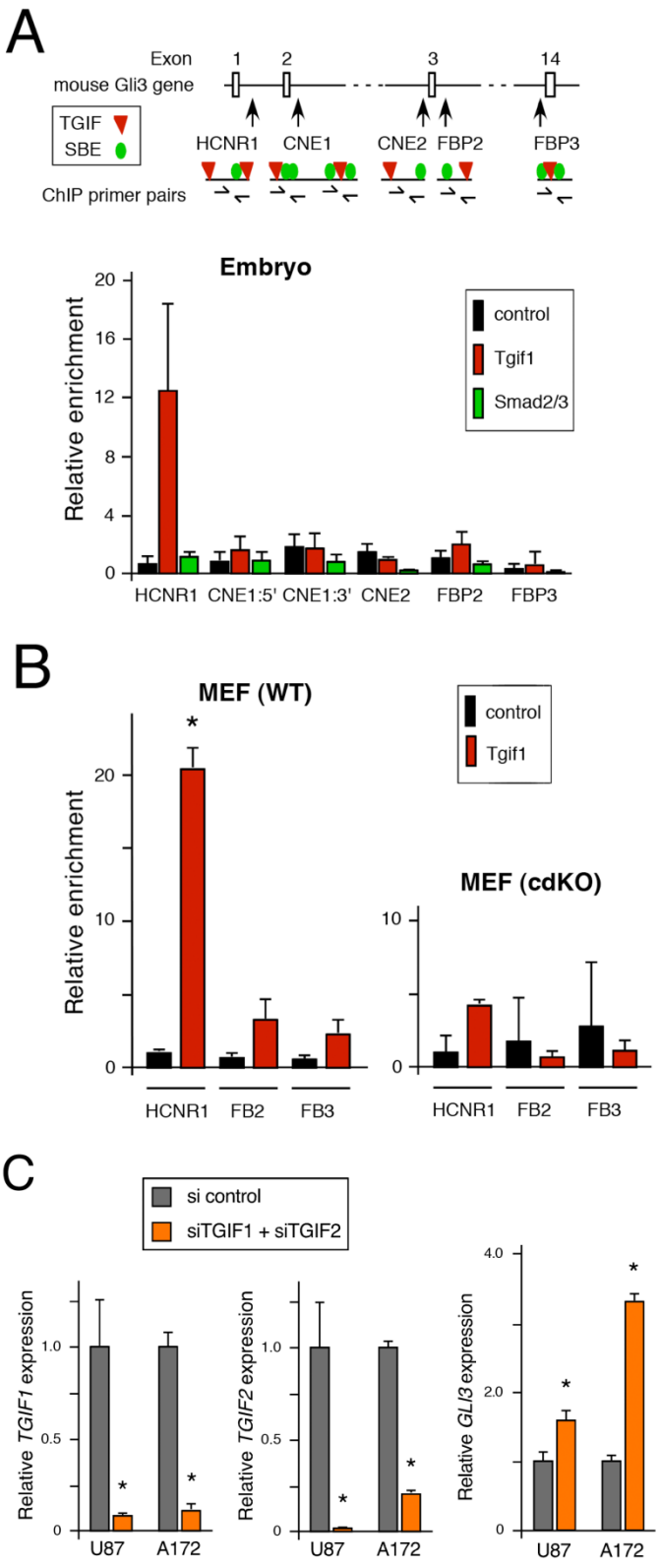
A
Exon
1
2
3
14
mouse Gli3 gene
TGIF
SBE
HCNR1
CNE1
CNE2
FBP2
FBP3
ChIP primer pairs
Embryo
Relative enrichment
control
Tgif1
Smad2/3
HCNR1
CNE1:5'
CNE1:3'
CNE2
FBP2
FBP3
B
MEF (WT)
MEF (cdKO)
control
Tgif1
Relative enrichment
HCNR1
FB2
FB3
C
si control
siTGIF1 + siTGIF2
Relative TGIF1 expression
Relative TGIF2 expression
Relative GLI3 expression
U87
A172

we obtained at least 75% knock-down of each gene, and also observed a significant increase in *GLI3* expression in both cell lines. Taken together, this data suggests that Tgifs are able to bind to a conserved region of the *GLI3* gene and that in both mouse and human *GLI3* expression is repressed by Tgifs.

Disruption of the neuroepithelium apical surface in cdKO embryos.

Close examination of the H&E stained sections through the forebrain NE suggested that the stratification of the NE might be disrupted in cdKO embryos. The NE is a pseudostratified epithelium, in which each cell has an apical domain at the ventricular surface and a basal region that is in contact with the neuroectoderm. Nuclei undergo interkinetic movement, such that they go through S phase at a relatively basal location and migrate towards the apical surface to undergo mitosis. During the normal growth of the NE, the nuclei divide perpendicularly to the apical surface of the cell, allowing for continued expansion of the NE (147,148). To examine NE cell polarity, we first stained sections through the forebrain of control and cdKO embryos at 9.0 dpc with antibodies specific for N-cadherin or atypical PKC (aPKC). aPKC is normally localized primarily at the apical domain of polarized epithelial cells, and in control NE we observed a clear concentration of aPKC towards the apical (ventricular) surface (Figure 4A). In contrast, in the cdKO NE aPKC staining was much more diffuse and lacked the sharp line of staining along the apical surface that was seen in most sections through control NE. The N-cadherin staining in the control was stronger towards the apical surface and clearly outlined the cell boundaries, whereas in cdKO sections, N-cadherin staining was more

diffuse and less apically concentrated (Figure 4A). Analysis of H&E stained sections at higher magnification showed the disorganized NE in the cdKO, and confocal imaging clearly showed that aPKC staining was disorganized in the cdKO NE (Figure 4B). This analysis suggests that there is disruption of the apical domain of the forebrain NE in cdKO embryos. To test if there was also a more wide-spread disruption of polarity, we examined expression of Collagen type IV (ColIV), which marks the basement membrane. As shown in Figure 4C, ColIV staining was present surrounding the basal region of the NE in both control and cdKO embryos. In the cdKO there were some regions where ColIV staining was disorganized. However, the contiguous basement membrane appeared to be generally intact, even in sections where co-staining for ß-catenin, which is normally present at the cell junctions, was more diffuse and disorganized in the cdKO (Figure 4C).

Examination of RNA-seq data from control and cdKO embryos isolated at approximately 8.75 dpc suggested that expression of *Snail2* (Slug) and *Twist2* may be higher in the cdKO, although *Twist2* expression was too variable to reach significance in this RNA-seq data-set. To confirm these changes, we tested expression of both genes by qRT-PCR in control and cdKO embryos isolated at approximately 8.75-9.0 dpc. *Snail2* and *Twist2* expression was significantly higher in the cdKO embryos than in control; we did not observe any difference in expression of *Snail1* or *Twist1*, in agreement with the RNA-seq data (data not shown). This analysis suggests there is defective apical polarization of the NE in cdKO embryos. Additionally, although we do not observe a complete epithelial-to-mesenchymal transition (EMT), there is some increase in both

Figure 4. Disrupted apical polarity in the cdKO neuroepithelium.

A and B) Sections through the forebrain of 9.0 dpc control and cdKO embryos were stained with antibodies for aPKC or N-cadherin and with DAPI for DNA. In A, 40x wide-field immunofluorescent images are shown. In B 100x confocal images and equivalent image of H&E stained sections are shown. C) Forebrain sections were stained with antibodies against Collagen IV and ß-catenin, and with DAPI. 20x and 40x confocal images are shown.

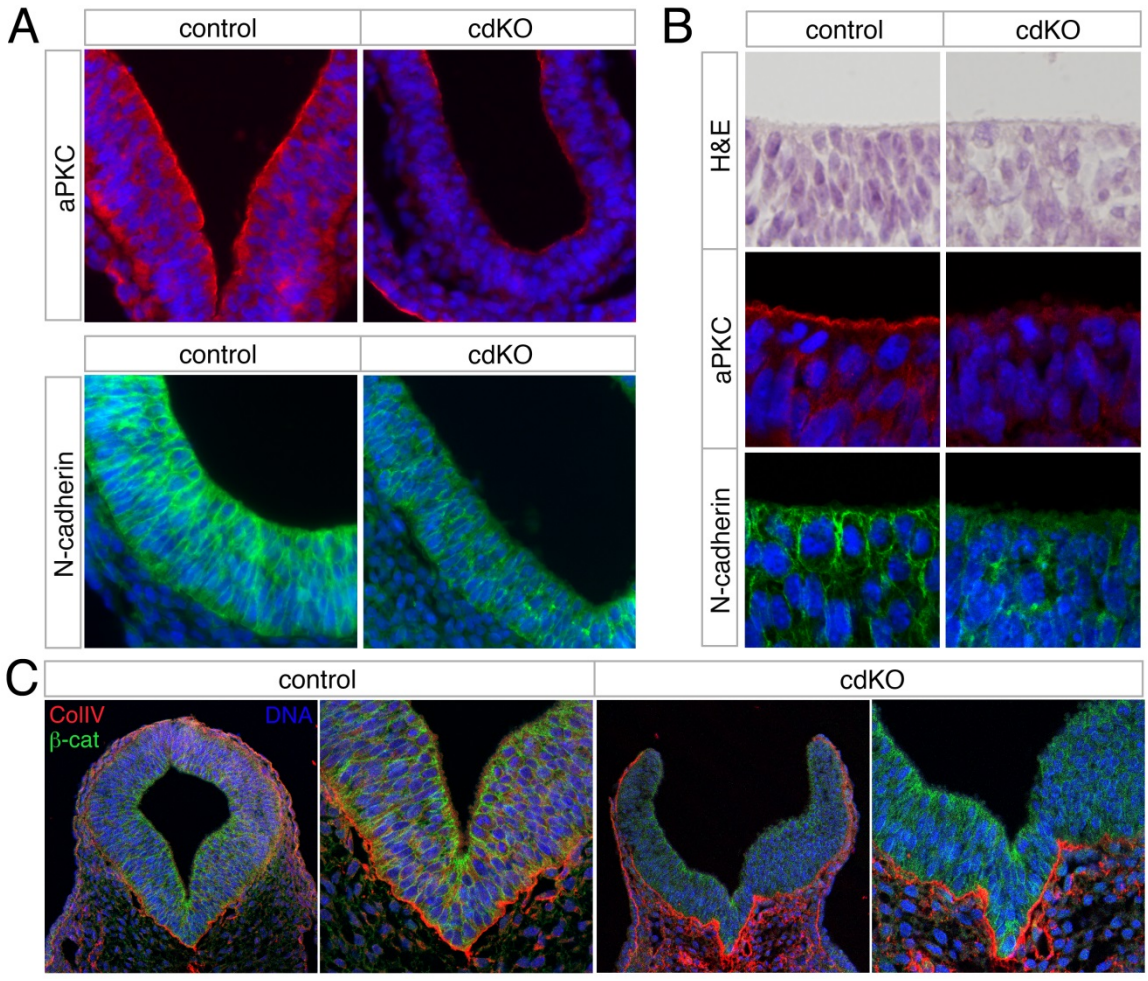
A
control
cdKO
aPKC
control
cdKO
N-cadherin
B
control
cdKO
H&E
aPKC
N-cadherin
C
control
cdKO
ColIV
β-cat
DNA

expression of canonical EMT driver transcription factors and disorganization of the basement membrane.

Reduced Nodal signaling rescues polarity defects.

To test if the improvement in NE organization observed by H&E staining in *Nodal*$^{z/+}$ cdKO embryos (see Figure 2) was due to improved apical polarity, we stained forebrain sections for aPKC and N-cadherin. As shown in Figure 5A, introduction of a *Gli3* mutation did not affect aPKC localization, whereas aPKC localization at the apical surface of the NE in *Nodal*$^{z/+}$ cdKO embryos was similar to that seen in controls. The localization of N-cadherin in *Nodal*$^{z/+}$ cdKO embryos was also similar to the control embryos, but in cdKO and *Gli3*$^{r/+}$ cdKO embryos, N-cadherin staining was more diffuse (Figure 5A). One consequence of disrupting the apical-basolateral organization of polarized epithelial cell layers is that the plane of cell division becomes randomized, rather than dividing predominantly perpendicular to the apical surface. To examine this in the forebrain NE, we stained sections with an antibody against γ-tubulin to identify cells with two centrosomes that were undergoing mitosis. We then measured the angle between the apical surface of the NE and the plane of division, estimated by drawing a line connecting the two centrosomes (see Figure 5B for an example). When we plotted the distribution of angles, the majority of mitotic cells in the control NE clustered with a relative angle of division close to 90° (Figure 5B). In contrast, in the cdKO NE the angle of division was scattered between 0° and 90° relative to the apical surface. We next examined *Nodal*$^{z/+}$ cdKO embryos and observed an intermediate phenotype. The

distribution of angle of division in control embryos was significantly different from a uniform distribution, consistent with the clustering around 90° and almost all of the spindle angles were greater than 60° relative to the apical surface (Figure 5C). In contrast to the control, cdKO mitotic angles were uniformly distributed between 0° and 90°, whereas in the *Nodal*$^{z/+}$ cdKO there was a significant skew towards 90°, with two thirds being greater than 60° relative to the apical surface. We have previously shown that cdKO embryos have a reduced mitotic index in the forebrain NE, and we again noticed this here while examining mitotic spindle angles. To test whether the reduced proliferation was due to altered Nodal signaling or reduced *Gli3* expression, we stained forebrain sections for phospho-Histone H3 (pHH3) to identify cells in late G2 and M phases of the cell cycle. As shown in Figure 5D, the mitotic index of the cdKO forebrain NE was significantly lower than the controls, and in agreement with previous work, deletion of one copy of *Gli3* did not affect the mitotic index. However, removing one copy of Nodal restored the cdKO mitotic index to close to that seen in control embryos (Figure 5D). This analysis suggests that in the cdKO forebrain NE, there is reduced proliferation and a disruption of apical polarity and both of these phenotypes are downstream of excess Nodal signaling.

Partial disruption of apical polarity within the cdKO neural tube

To determine whether polarity defects similar to those found in the forebrain extended to the developing neural tube of cdKO embryos, we analyzed the structure of the neural tube between the midbrain-hindbrain boundary and the forelimb region of control and

Figure 5. Defective polarity and proliferation are downstream of Nodal.

A) Confocal images of forebrain sections of the indicated genotypes, stained with antibodies against aPKC or N-cadherin, are shown. B) Forebrain sections were stained with an antibody for γ-tubulin. Representative images with the apical surface and spindle angle are shown, together with a graphical representation of the spindle angles from control and cdKO forebrain sections. B) The relative spindle angle for neuroepithelial cells from the indicated genotypes were separated into 15° bins and compared to the distribution expected if spindle angle was uniform. D) The mitotic index in the forebrain neuroepithelium at 9.0 dpc was analyzed by staining for pHH3. The mean (+ s.d.) is shown for at least three embryos of each genotype.

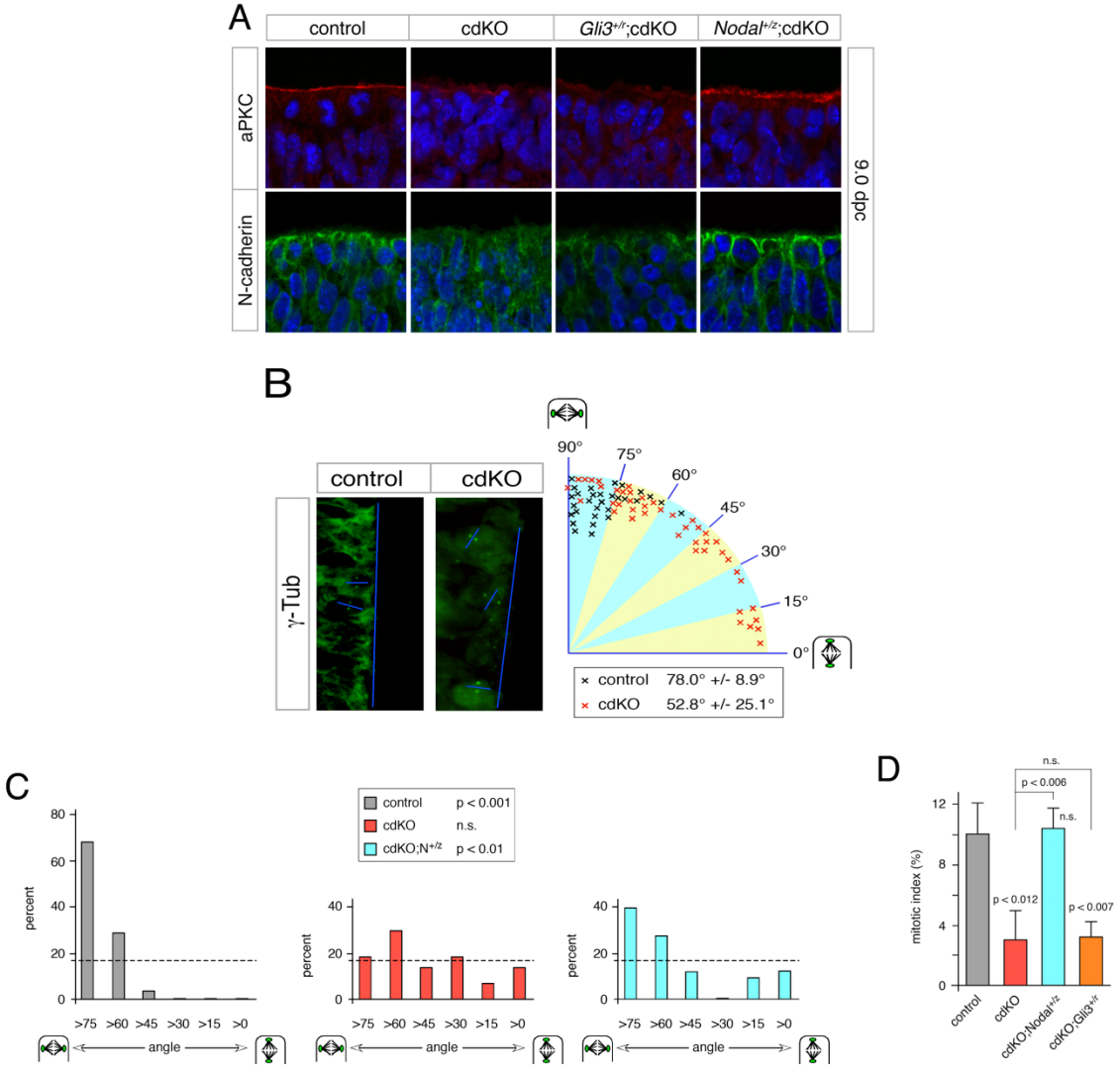
A
control
cdKO
Gli3+/r;cdKO
Nodal+/z;cdKO
aPKC
N-cadherin
9.0 dpc
B
control
cdKO
γ-Tub
90°
75°
60°
45°
30°
15°
0°
control 78.0° +/- 8.9°
cdKO 52.8° +/- 25.1°
C
control p < 0.001
cdKO n.s.
cdKO;N+/z p < 0.01
percent
>75 >60 >45 >30 >15 >0
angle
D
mitotic index (%)
n.s.
p < 0.006
n.s.
p < 0.012
p < 0.007
control
cdKO
cdKO;Nodal+/z
cdKO;Gli3+/r

cdKO embryos. H&E staining of transverse sections showed a closed neural tube with a single-cell-thick ventral floor plate in control embryos. In cdKO embryos, the neural tube was not always closed and the floor plate had variable thickness. In contrast to the disorganization in the forebrain, neural tube disorganization was patchy and less consistent along the length of the neural tube. N-cadherin mediates cell-cell contacts within neuroepithelium. Within both control and cdKO embryos N-cadherin was expressed strongly at the cell surface, suggesting that cell-cell contacts are largely maintained within the cdKO neural tube. Similarly aPKC, a marker for the apical surface of polarized cells, was concentrated at the apical surface in both control and cdKO neural tube. Examination of multiple sections of multiple embryos for these polarity markers revealed that epithelial polarity is disrupted in some areas of the neural tube and intact in others. Figure 6A gives an example of disrupted polarity within the neural tube.

To determine if the neural tube had proliferation defects, we stained both 9.0 dpc and 10.0 dpc sections for pHH3 and counted the proportion of neural tube cells that were pHH3-positive as a measure of proliferation. While there was no difference in proliferation rates at 9.0 dpc, there was a small but significant decrease in proliferation in the cdKO at 10.0 dpc (Figure 6C). As pseudostratified epithelium, cells within the neural tube undergo interkinetic nuclear migration. During growth phase nuclei are positioned near the basal cell surface and travel to the apical surface in preparation for division.(148) As an illustration of the disruption of epithelial polarity within the neural tube, we also grouped the pHH3-positive cells based on their location, namely those pHH3-positive nuclei adjacent to the inner (apical) surface and those not touching the apical surface.

Once again there was no significant difference in location of pHH3 positive nuclei at 9.0 dpc, but at 10.0 dpc there were significantly more pHH3 positive nuclei away from the apical surface in the cdKO as compared to control sections (Figure 6C). We also stained 9.75 dpc sections for cleaved caspase-3. This staining showed an increase of apoptosis within the neural tube. This phenotype was inconsistent along the length of the neural tube (Figure 6B). This decreased proliferation, increased apoptosis and inappropriate location of mitotic nuclei all suggest a more pronounced disruption in epithelial polarity within the neural tube at later stages of development.

Reduced Nodal signaling partially rescues neural tube defects

While examining the neural tube for polarity defects we noticed a strange structural defect present within the cdKO. Intermittently along the length of the neural tube we noticed extensive disruption of epithelial structure in the ventral tube progressing into an isolated tube-like structure with its own lumen between the notochord and the dorsal neural tube (Figure 7A). *Shh* is expressed at the notochord and floor plate and establishes patterning via concentration gradient through the ventral neural tube.(105) In the same manner, *Gli3* is expressed in the dorsal neural tube and gradually decreases towards the ventral neural tube. We hypothesized that disruption of ventral structure and the isolated tube would disrupt the propagation of Shh signaling and ventral identity within the neural tube. To test this, we performed WISH with a probe recognizing *Shh*. We sectioned the stained embryos. Control embryos had strong *Shh* expression within the notochord and floor plate. *Shh* was also expressed in the notochord of cdKO embryos and in the ventral

Figure 6. Defective polarity and proliferation within the neural tube.

A) Transverse sections of neural tube of control and cdKO embryos at 9.0 dpc stained by H&E and IF for N-cadherin and aPKC. B) Transverse sections of neural tube of control and cdKO embryos at 9.75 dpc stained by IF for cleaved caspase 3. C) Analysis of pHH3 by IF as a measure of proliferation in control and cdKO embryo, at both 9.0 dpc and 10.0 dpc. From left to right, charts represent number of cells positive for pHH3, relative number of cells positive for pHH3 and the percent of cells positive for pHH3. For first and second charts, counts are divided into pHH3-positive cells touching the apical surface (inner) and those not touching the apical surface (outer). T-test performed for statistical significance.

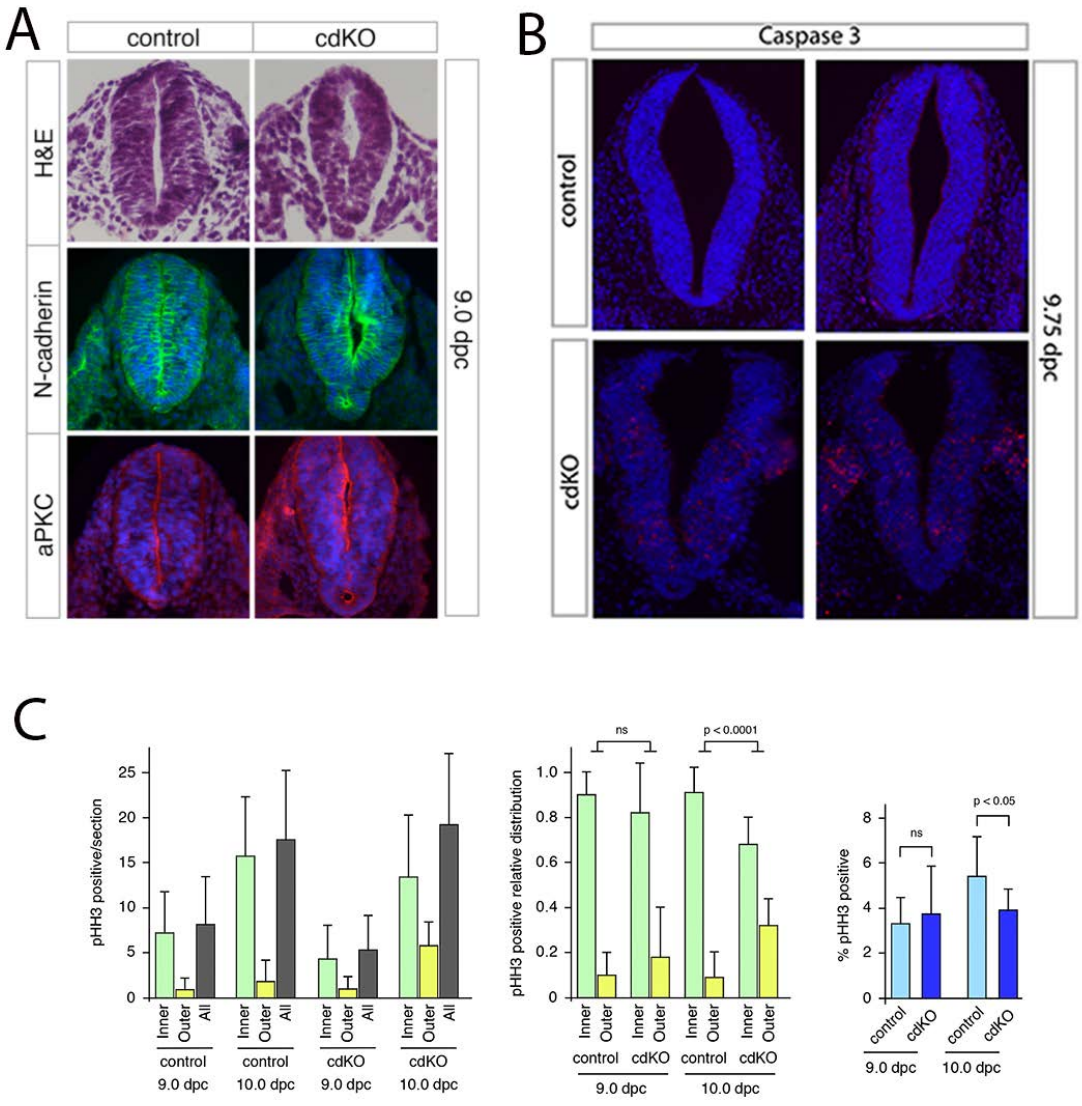
A
control
cdKO
H&E
N-cadherin
aPKC
9.0 dpc
B
Caspase 3
control
cdKO
9.75 dpc
C
pHH3 positive/section
Inner
Outer
All
control
9.0 dpc
control
10.0 dpc
cdKO
9.0 dpc
cdKO
10.0 dpc
pHH3 positive relative distribution
ns
p < 0.0001
control
cdKO
9.0 dpc
10.0 dpc
% pHH3 positive
ns
p < 0.05
control
cdKO
9.0 dpc
10.0 dpc

isolated tube but was absent from the dorsally located neural tube. The presence of an isolated tube appeared to prevent potentiation of the Shh signal through the neural tube (Figure 7B).

To understand the frequency of normal (N), disorganized (D), and isolated tube (IT) regions of the neural tube, we analyzed 95 serial transverse sections of control and cdKO embryos and classified them based on the appearance of the neural tube at several stages of development. In all control embryos, the majority of the neural tube was normal with few sections categorized as disorganized and no isolated tubes. At 9.0 dpc the cdKO exhibited an isolated tube in approximately 70% of the sections counted, with approximately 25% of sections classified as disorganized. We hypothesized that decreasing the genetic dose of *Nodal* would partially rescue this phenotype as it had rescued polarity in the forebrain, and decreasing the genetic dose of *Gli3* would not affect the neural tube structure. When we analyzed serial sections from the $Nodal^{z/+}$ cdKO, the proportion of sections with an isolated tube significantly decreased, while the proportion of sections with disrupted or normal epithelial morphology both increased. Consistent with our hypothesis there was no significant change in the proportion of disrupted sections or those with an isolated tube in the $Gli3^{r/+}$ rescue (Figure 7C). When these phenotypes were plotted and cdKO and $Nodal^{z/+}$ cdKO were viewed together, we noticed that in cdKO embryos the majority of the anterior neural tube exhibits an isolated tube phenotype, whereas the $Nodal^{z/+}$ cdKO had greatly reduced number of sections with an isolated tube. This information suggests that the isolated tube is a more severe phenotype,

and when the dose of Nodal is decreased, the neural tube can become disorganized but is less likely to progress into an isolated tube (Figure 7C).

With the disruption of Shh in the neural tube we wanted to examine DV patterning. We stained transverse sections with antibodies to different neural tube patterning markers (Nkx2.2, Nkx6.1, Olig2, Pax3). These patterning markers are expressed in specific bands, progressing from the ventral neural tube to the dorsal neural tube. They are dependent on the expression of *Shh* and *Gli3* in a gradient-dependent manner. As shown in Figure 8, patterning within the neural tube is basically maintained and only disrupted in the presence of a completely isolated tube ventral to the neural tube.

HPE in late-stage cdKO embryos with *Nodal* heterozygous mutations.

cdKO embryos typically do not survive beyond 11.0 dpc. However, from a large number of litters (118 embryos) isolated at 12.5 dpc, we identified two cdKO embryos with cyclopia and clear signs of HPE. Both these embryos were severely defective and likely would not have survived much longer beyond this stage. To test whether reducing Nodal signaling might allow cdKO embryos to survive to later in embryogenesis, we isolated embryos at 18.5 dpc from crosses between *Sox2cre*$^{+}$; *Tgif1*$^{r/r}$; *Tgif2*$^{+/-}$ and *Nodal*$^{z/+}$; *Tgif1*$^{f/f}$; *Tgif2*$^{-/-}$ mice. One fourth of the resulting embryos were expected to be cdKO and half were expected to be heterozygous for *Nodal*. As shown in Figure 9A, we recovered two cdKO embryos at this stage, both of which were also heterozygous for *Nodal*. We did not identify any cdKO embryos with control *Nodal* alleles from this analysis. Embryos with one, two or three wild type alleles of *Tgif1* or *Tgif2* were found at about

Figure 7. Isolated tube present in cdKO rescued by Nodal heterozygosity.

A) Paraffin-embedded sections of neural tube in control and cdKO embryos 9.0 dpc illustrating normal (N), disorganized (D), and isolated tube (IT). B) WISH for *Shh* in 9.0 dpc neural tube in both control and cdKO. C)95 serial sections from 3 cdKO embryos, 3 $Gli3^{r/+}$ cdKO embryos, 3 $Nodal^{z/+}$ cdKO embryos at 8.5 dpc and 9.0 dpc were stained with H&E and scored according to above defined phenotype (N, D, IT). Results were plotted by both percent of sections exhibiting each phenotypic classification and plotted linearly anterior to posterior (left to right). T-test was performed for statistical significance. Ken Taniguchi helped with IT phenotype analysis.

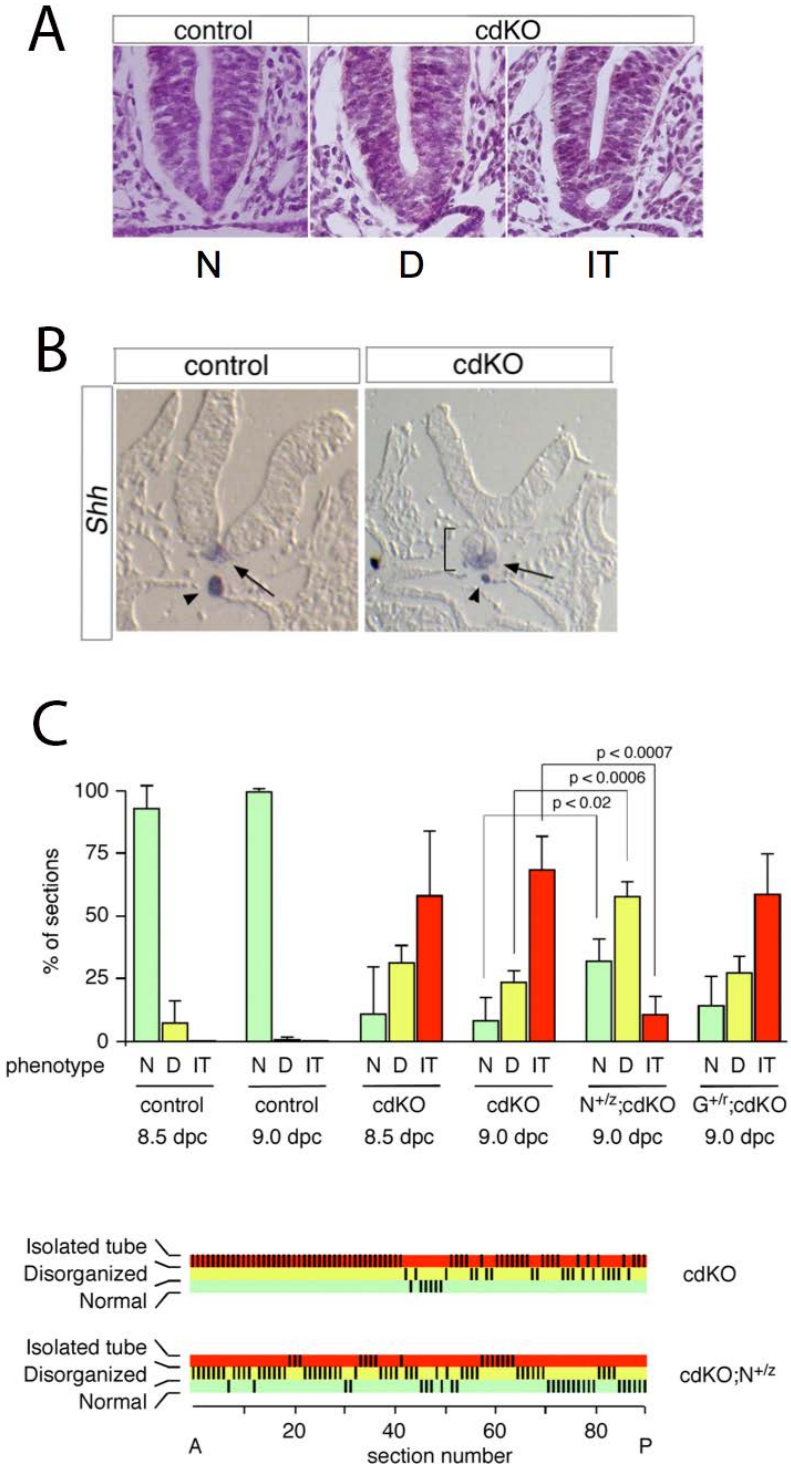
A
control
cdKO
N
D
IT
B
control
cdKO
Shh
C
p < 0.0007
p < 0.0006
p < 0.02
100
75
50
25
0
% of sections
phenotype
N D IT
control
8.5 dpc
control
9.0 dpc
cdKO
8.5 dpc
cdKO
9.0 dpc
N+/z;cdKO
9.0 dpc
G+/r;cdKO
9.0 dpc
Isolated tube
Disorganized
Normal
cdKO
cdKO;N+/z
20
40
60
80
A
P
section number

Figure 8. Neural tube patterning maintained despite polarity defects.

Cryosectioned sections of neural tube in control and cdKO embryos at 9.0 to 10.0 dpc, stained by IF for Nkx2.2, Nkx6.1, Olig2 and Pax3.

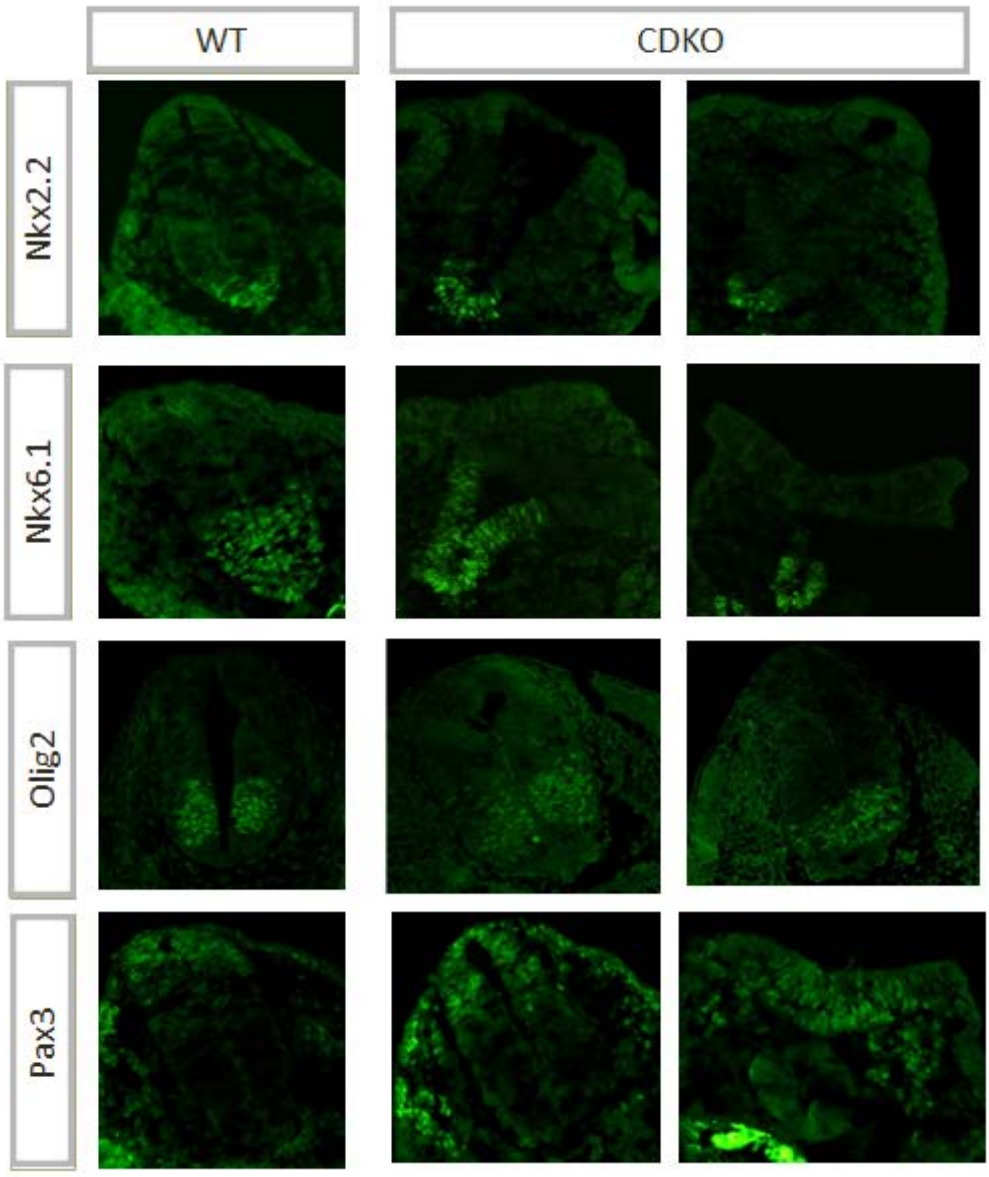
WT
CDKO
Nkx2.2
Nkx6.1
Olig2
Pax3

the expected frequencies with slightly fewer embryos having a *Nodal* heterozygous mutation than those with two control alleles (Figure 9A). Among the 53 embryos in this analysis, we identified several with severe phenotypes, including three with a classic HPE phenotype. Interestingly, both of the $Nodal^{z/+}$ cdKO embryos, as well as one three-allele mutant that was also heterozygous for *Nodal*, had HPE (Figure 9A-C). The other, clearly defective embryos were also *Nodal* heterozygous three-allele mutants, with two having exencephaly and one with agnathia. It seems reducing excess Nodal signaling can allow cdKO embryos to develop to late embryogenesis, but does not appear to rescue the HPE phenotype. This suggests a model in which Tgifs directly repress *Gli3* to maintain anterior DV patterning, and limiting Nodal signaling allows for normal NE cell polarity and proliferation. With misregulated Nodal and Gli3 signaling, cdKO embryos develop a precursor HPE-like phenotype, but die by approximately 11 dpc with multiple defects, including reduced proliferation, defective polarity and increased apoptosis. Reducing Nodal signaling in this context restores cell polarity and proliferation but excess *Gli3* expression still causes HPE. Thus, it appears that Tgifs may regulate forebrain development by two independent pathways (Figure 10).

Figure 9. HPE in Nodal heterozygous cdKO embryos at late gestation.

A) Embryos with various combinations of *Tgif1* and *Tgif2* alleles that were either wild type or heterozygous for *Nodal* were examined at 18.5 dpc. A summary of the genotypes and phenotypes is shown. Embryos with two or three wild type *Tgif1* and *Tgif2* alleles (of the four) are included as one group, with the *Nodal* genotypes (wild type [+/+] or heterozygous [z/+]) separated. The total number of embryos and percentage that were grossly normal are shown. Defects are listed separately for each embryo where applicable. B and C) Examples of whole mount images of $Nodal^{z/+}$ cdKO embryos are shown. Tiffany Melhuish helped with dissection.

A

WT alleles Tgif1 + Tgif2	Nodal	N	% normal	defects
2 or 3	+/+	15	100	-
2 or 3	+/z	8	100	-
1	+/+	18	100	-
1	+/z	10	60	HPE Exencephaly Exencephaly Agnathia
0	+/+	0	-	-
0	+/z	2	0	HPE HPE

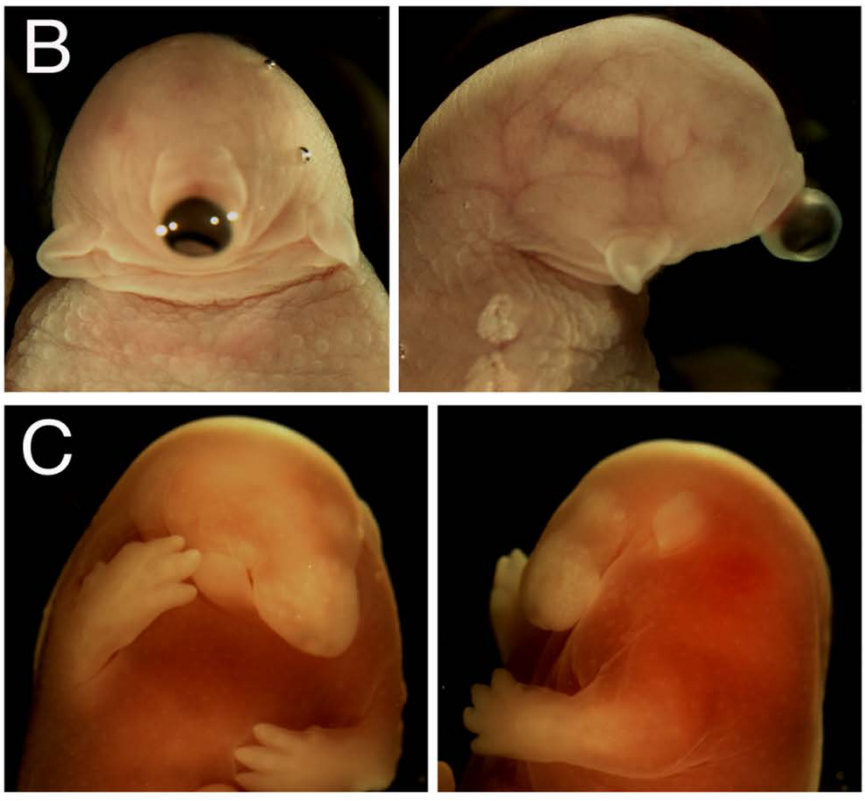

Figure 10. A tentative model for the function of Tgifs in forebrain development. TGIFs regulate Gli3 gene expression and the transcriptional activity of Smad2, in the Nodal pathway via independent mechanisms. Green arrows indicate a positive effect, red lines indicate an inhibitory effect. See text for further discussion.

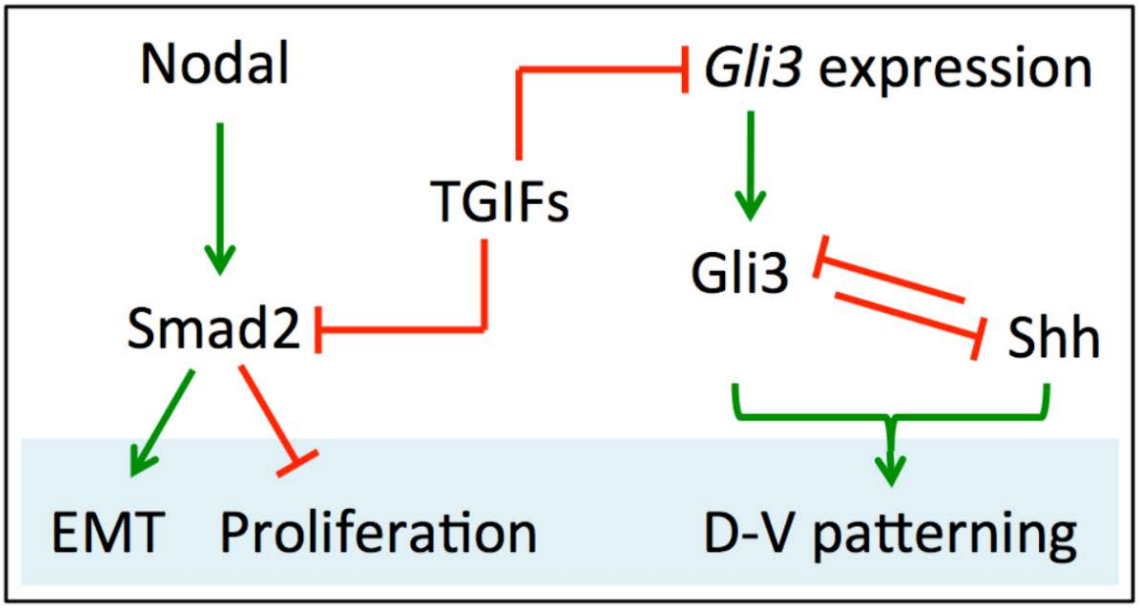
Nodal
Gli3 expression
TGIFs
Gli3
Smad2
Shh
EMT
Proliferation
D-V patterning

Discussion

In mice loss of Tgif1 and Tgif2 together causes HPE and disrupts Nodal and Shh signaling (91). Here we show that excess Gli3 contributes to patterning defects in cdKO embryos and Tgifs repress *Gli3* gene expression. In contrast, excess Nodal signaling in the absence of Tgifs causes defects in NE polarity and proliferation. Reducing both Nodal and Gli3 levels results in improved overall rescue of the cdKO defects, consistent with two independent pathways causing this phenotype in the absence of Tgif function (Figure 10).

We have previously shown that embryos lacking both Tgifs have phenotypes consistent with an early precursor form of HPE and at these early stages appear quite similar to *Shh* null embryos (91). The majority of cdKO embryos do not survive past approximately 11.0 dpc, so it is difficult to examine later phenotypes more clearly representative of HPE. In previous analyses, we identified two cdKO embryos at 12.5 dpc. Both embryos had cyclopia and an anterior proboscis-like structure, as seen in *Shh* null embryos at this age. However, these embryos were quite rare, were very fragile and were not likely to survive much beyond this stage.

From a smaller cohort of embryos analyzed here at 18.5 dpc, we found three with clear HPE, including cyclopia and proboscis. Two of these embryos were cdKOs and one had three mutant alleles (*Tgif1* $^{r/r}$; *Tgif2* $^{+/-}$). The presence of an HPE phenotype in a three allele mutant is consistent with previous work suggesting that a small proportion (approximately 5-10%) of embryos of this genotype are indistinguishable from cdKOs at

approximately 9.0-10.5 dpc. What is most striking from the analysis here is that all three embryos with HPE, including the only two cdKO embryos identified at 18.5 dpc, were also heterozygous for *Nodal*.

Previous analyses have shown that reducing *Gli3* dosage in the background of a *Shh* null mutation can partially rescue the defects in DV patterning and the HPE phenotype (181). Based on our analysis here and in previous work, it appears that *Gli3* heterozygosity can do the same in the context of loss of Tgif function. The bisection of the neuroectoderm by the NE was improved in $Gli3^{r/+}$ cdKO embryos compared to the cdKO, and patterning of the forebrain and facial fields was improved. However, defects in cell proliferation and NE polarity within the forebrain and neural tube appear to be downstream of excess Nodal signaling.

The increase in *Gli3* expression appears to be independent of the TGFß/Nodal pathway. Since Tgifs are transcriptional repressors, direct target genes would be expected to have higher expression in the cdKO than in control embryos, and we show that Tgif1 can indeed bind to a conserved region of the *Gli3* gene that contains two consensus Tgif sites.

In summary, we show both the Nodal and Shh signaling pathways are disrupted in embryos lacking Tgif function, and these pathway disruptions appear to be independent of each other (Figure 10). Our genetic analysis suggests a context in which mutations that reduce TGFß/Nodal signaling could contribute to the pathogenesis of HPE, and we propose a refined model for the involvement of Tgif function in Nodal and Shh signaling in the pathogenesis of HPE.

Materials and Methods

Ethics statement

All animal procedures were approved by the Animal Care and Use Committee of the University of Virginia, which is fully accredited by the AAALAC.

Mice and DNA analysis

The *loxP* flanked *Tgif* allele (86) and *Tgif2 null* (90) alleles and the *loxP* flanked *Gli3* allele (173) and *Nodal* mutant (56) are as described. The *Sox2-Cre* line (182) was obtained from Jax (# 4783). The *Gli3* allele contains a loxP flanked exon, which when recombined results in a null allele, referred to here as 'r' for recombined (null). The *Nodal* null allele is referred to as 'z', for an introduced lacZ reporter. All mouse lines were maintained on a mixed C57BL/6J x 129Sv/J background. Genomic DNA for PCR genotype analysis was purified from ear punch, at post-natal day 21 (P21), yolk sac (7.0-10.0 dpc), or tail (18.5 dpc) by HotShot (183).

In situ hybridization

Whole-mount in situ hybridization was performed with digoxigenin-labeled riboprobes, as described (184). All images are representative of at least three embryos analyzed.

Histology, immunohistochemistry (IHC) and whole-mount analysis

Embryos were fixed overnight in 4% paraformaldehyde at 4^{o}C, or for 48 hours for 18.5 dpc, dehydrated through an ethanol series (70%, 90%, 95%, 100% x2 for 30 minutes each), incubated in xylene twice for 60 minutes and 1:1 xylene/paraffin for 60 minutes at 60^{o}C, then embedded in paraffin wax, and sectioned at 7μm. For Hematoxylin and Eosin (H&E) staining for histological analysis, sections were de-paraffinized with xylene and stained with H&E. Embryos cryosectioned were flash frozen in OTC and were incubated in PBS prior to application of primary antibody. Multiple sections per embryo were incubated with primary antibodies for rabbit polyclonal phospho-histone H3 (1:200, Upstate 06-570) , rat monoclonal N-Cadherin (1:50, DSHB MNCD2), rabbit polyclonal aPKC (ζ isoform; 1:250, Santa CruzSC-216), rabbit polyclonal collagen IV (1:100, Chemicon AB756P), mouse monoclonal β-Catenin (1:100, BD Transduction Laboratories 610153), mouse monoclonal γ-tubulin (1:200, Sigma, T6557), rabbit polyclonal ACTIVE Caspase-3 (1:250, Promega, G7481), mouse monoclonal Nkx2.2 (1:50, DSHB, 74.5A5), mouse monoclonal Nkx6.1 (1:250, DSHB, F55A10), mouse Pax3 (1:250, DSHB, PAX3), or polyclonal rabbit Olig2 (1:500, Millipore, AB9610) as described (90). For IHC, antibody staining was detected using Vectastain ABC (Vector Laboratories) and developed with Impact DAB (Vector Laboratories). For H&E and IHC images were captured using an Olympus BX51 microscope and either an Olympus SZX12 or DP70 digital camera, and manipulated in Adobe Photoshop. Images of 7.0-10.0 dpc embryos were captured using a Leica MZ16 stereomicroscope and QImaging 5.0 RTV digital camera.

Chromatin immunoprecipitation

Chromatin immunoprecipitation was performed as previously described.(185,186) Briefly, MEFs or NIH3T3 cells were cross-linked with 1% formaldehyde for 20 minutes at 37°C. Following chromatin isolation, DNA was sheared by sonication to between 200 and 1000bp in length using a Branson digital sonifier with microtip. For ChIP from whole embryos, freshly isolated tissue was gently dissociated into a conical tube and cross-linked for 20 minutes at 37°C. Immunoprecipitations were carried out using 2µl of a polyclonal Tgif1 antiserum (78), or 2µl of preimmune serum.

siRNA knock-down and qRT-PCR

RNA was isolated and purified using Absolutely RNA kit (Agilent). cDNA was generated using Superscript III (Invitrogen), and analyzed in triplicate by real time PCR using a BioRad MyIQ cycler and Sensimix Plus SYBRgreen plus FITC mix (Bioline), with intron spanning primer pairs, selected using Primer3 (http://frodo.wi.mit.edu/). Expression was normalized to Rpl4 and Actin using the delta Ct method, and is shown as mean plus standard deviation of triplicates. For knock-down, cells were plated in 6 well plates and transfected with Dharmacon SMARTpool oligonucleotides against *TGIF1* and *TGIF2*, using DharmaFECT reagent 1. The control pool (siGENOME Non-targeting siRNA pool #3) was used for the non-targeting control.

Cell culture and luciferase assays

U87 and A172 cells were grown in DMEM with 10% FBS. Primary MEFs were isolated from 13.5 day mouse embryos, and cultured in DMEM (Invitrogen) with 10% Fetal Bovine Serum (Hyclone) as described. Cells were transfected using TransFectin (Biorad) according to the manufacturer's instructions. Cells were transfected with firefly luciferase reporters, a Renilla transfection control (phCMVRLuc; Promega), and the indicated constructs. After 48 hours firefly luciferase activity was assayed using firefly substrate (Biotium) and Renilla luciferase was assayed with 0.09μM coelenterazine (Biosynth), using a Berthold LB953 luminometer.

Chapter Three

Tgif1 and Tgif2 control ciliogenesis by limiting expression of the RabGAP, Evi5l

Anoush E. Anderson[1], Kenichiro Taniguchi[1,#], Tiffany A. Melhuish[1], Anant Shah[1], Ann E. Sutherland[2] and David Wotton[1]*

[1] Department of Biochemistry and Molecular Genetics,
and Center for Cell Signaling, University of Virginia, Charlottesville, USA

[2] Department of Cell Biology, University of Virginia, Charlottesville, USA

[#] Present address: Department of Cell and Developmental Biology,
University of Michigan Medical School, Ann Arbor, MI 48109

Ann Sutherland helped with whole embryo immunofluorescence. Anant Shah helped with immunofluorescence of forebrain sections. Tiffany Melhuish helped with ChIP-qPCR.

Abstract

The human *TGIF1* gene is implicated in holoprosencephaly (HPE). In mice, deletion of both *Tgif1* and the related *Tgif2* results in a failure of gastrulation. Conditional deletion of *Tgif1* (cdKO) allows survival to mid-gestation, but embryos lacking both Tgifs have HPE and defects in left-right asymmetry. To identify pathways that may be deregulated by loss of Tgif function during embryogenesis we performed transcriptome profiling on whole mouse embryos at approximately nine days after fertilization. This analysis revealed a large number of differentially expressed genes with most being increased in the Tgif mutant embryos, consistent with the function of Tgifs as transcriptional repressors. Among the differentially expressed genes we noticed a number of genes with links to cilia function. This included a small number that were increased in the mutants and are predicted to inhibit cilia formation. One of these, the RabGAP *Evi5l*, is known to block cilia formation when overexpressed and was among the most significantly altered genes in *Tgif* mutant embryos. We show that *Evi5l* expression is increased in cdKO embryos and in double null primary mouse embryonic fibroblasts (MEFs). Knock-down of *TGIFs* in a human retinal pigment epithelial cell line (ARPE19) also increased *EVI5L* expression. TGIF1 binds a conserved consensus TGIF site in the 5' of the human and mouse *Evi5l* genes, suggesting *Evi5l* is a direct target of TGIF repression. In *Tgif* null MEFs we show that the number of cells with primary cilia is significantly decreased. Similarly, transient TGIF knock-down in ARPE19 cells reduced cilia numbers. Reducing the expression of *Evi5l* in primary cells lacking both *Tgifs* resulted in a partial restoration

of cilia numbers. In summary, this work shows Tgifs may regulate ciliogenesis and suggests Evi5l mediates at least part of the effect of Tgifs on cilia formation.

Introduction

Tgif1 and Tgif2 are related homeodomain proteins of the TALE superfamily and primarily act as transcriptional repressors (75,81,82,187). Tgif1 and Tgif2 have been shown to repress TGFß responsive gene expression by binding to TGFß-activated Smads (78,82,188). Tgif1 has been shown to interact with general transcriptional corepressors, including CtBP1 and mSin3a; the related Tgif2 binds mSin3a but lacks the CtBP-interaction motif (79,80,189). Thus, repression of TGFß dependent gene expression by Tgifs likely involves recruitment of general corepressors to the Smad complex, although other mechanisms for regulating TGFß responses have been proposed (42,190).

Tgifs also regulate gene expression when bound directly to DNA in the absence of Smads or nuclear receptors (81). Unlike many homeodomain proteins which recognize a relatively short binding site and often bind in complex with other related proteins, Tgifs bind to a 7-base consensus site (75). Binding of TGIF1 to this site represses transcription, likely by recruiting general corepressors. Relatively few direct Tgif target genes have been identified.

Loss-of-function mutations in the human *TGIF1* gene are associated with holoprosencephaly (HPE), a severe craniofacial disorder affecting forebrain development and midline patterning (84,191). Although these human *TGIF1* mutations are heterozygous, deletion of *Tgif1* in mice has relatively mild phenotypes, even as a homozygous mutation (86–88,192). However, deletion of both *Tgif1* and *Tgif2* results in gastrulation defects and altered Nodal responses, consistent with the role of Tgifs in

TGFß family signaling (90). Conditional mutation of *Tgif1* in the background of a *Tgif2* null mutation allows embryos to bypass gastrulation defects. The resulting embryos have HPE and changes in the Shh signaling pathway, confirming Tgifs as regulators of forebrain development, as suspected from the human HPE association (90,91). In addition to the HPE-like phenotypes, conditional double mutants have a number of other defects, including defects in left-right asymmetry, and do not survive past approximately eleven days of embryogenesis. Direct gene targets for Tgifs that may mediate these embryonic phenotypes have not been identified.

Primary cilia are specialized organelles that are assembled over the basal body during the G1 phase of the cell cycle. The cilium, which protrudes from the surface of many cell types, consists of a central core of acetylated tubulin that is surrounded by a compartmentalized cell membrane domain. Transport into and out of the primary cilium is mediated by specific IFT complexes which are also responsible for the regulated assembly and disassembly of cilia as cells progress through the cell cycle. Cilia perform a number of important functions, including mediating certain signaling pathways, e.g. Shh signaling (121,131). Components of the Shh signaling pathway, including the Patched and Smoothened transmembrane receptors and the intracellular mediators, the Gli proteins, are all present in primary cilia (132,193,194). This localization is required for the majority of Shh signaling, with the Gli proteins being activated in the primary cilium prior to translocation to the nucleus. Defects in ciliogenesis in certain mouse mutants cause phenotypes similar to those found as a result of mutations in the Shh pathway, further reinforcing the importance of this organelle in Shh signaling (131). At the PNC,

pit cells each have a single motile cilium. These cilia are thought to contribute to fluid flow across the PNC that is responsible for setting up left-right (L-R) asymmetry in the developing embryo (195,196). It is thought that fluid flow generated by motile cilia at the PNC results in the leftward transfer of signaling molecules which then induce left-specific gene expression in the left lateral plate mesoderm (123,124).Thus cilia play important roles in a number of early developmental processes.

In an effort to identify the genes and pathways regulated by Tgifs during embryogenesis, we performed transcriptome profiling by RNA-seq on control embryos and embryos lacking both Tgif1 and Tgif2. For this analysis, we chose embryos at the 9-10 somite stage, when the mutant embryos had relatively severe phenotypes but had not yet induced apoptosis. This analysis identified a large number of genes that were differentially expressed. We focused on a small sub-set of the differentially expressed genes that have been associated with ciliogenesis. We show increased expression of a RabGAP, encoded by the *Evi5l* gene, which was previously shown to limit ciliogenesis (140). Deleting *Tgifs* results in increased *Evi5l* expression and a reduction of cells with cilia. Finally, we show that Tgif1 binds directly to a conserved element in the *Evi5l* gene and represses its expression. This work identifies *Evi5l* as a direct Tgif target gene and suggests that Tgifs play a role in regulating ciliogenesis.

Results

Transcriptomic analysis of cdKO embryos

We have previously characterized embryos lacking both Tgif1 and Tgif2, generated with Sox2Cre and a conditional *Tgif1* allele (*Tgif1*$^{f/f}$;*Tgif2*$^{-/-}$;*Sox2Cre*$^{+}$, referred to as cdKO (conditional double knock-out). cdKO embryos have a number of phenotypes, including holoprosencephaly, defects in Shh signaling, and left-right (L-R) asymmetry, and they do not typically survive beyond ~11.0 dpc (days post coitum) (90,91). In an effort to identify pathways and/or transcriptional programs altered in the absence of Tgifs, we performed RNA-seq analysis on whole embryos isolated at 8.5 - 9.0 dpc, a stage at which defects are clearly evident. Control and cdKO embryos were isolated from separate litters and approximately stage matched such that the control embryos had 9-10 somites, equivalent to 8.5 to 8.75 dpc in this strain background. Since somite structure is poorly defined in the cdKO embryos, we stage matched cdKOs by embryo size and overall appearance, focusing on litters that were isolated at around 9.0 dpc. Representative images of embryos used for this analysis are shown in Figure 11A. Although analysis of whole embryos could mask changes in gene expression restricted to part of the embryo, we thought this approach might identify more fundamental changes in gene expression in the absence of Tgifs. As shown in Figure 11A, principle component analysis (PCA) showed that the embryos clustered quite tightly by genotype, with some spread in the cdKOs. However, the majority of the variation in the data is accounted for by PC1, with only 13.2% being attributed to PC2. The two cdKO embryos shown in Figure 11A span most

of the range of the data as separated by PC2. We also performed unsupervised hierarchical clustering of the data based on the 100 most variable genes, again yielding results clustering control and cdKO embryos into two separate groups (Figure 11B). Within each group in this analysis, embryos also clustered by expression of *Xist*, an X-chromosome-specific gene involved in X-inactivation in females, and the reciprocal expression of a small group of genes on the Y chromosome. Using this as an indicator of gender, it appears that gender difference was not a major driver of the clustering in the PC analysis (m: male embryos, Figure 11A).

Comparing control and cdKO embryos identified 1676 genes that were differentially expressed (log2-fold change of greater than +/-0.5, adjusted p-value of < 0.0001), of which 1172 (70%) increased in the cdKO compared to control (data available upon request). Displaying the z-scores of each of these genes for all embryos revealed some variability, particularly in the cdKOs; however, it was not possible to identify any embryos as extreme outliers in their overall patterns from this analysis or from the PCA (Fig 1A and C).

We previously analyzed gene expression in primary mouse embryonic fibroblasts (MEFs) lacking *Tgif1* by Affymetrix expression array and identified 2095 probe-sets that collapsed to 340 genes that increased and 255 that decreased in the absence of *Tgif1 (188)*. We used this to filter the aforementioned RNA-seq data in an effort to focus on higher-confidence potential Tgif target genes. Comparing these two data-sets identified 131 differentially expressed genes in common, with the majority (93 genes) increased in both analyses (Figure 11D and E). We, therefore, focused on this common list of

increasing genes and tested a small panel of them (red dots in Figure 11E) by qRT-PCR in a set of four control and four cdKO embryos that were distinct from those used for the initial RNA-seq analysis. Of the five genes tested, four increased significantly. Expression of the fifth gene increased in the cdKO, but was too variable to reach significance in this smaller set of embryos (Figure 11F). This analysis suggests that genes that overlap between the two data-sets are likely to be Tgif targets.

Disrupted expression of ciliogenesis genes in cdKO embryos

GO-term analysis of the RNA-seq data revealed enrichment for genes involved in DNA metabolic processes and patterning in the down-regulated gene list, consistent with previously identified phenotypes (Table 1). There was enrichment for genes associated with the extra-cellular matrix and cytoskeleton among the up-regulated genes, suggesting alterations in cell architecture. Among the most significantly up-regulated genes was *Evi5l* (see Figure 11E and data not shown). *Evi5l* encodes a RabGAP that was identified in a screen for RabGAPs involved in ciliogenesis. When *Evi5L* is over-expressed cilia numbers are reduced in retinal pigment epithelial cells (140). Additionally, expression of a small group of *Ift* genes that encode components of the ciliary transport machinery was decreased in the cdKO (see Figure 12A and data not shown). Given the changes seen in *Evi5l* and *Ift* genes, we used PubMed to create a list of genes associated with ciliogenesis or cilia function and examined their expression patterns within our RNA-seq data. This list included *Hdac5*, *Hdac6* and *Sirt2*, all of which have been shown to deacetylate tubulin (197–199). We also included other Hdacs and Sirtuins (see Supplementary Table

Figure 11. Transcriptome analysis of cdKO embryos.

RNA was isolated from four control and eight cdKO embryos and analyzed by RNA-seq. A) Principal component analysis of the RNA-seq data is shown. The three numbered points correspond to the three numbered embryos shown to the right, 'm' represents male embryos as determined by analysis of the RNA-seq data. B) Unsupervised hierarchical clustering of the RNA-seq data is shown, based on the 100 most variable genes. The positions of *Xist* and a small cluster of male specific genes from the Y chromosome are shown, as is the position of *Evi5l*. C) RNA-seq data was filtered using a log-fold change of +/- 0.5 and a p-value cutoff of < 0.0001, and is displayed as the z-scores for the 1676 genes that passed this cutoff when comparing control to cdKO. D) Analysis of the overlap between this data and Affymetrix expression array data from wild type and *Tgif1* null primary MEFs is shown. The distribution of the genes in the four overlap segments was compared by chi squared analysis using a 2x2 contingency table. E) A volcano plot for the p-value vs the fold change for the 93 and 22 genes that increase or decrease in both analyses from D is shown. Red dots are genes tested in F, and *Nphp1* and *Evi5l* are indicated. F) Four control and four cdKO embryos were analyzed by qRT-PCR for expression of a selection of the genes in the overlap between the embryo RNA-seq and the MEF expression analysis. Relative expression compared to the control is shown. * : $p < 0.05$, ** : $p < 0.01$.

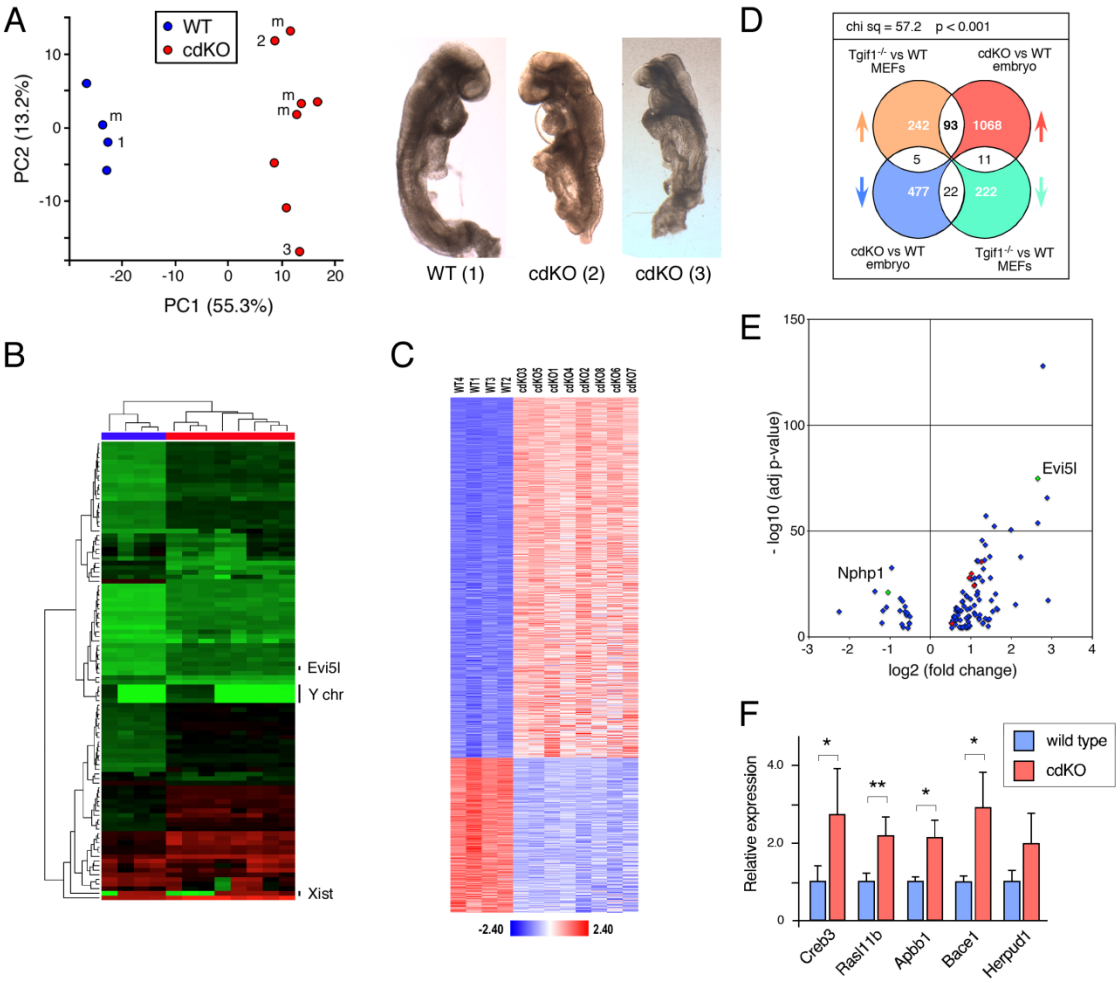
A
WT
cdKO
PC2 (13.2%)
PC1 (55.3%)
WT (1)
cdKO (2)
cdKO (3)
D
chi sq = 57.2 p < 0.001
Tgif1-/- vs WT MEFs
cdKO vs WT embryo
242
93
1068
5
11
477
22
222
cdKO vs WT embryo
Tgif1-/- vs WT MEFs
B
Evi5l
Y chr
Xist
C
WT4
WT1
WT3
WT2
cdK03
cdK05
cdK01
cdK04
cdK02
cdK08
cdK06
cdK07
-2.40
2.40
E
- log10 (adj p-value)
log2 (fold change)
Evi5l
Nphp1
F
Relative expression
wild type
cdKO
Creb3
Rasl11b
Apbb1
Bace1
Herpud1

Table 1. GO-term analysis of RNA-seq.

GO Term	fold enrichment	FDR	Up/Down
Extracellular matrix	2.63	3.71E-06	Up
proteinaceous extracellular matrix	2.62	9.64E-06	Up
Cytoskeleton	1.56	0.0085	Up
Intracellular signaling cascade	1.64	0.0094	Up
Endosome	2.26	0.0309	Up
Muscle system process	3.90	0.0370	Up
Regionalization	4.55	4.94E-06	Down
DNA metabolic process	2.99	2.94E-04	Down
Anterior/posterior pattern formation	4.77	3.69E-04	Down
Pattern specification process	3.43	9.47E-04	Down
DNA repair	3.65	0.0041	Down
Response to DNA damage stimulus	3.25	0.0042	Down
Cellular response to stress	2.61	0.0382	Down

1 for full list). Clustering the gene expression data for this list generated four major clusters: three smaller clusters contained genes that were quite consistently increased in the cdKO compared to the control embryos and a fourth larger group contained genes with decreased expression in the cdKO, including the sub-set of aforementioned *Ift* genes (Figure 12A). We next compared our gene expression data to specific well-characterized cilia sub-complexes, here including only genes that made the statistical cut-offs described earlier. As shown in Figure 12B, expression of the genes encoding four transition zone components (129) and five components of the IFT-B complex (200) decreased significantly in the absence of Tgifs. Although these changes could be consistent with decreased cilia numbers, putative direct Tgif target genes would be expected to show increased expression in the cdKO.

While a number of genes showed increased expression in the z-score heat-map, not all of these were significantly changed based on our statistical cut-offs. Among the genes from the cilia list that significantly increased in the cdKO were *Evi5l, Kif19a* and two histone deacetylases (*Hdac5* and *Sirt2*) (Figure 12A). Both Hdac5 and Sirt2 have been reported to be tubulin deacetylases, and Kif19a limits cilia formation by aiding in microtubule depolymerization at the cilia tip (201). As previously mentioned, *Evi5l* encodes a RabGAP that, when overexpressed in human RPE cells, decreased the number of cells with cilia (140). Two other RabGAPs (Tbc1d7 and Tbc1d30) also decreased cilia numbers in this screen, but did not change significantly in our RNA-seq data (Figure 12C). In addition, no change in their cognate Rabs was observed here, whereas *Rab23* (the Evi5l-associated Rab) showed a small but significant decrease in expression in the

RNA-seq data. To validate these changes, we analyzed the additional set of embryos by qRT-PCR for *Evi5l* and a small number of other cilia related genes. As shown in Figure 12D, *Evi5l* expression was significantly higher in cdKO than in control embryos and *Rab23* expression did not change significantly. We also confirmed the changes observed by RNA-seq for *Kif19a*, *Hdac5* and *Sirt2*, and the decrease in *Nphp1* expression (Figure 12D).

Embryos lacking Tgif1 and Tgif2 have defective PNC cilia

We have previously shown that cdKO embryos have defects in L-R asymmetry (90). One possible explanation for this might be defective cilia at the PNC. To determine whether there were structural defects in the cdKO PNC, we performed whole-mount confocal immunofluorescence on control and cdKO embryos at ~7.25 dpc. As shown in Figure 13A, in control embryos stained with phalloidin to detect actin, the PNC pit was readily identifiable and contained numerous cells with long cilia marked by robust staining with an antibody against Arl13b. In contrast, few, if any, PNC cilia were present in cdKO embryos, and the PNC pit appeared to be disorganized compared to the control (Figure 13B and C). This suggests that L-R asymmetry defects in cdKO embryos may be due to structural defects in the PNC, including a reduction in the number of cilia.

In addition to L-R asymmetry problems, cdKO embryos have holoprosencephaly and defects in the Shh signaling pathway, including reduced expression of *Shh* itself in the ventral forebrain (91). Given that Shh signaling is dependent on primary cilia, we next examined whether cdKO embryos had normal primary cilia present on the

Figure 12. Analysis of ciliogenesis related genes in cdKO embryos.

A) Clustering analysis of RNA-seq data (z-score) for 151 genes that may be involved in cilia function was performed and heat maps of the top three clusters are shown. Red and blue arrows indicate genes that are significantly changed between control and cdKO and are analyzed further. B) A summary of components of specific cilia sub-complexes, with genes that decrease in the cdKO shown in blue and those that increase in orange. C) The relative expression (RNA-seq) of three RabGAPs and their associated Rabs is shown. D) Control and cdKO embryos were analyzed by qRT-PCR for five genes with significantly different expression by RNA-seq, and for *Rab23*. Relative expression compared to the control is shown. * : $p < 0.05$, ** : $p < 0.01$, *** : $p < 0.001$.

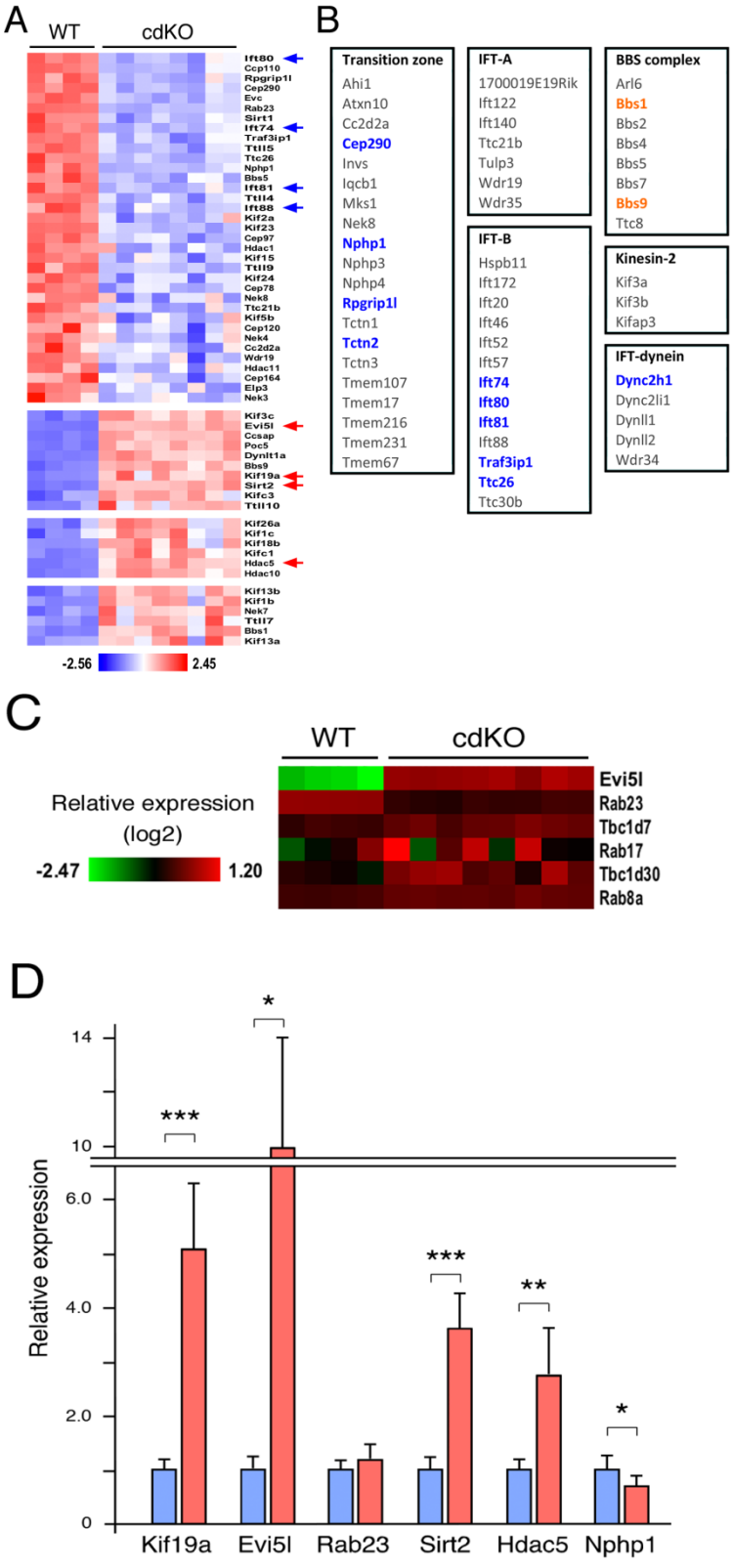
A
WT
cdKO
Ift80
Ccp110
Rpgrip1l
Cep290
Evc
Rab23
Sirt1
Ift74
Traf3ip1
Ttll5
Ttc26
Nphp1
Bbs5
Ift81
Ttll4
Ift88
Kif2a
Kif23
Cep97
Hdac1
Kif15
Ttll9
Kif24
Cep78
Nek8
Ttc21b
Kif5b
Cep120
Nek4
Cc2d2a
Wdr19
Kif11
Cep164
Elp3
Nek3
Kif3c
Evi5l
Ccsap
Poc5
Dynlt1a
Bbs9
Kif19a
Sirt2
Kifc3
Ttll10
Kif26a
Kif1c
Kif18b
Kifc1
Hdac5
Hdac10
Kif13b
Kif1b
Nek7
Ttll7
Bbs1
Kif13a
-2.56
2.45
B
Transition zone
Ahi1
Atxn10
Cc2d2a
Cep290
Invs
Iqcb1
Mks1
Nek8
Nphp1
Nphp3
Nphp4
Rpgrip1l
Tctn1
Tctn2
Tctn3
Tmem107
Tmem17
Tmem216
Tmem231
Tmem67
IFT-A
1700019E19Rik
Ift122
Ift140
Ttc21b
Tulp3
Wdr19
Wdr35
IFT-B
Hspb11
Ift172
Ift20
Ift46
Ift52
Ift57
Ift74
Ift80
Ift81
Ift88
Traf3ip1
Ttc26
Ttc30b
BBS complex
Arl6
Bbs1
Bbs2
Bbs4
Bbs5
Bbs7
Bbs9
Ttc8
Kinesin-2
Kif3a
Kif3b
Kifap3
IFT-dynein
Dync2h1
Dync2li1
Dynll1
Dynll2
Wdr34
C
WT
cdKO
Relative expression
(log2)
-2.47
1.20
Evi5l
Rab23
Tbc1d7
Rab17
Tbc1d30
Rab8a
D
Relative expression
14
10
6.0
4.0
2.0
0
***
*
***
**
*
Kif19a
Evi5l
Rab23
Sirt2
Hdac5
Nphp1

Figure 13. PNC cilia defects.

Whole mount confocal images of the PNC are shown, for a control (A) and two cdKO (B, C) embryos. Embryos were stained with phalloidin to visualize actin and an antibody against Arl13b to visualize cilia. Asterisks are placed to the upper left of the PNC in each low magnification merged image, and the white arrowhead indicates the end of the neural tube. Individual false-colored images (Actin: red, Ac-tubulin: cyan) and the overlaid images are shown with higher resolution images to the right. Ann Sutherland provided microscopy expertise.

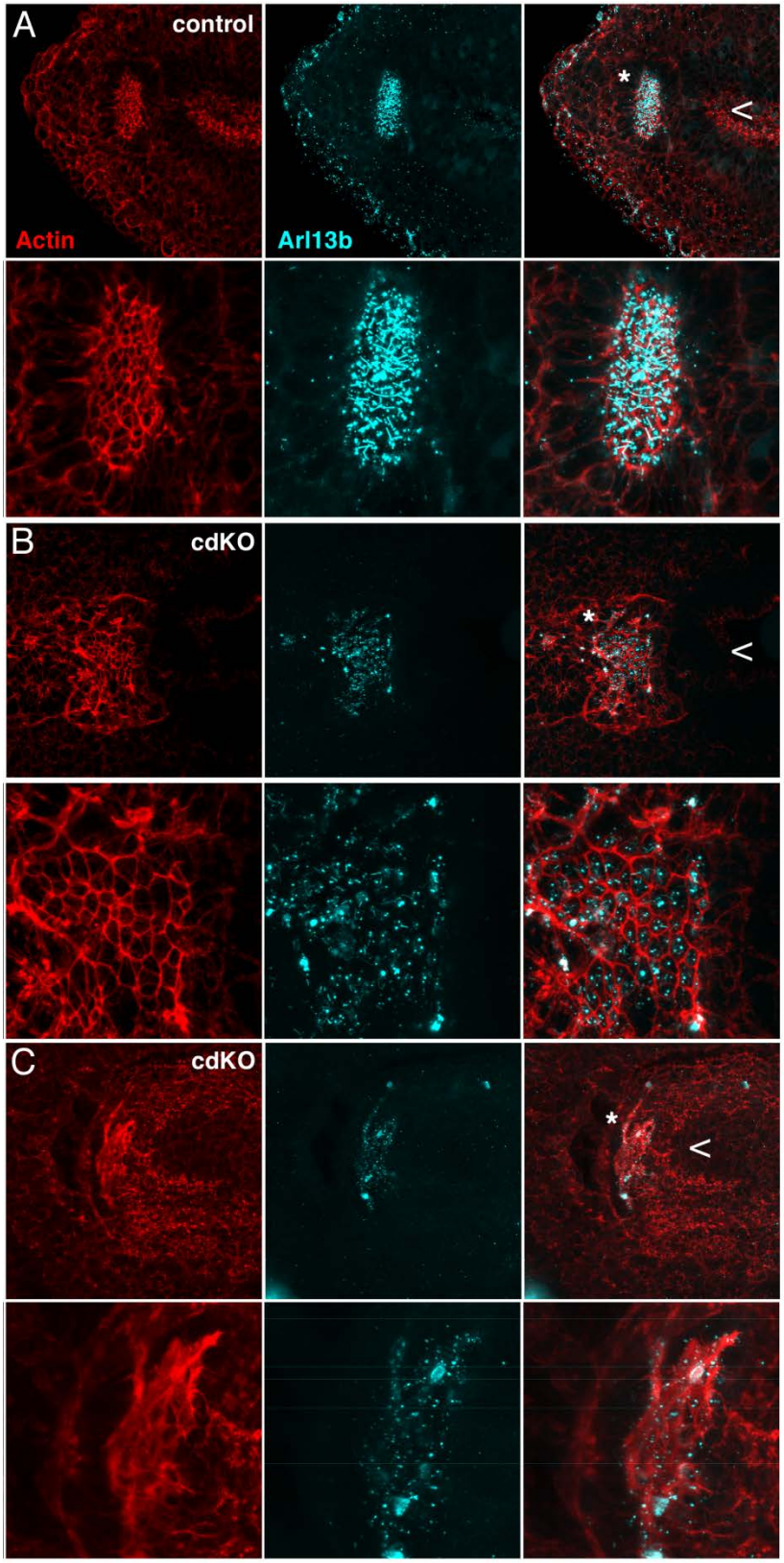
A
control
Actin
Arl13b
*
V
B
cdKO
*
V
C
cdKO
*
V

ventricular surface of the ventral forebrain. This region of the forebrain was surgically isolated from ~9.0 dpc embryos and stained with antibodies to Arl13b and pericentrin to identify primary cilia and the basal body, in addition to phalloidin for visualization of cell structure. Comparison of control and cdKO forebrain samples revealed that there was some overall disorganization of the forebrain neuroepithelium in the cdKO, as evidenced by the more diffuse phalloidin staining and irregular cell shape in the cdKO (Figure 14A and B). Although the majority of the forebrain neuroepithelial cells in the cdKO had primary cilia, we observed regions of the cdKO forebrain in which cilia numbers were decreased (Figure 14B-D). Additionally, when we stained sections of the forebrain for acetylated tubulin and total α-tubulin, it appeared that there was a decrease in the apical concentration of acetylated tubulin in the cdKO (Figure 14E and F). Thus it appears that in the forebrain, loss of Tgifs results in some disruption of neuroepithelial cell organization and may also limit cilia formation, although any ciliogenesis defect in the forebrain is much less severe than that observed in the PNC. This analysis, together with previous work showing defects in forebrain patterning and L-R asymmetry, suggests that embryos lacking *Tgif1* and *Tgif2* have widespread defects in neural tissue. The reduced cilia numbers may also suggest that changes in cilia related gene expression seen by RNA-seq may contribute to the embryonic phenotypes observed.

Primary MEFs lacking Tgifs have reduced cilia numbers

To better understand the more immediate effects of reducing Tgif function on primary cilia we transiently knocked down *TGIF1* and *TGIF2* in the human retinal pigment

Figure 14. Analysis of forebrain cilia.

A-D) Whole mount confocal images of the ventricular surface of the ventral forebrain are shown, stained for actin (phalloidin, white) and with antibodies against Arl13b and Pericentrin (false colored green and red respectively). Individual images and the three-color merge are shown for control (A) and cdKO (B). The cyan boxes are magnified in C and D for control and cdKO respectively, shown as three color merge and actin plus Arl13b only (white and green). E, F) Paraffin sections through the ventral forebrain were stained with antibodies for α-tubulin (red), acetylated tubulin (green) and DAPI (blue). The merged images and an overlay of acetylated tubulin and DAPI only are shown for control (E) and cdKO (F). Ann Sutherland helped with imaging.

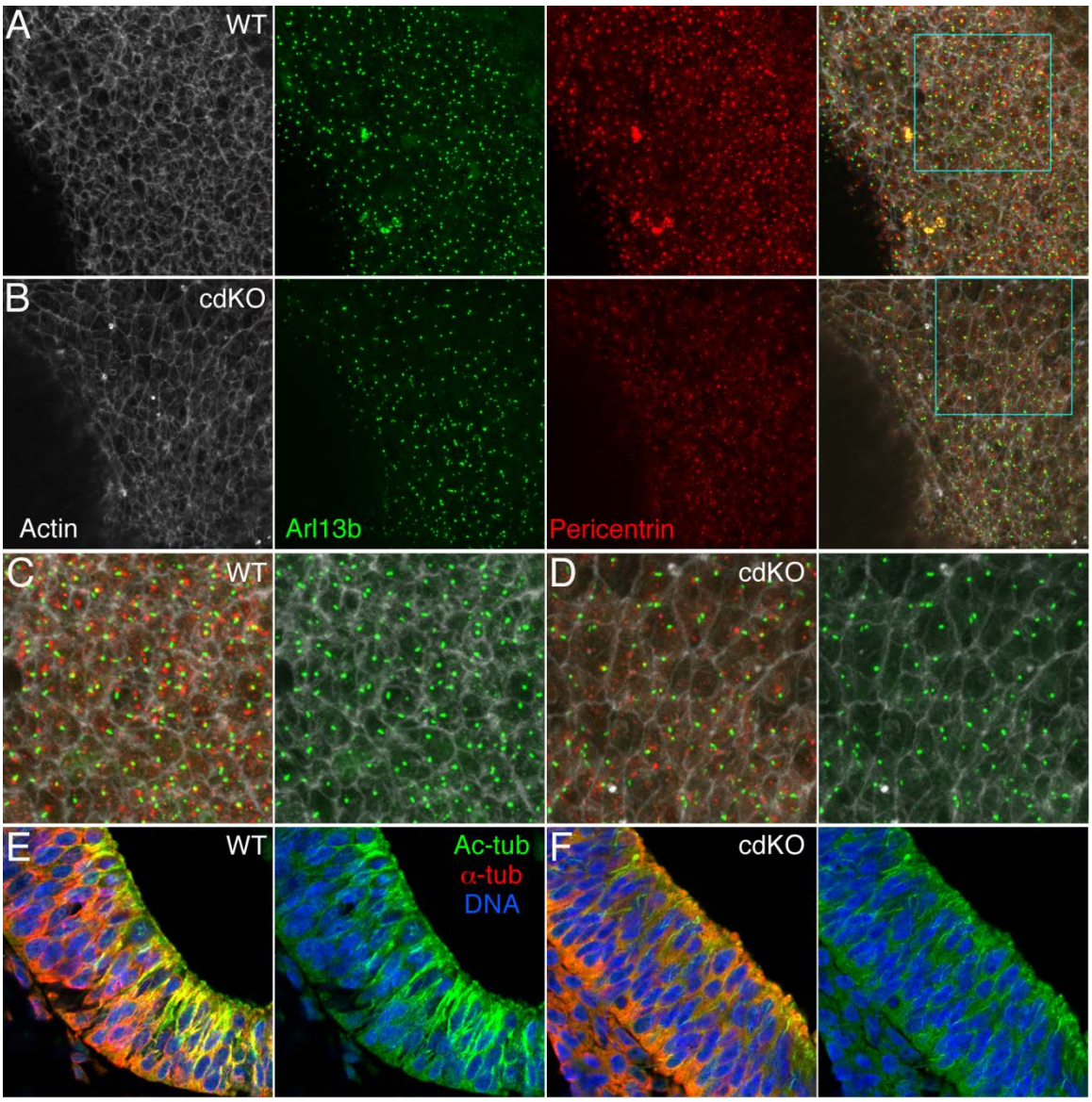
A
WT
B
cdKO
Actin
Arl13b
Pericentrin
C
WT
D
cdKO
E
WT
Ac-tub
α-tub
DNA
F
cdKO

epithelial cell line, ARPE19. As shown in Figure 15A, we achieved approximately 70% knock-down of both genes in cells transfected with siRNA pools against *TGIF1* and *TGIF2*. Analysis of these samples for expression of several of the genes previously shown to change in cdKO embryos revealed a significant increase in expression of *EVI5L* and *HDAC5* (Figure 15B). To determine whether reduced TGIF levels affected the number of cells with primary cilia, we starved control and knock-down cells for 72 hours, analyzed them by immunofluorescence microscopy for acetylated tubulin and pericentrin, and counted the proportion of cells with cilia. There were significantly fewer cells with primary cilia when both *TGIFs* were knocked down, suggesting that TGIFs may play a direct role in regulating ciliogenesis (Figure 15C). We also examined control and knock-down cells for cilia structure by confocal imaging of cells stained for acetylated tubulin and Ift46. This did not reveal any consistent changes in cilia length, shape or overall structure at this level of resolution (Figure 15D).

To generate a more amenable system to test potential effects of Tgifs on cilia we created cdKO primary MEFs (mouse embryonic fibroblasts). MEFs were isolated at 13.5 dpc from mice with a *Tgif2* null allele, loxP flanked *Tgif1* alleles and a Tamoxifen-inducible Cre transgene (*Tgif1*^{ff}*; Tgif2*$^{-/-}$*; CreER*$^{+}$). At passage 2, cells were treated with 1 µM 4-hydroxy-tamoxifen for 48 hours and then analyzed for gene expression after one more passage and one additional day in culture (see Figure 16A). For comparison, we used wild type MEFs that were passaged similarly. RNA was isolated three days after the initial tamoxifen treatment and analyzed for expression of *Tgif1* and *Tgif2*. As expected *Tgif2* was not detectable using primers to the deleted region, and *Tgif1* expression was

Figure 15. Analysis of TGIFs in ARPE19 cells.

A) *TGIF1* and *TGIF2* were transiently knocked down in ARPE19 cells, and expression levels were tested by qRT-PCR 48 hours after knock-down. B) Expression of a panel of cilia related genes was tested by qRT-PCR in ARPE19 with and without TGIF1/2 knock-down. Relative expression compared to the control is shown. * : $p < 0.05$, *** : $p < 0.001$. C) 48 hours after knock-down, ARPE cells were transferred to media without serum for 72 hours and cilia numbers counted after staining for acetylated tubulin. % of cells with cilia is shown (mean + s.d. for four replicates). * : $p < 0.05$. D) representative images of cilia in control and *TGIF1/2* knock-down cells are shown, stained for acetylated tubulin (red), Ift46 (green) and for DNA with DAPI (blue). Larger images of individual cilia are shown below as the three-color overlay; individual red and green channels and red and green together.

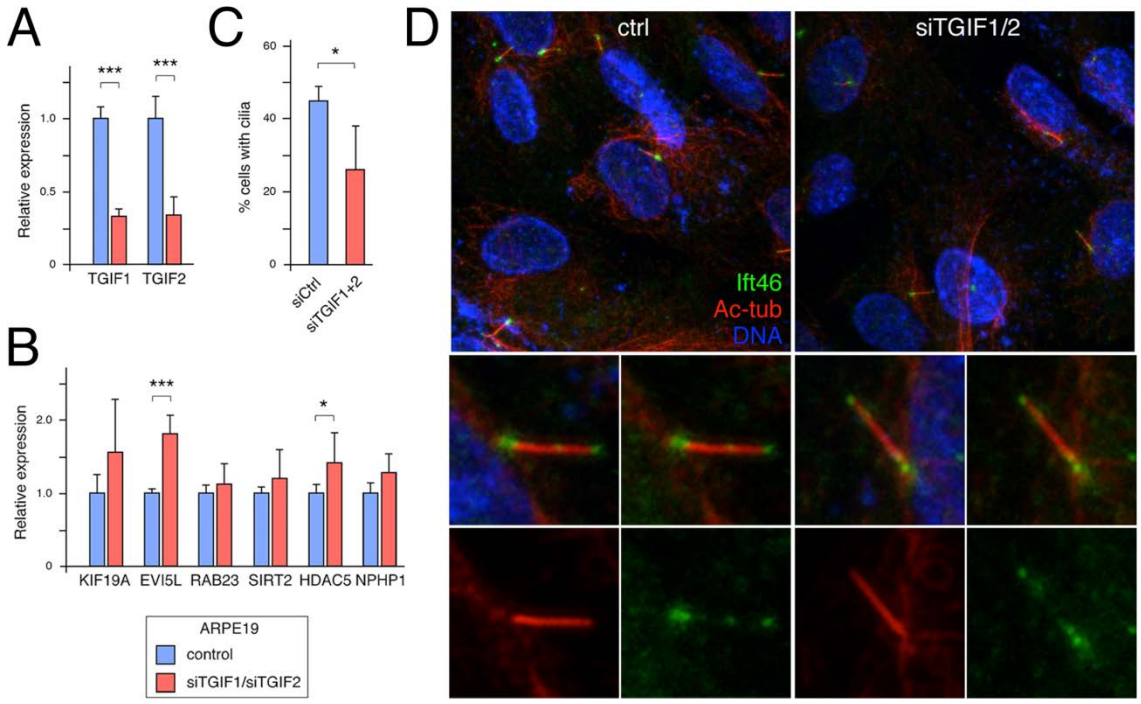
A
Relative expression
1.0
0.5
0
***
***
TGIF1
TGIF2
C
% cells with cilia
60
40
20
0
*
siCtrl
siTGIF1+2
B
Relative expression
2.0
1.0
0
***
*
KIF19A
EVI5L
RAB23
SIRT2
HDAC5
NPHP1
ARPE19
control
siTGIF1/siTGIF2
D
ctrl
siTGIF1/2
Ift46
Ac-tub
DNA

less than 1% of that seen in the wild type cells after tamoxifen treatment, confirming efficient Cre-mediated deletion (Figure 16B). Since *Tgif1* null MEFs had a decreased proliferation rate compared to wild type (188) we also analyzed wild type and cdKO MEFs for Ki-67 labeling three days after the initial tamoxifen treatment. There was a significant decrease in Ki-67 positive cells in the cdKO, further suggesting that the deletion of *Tgif1* in the background of a *Tgif2* null mutation had functional consequences in primary MEFs (Figure 16C).

We next tested expression of a panel of genes that were either present in the overlap between our RNA-seq data and our expression array analysis of *Tgif1* null MEFs or that we had previously analyzed in *Tgif1* null MEFs. As shown in Figure 16D, we observed significant changes by qRT-PCR that were consistent with those seen by RNA-seq and/or Affymetrix array analysis. To examine changes in potential ciliogenesis genes, we tested expression of *Evi5l* and several other candidate genes by qRT-PCR. Given the cilia defects in cdKO embryos, we primarily focused on genes that might be expected to result in fewer cilia when over-expressed. In cdKO MEFs, *Evi5l, Kif19a*, *Sirt2* and *Hdac5* expression increased significantly, further verifying them as potential Tgif1 target genes (Figure 16E). No significant changes were seen in the three *Ift* genes tested; however, it should be noted that very few of these cells generate cilia when grown in high serum.

To test effects of Tgifs on cilia in MEFs, we maintained wild type and cdKO MEFs (after tamoxifen treatment) in media lacking serum to induce cilia formation and then examined cilia by immunofluorescence microscopy with antibodies that detected

Figure 16. Analysis of gene expression in cdKO MEFs.

A) The time-course of generating cdKO MEFs and when they were analyzed is shown. 'T' indicates when tamoxifen was added to activate the Cre transgene. B) Expression of *Tgif1* and *Tgif2* was analyzed by qRT-PCR in control and cdKO embryos after tamoxifen treatment. C) Proliferation in wild type and cdKO MEFs was analyzed by staining for Ki-67. % positive cells is shown (mean + s.d. for four replicates). D) Expression of a selection of genes (primarily from the overlap between the cdKO MEFs and cdKO embryo RNA-seq) was analyzed by qRT-PCR in wild type and cdKO MEFs. E) Analysis of cilia related gene expression by qRT-PCR in wild type and cdKO MEFs. The relative expression based on embryo RNA-seq is shown above in gray for comparison. * : $p < 0.05$, ** : $p < 0.01$, *** : $p < 0.001$.

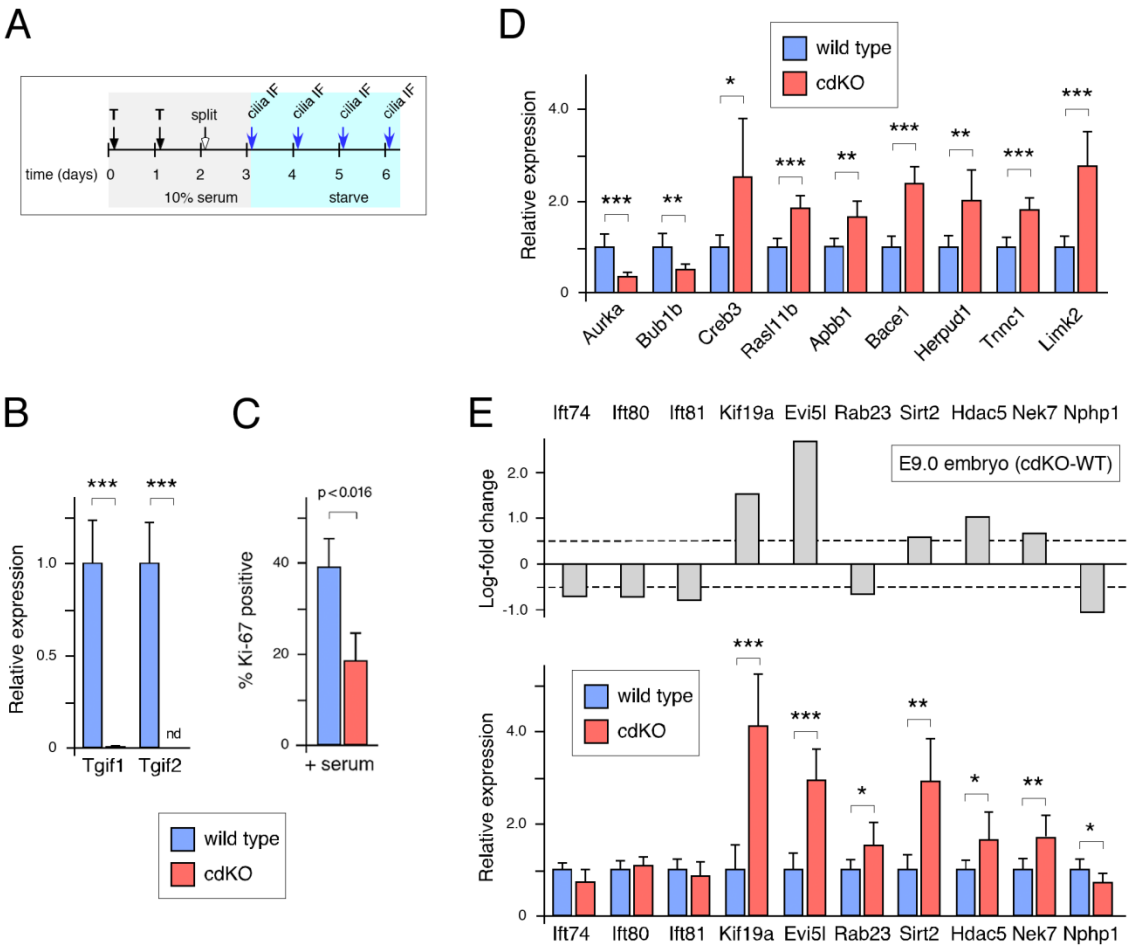
A
T
T
split
cilia IF
cilia IF
cilia IF
cilia IF
time (days) 0 1 2 3 4 5 6
10% serum
starve
B
Relative expression
***
***
1.0
0.5
0
Tgif1
Tgif2
nd
C
% Ki-67 positive
p<0.016
40
20
0
+ serum
wild type
cdKO
D
wild type
cdKO
Relative expression
4.0
2.0
0
*
***
**
***
**
***
**
***
Aurka
Bub1b
Creb3
Rasl11b
Apbb1
Bace1
Herpud1
Tnnc1
Limk2
E
Ift74 Ift80 Ift81 Kif19a Evi5l Rab23 Sirt2 Hdac5 Nek7 Nphp1
E9.0 embryo (cdKO-WT)
Log-fold change
2.0
1.0
0
-1.0
wild type
cdKO
Relative expression
4.0
2.0
0
***
***
*
**
*
**
*
Ift74 Ift80 Ift81 Kif19a Evi5l Rab23 Sirt2 Hdac5 Nek7 Nphp1

acetylated tubulin and either pericentrin or Ift46. Cilia were present in both wild type and cdKO MEFs and did not appear to be structurally different between the two genotypes at this resolution (Figure 17A, B). We next counted the proportion of cells with cilia when maintained in 10% serum, or after 24-72 hours in starvation media. At all time-points analyzed, we observed a significant decrease in the proportion of cdKO MEFs with cilia compared to the wild type controls (Figure 17C). The fraction of cells with cilia was relatively constant after 24 hours in starvation media, although the length of cilia increased somewhat over time (Figure 17C and data not shown). Loss of Tgifs had little effect on cilia length, but clearly decreased the overall proportion of cells that had cilia.

Due to significant upregulation of *Evi5l* in the RNA-seq and changes in *Evi5l* expression in MEFs, ARPE-19 cells and embryos, we first focused on manipulating *Evi5l* expression in an effort to rescue the cilia defect seen in MEFs. We analyzed wild type and cdKO MEFs by western blot to show that change in *Evi5l* gene expression translated to a change in protein levels. Expression of Evi5l was clearly higher in the cdKO MEFs than the wild type control (Figure 17D). To test if the increased *Evi5l* expression seen in cdKO MEFs contributed to the decrease in cilia numbers, we transiently knocked down *Evi5l* in cdKO MEFs prior to starvation. As shown in Figure 17E, Evi5l protein levels were reduced by siRNA knock-down in MEFs, and we did not see any change in expression of a panel of other cilia related genes after *Evi5l* knock-down (data not shown). We next counted the proportion of cdKO MEFs with cilia after 48 hours in serum free media following transfection with control or Evi5l siRNA. As shown in

Figure 17E, reducing *Evi5l* levels in cdKO MEFs resulted in increased cilia numbers, consistent with the idea that excess Evi5l in the cdKO MEFs may limit ciliogenesis.

Evi5l is a direct TGIF target gene

Tgif1 and Tgif2 are transcriptional corepressors for TGFß activated Smads, and have been shown to limit TGFß-responsive gene expression in primary MEFs and to regulate Nodal-dependent phenotypes in early mouse embryos (90,188). However, Tgifs can also bind directly to DNA and interact with some nuclear receptors, allowing for transcriptional regulation independent of TGFß signaling (75,76). To test whether TGFß signaling affected cilia formation in primary MEFs, we starved cells for 24 hours and then added back serum, TGFß, or both and counted cilia by immunofluorescence microscopy 24 hours later. TGFß addition had no effect on the number of ciliated cells but clearly reduced proliferation, as measured by the proportion of Ki-67 positive cells (Figure 18A). Experiments in ARPE19 cells yielded similar results, although the reduction in Ki-67 labeling with TGFß addition was less dramatic. Treating MEFs with TGFß resulted in induction of expression of *Smad7* and *Serpine1*, two well-characterized TGFß-responsive genes, whereas we observed no change in *Evi5l* expression in Figure 18B. Similar results were observed in ARPE19 cells treated with TGFß, although the induction of *SMAD7* and *SERPINE1* in ARPE19 cells was less than that seen in MEFs. Taken together, these data suggest that changes in cilia numbers and *Evi5l* expression upon knock-down or deletion of Tgifs cannot be mimicked by increased TGFß signaling.

Figure 17. Analysis of cilia and Evi5l in MEFs.

Wild type and cdKO MEFs were analyzed by immunofluorescence microscopy with antibodies against acetylated tubulin and Pericentrin (A) or acetylated tubulin and Ift46 (B). Confocal images of representative cilia are shown for each. C) Wild type and cdKO MEFs were incubated in regular medium (+serum) or starved for 24-72 hours, then analyzed for cilia numbers by staining for acetylated tubulin and pericentrin. The % of cells with cilia is shown (mean +s.d. of quadruplicates), together with p-values for the comparison of wild type to cdKO. D) Evi5l expression was analyzed by western blot in wild type and cdKO MEFs. Tgif1 and tubulin are shown as controls. E) *Evi5l* was transiently knocked down in cdKO MEFs and expression of Evi5l was analyzed by western blot (left). Cilia numbers were analyzed in cdKO MEFs with control or *Evi5l* knock-down. % of cells with cilia is shown (mean +s.d. of quadruplicates), with p-value for the comparison of control to si*Evi5l*.

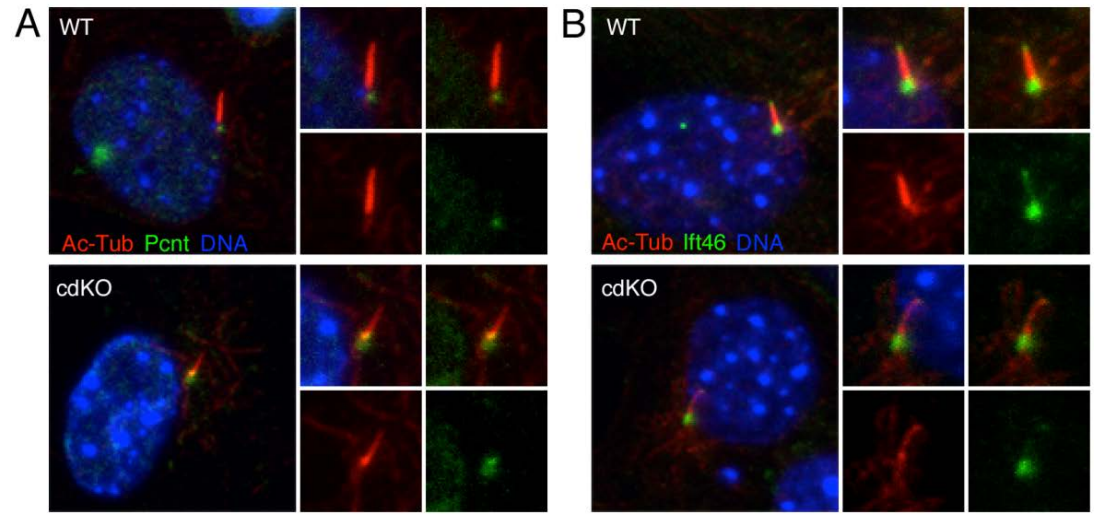
A
WT
Ac-Tub Pcnt DNA
cdKO
B
WT
Ac-Tub Ift46 DNA
cdKO

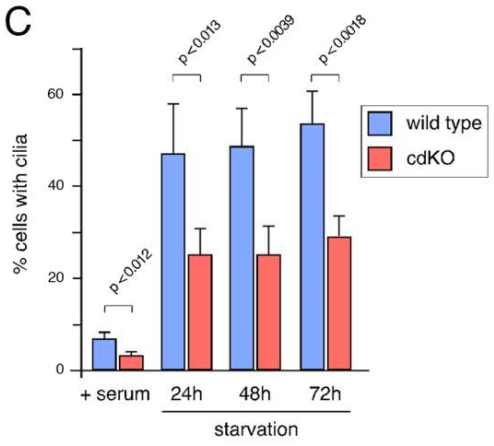
C
% cells with cilia
60
40
20
0
p<0.012
p<0.013
p<0.0039
p<0.0018
wild type
cdKO
+ serum
24h
48h
72h
starvation

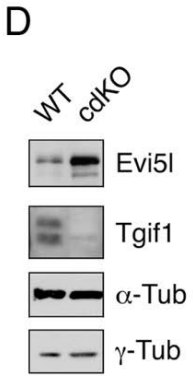
D
WT
cdKO
Evi5l
Tgif1
α-Tub
γ-Tub

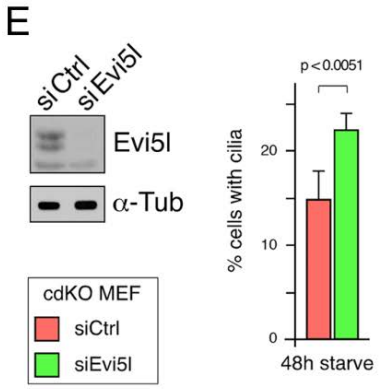
E
siCtrl
siEvi5l
Evi5l
α-Tub
cdKO MEF
siCtrl
siEvi5l
p<0.0051
% cells with cilia
20
10
0
48h starve

Since *Evi5l* expression did not appear to respond to TGFß, we considered the possibility that Tgifs might bind directly to *Evi5l* regulatory elements to limit its expression. We first scanned the human *EVI5L* gene for regions with peaks of H3K27Ac ChIP-seq signal from the ENCODE data using the UCSC genome browser (GRC37/hg19, 2009 assembly; http://genome.ucsc.edu/ENCODE/). We chose the human genome over mouse since the ENCODE project contains more information on the human genome, and we focused on H3K27Ac, as this histone mark is generally associated with transcriptionally active regulatory elements. This search identified four broad regions within or flanking the *EVI5L* gene with high H3K27Ac signal. We then scanned sequences in these regions that were conserved between human and mouse for consensus TGIF binding sites (CTGTCAA) (75). As shown in Figure 18C, a single conserved TGIF consensus site was identified within a highly conserved region overlapping the 5'-most transcriptional start sites of *EVI5L*, adjacent to a H3K27Ac peak.

To test whether Tgif1 could bind to this region in MEFs, we performed chromatin immunoprecipitation (ChIP) with a TGIF1-specific antiserum or with the pre-immune serum as a control. The *Evi5l* 5' region was clearly enriched in Tgif1 immunoprecipitates from wild type MEFs, but not from the cdKO MEFs (Figure 18D). We observed no Tgif1 binding to two intronic regions from the *Gli3* gene, supporting the specificity of this binding. Similar results were obtained in ARPE19 cells, with clear enrichment of the *EVI5L* 5' region and no binding to a control region from 5' to the *CDKN2B* gene (Figure 18D). To test whether this region could indeed respond to TGIF1, we amplified a 471bp region surrounding the putative TGIF site from mouse *Evi5l* and generated a luciferase

reporter in which this sequence was placed upstream of a minimal TATA element. We first tested the pEvi5l-TATA-luc vector in A549 lung carcinoma cells, as these respond well to transfected TGIF1 and to TGFß. As shown in Figure 18E, the pEvi5l-TATA-luc was over 5-fold more active than the parental TATA-luc, and its activity was significantly repressed by coexpression of TGIF1. As with the endogenous *Evi5l* gene, we did not observe any response of the luciferase reporter to TGFß signaling, consistent with a TGFß-independent effect of TGIFs (Figure 18E). When TGIF1 was co-expressed with the pEvi5l-TATA-luc reporter in ARPE19 cells, we again observed strong repression by TGIF1 with no effect of TGIF1 on the basic TATA-luc reporter (Figure 18F). Taken together, these data suggest that the *EVI5L* gene is a conserved TGIF target gene that is repressed by direct binding of TGIF1 to a consensus element in the proximal promoter.

Figure 18. Evi5l is a direct Tgif target gene.

A) Wild type MEFs or ARPE19 cells were starved and then treated with serum, TGFß, or both, and effects on cilia numbers and proliferation were analyzed. B) Expression of *Evi5l* and two known TGFß target genes was analyzed in MEFs and ARPE19 cells. Data is plotted as fold induction relative to untreated. C) A screenshot from the UCSC browser with the region of human chromosome 19 surrounding the transcriptional start of the *EVI5L* gene is shown. The gene prediction is shown in blue, composite RNA expression in rainbow, and composite H3K27Ac ChIP-seq data in purple. The lower two tracks show vertebrate conservation (blue) and mouse-human identity in green. The vertical red bar indicates the position of the conserved element shown below, in which the conserved TGIF consensus site is boxed in red. Colons show identity to human, dashes indicate deletions and differences from human are shown. D) Binding of TGIF1 to the EVI5L upstream region was analyzed by ChIP-qPCR in primary wild type and cdKO MEFs and in ARPE19 cells. Relative binding compared to pre-immune serum is shown, together with negative control regions. * : $p < 0.01$, ** : $p < 0.001$. E and F) The activity of the mouse *Evi5l* upstream region (cloned upstream of a minimal TATA element) was analyzed by transient transfection and luciferase assay. Activity is shown for the Evi5l reporter and the parental TATA-luc, with increasing TGIF1 co-expression in A549 (E) and ARPE19 cells (F). The right hand panel in E shows the effects of activating TGFß signaling on the Evi5l reporter or a positive control TGFß responsive reporter in A549 cells. Data are shown as mean (+ s.d.) relative activity of triplicates in arbitrary units. * : $p < 0.01$. Tiffany Melhuish assisted with ChIP-qPCR.

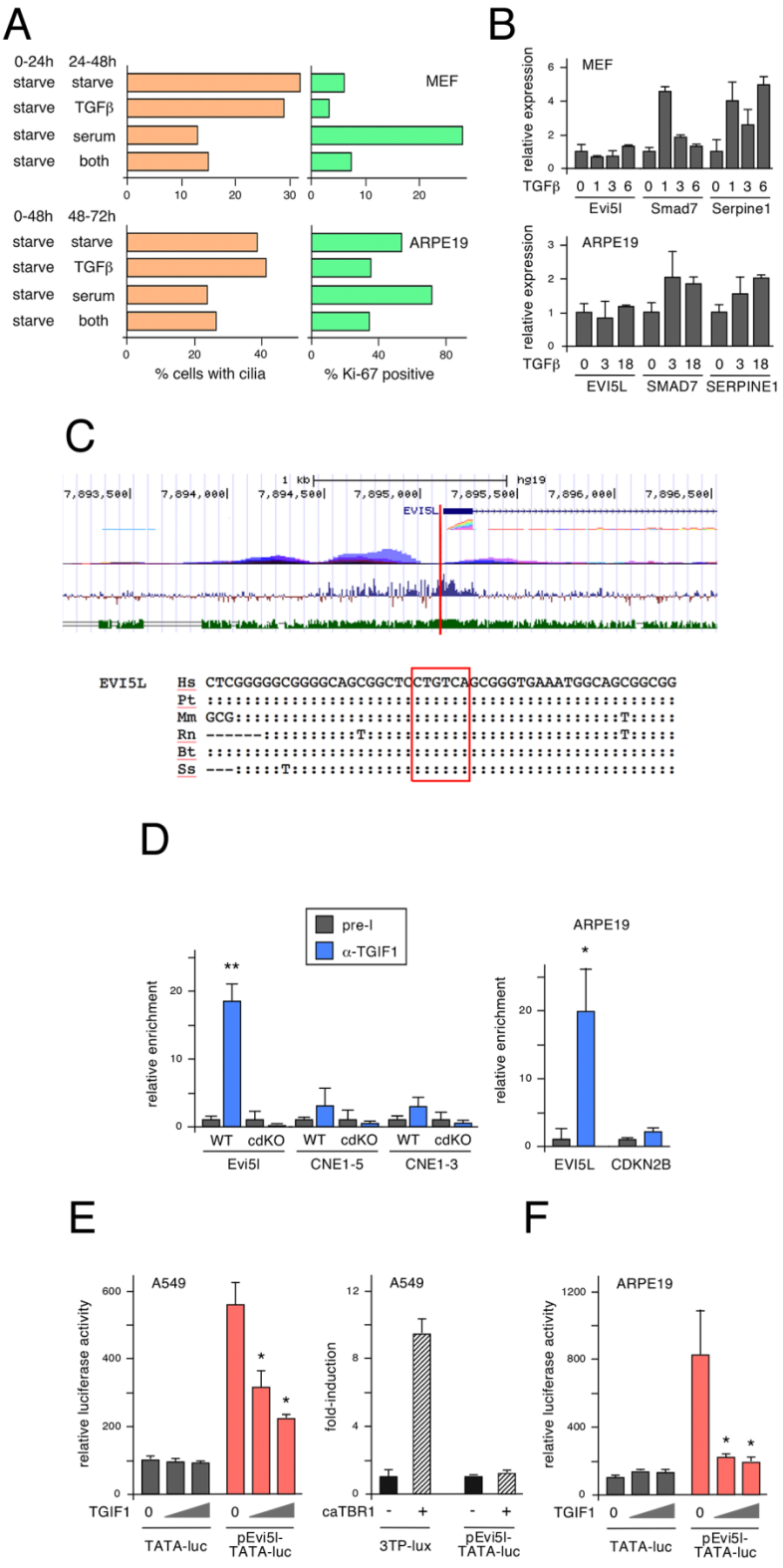
A
0-24h 24-48h
starve starve
starve TGFβ
starve serum
starve both
MEF
0-48h 48-72h
starve starve
starve TGFβ
starve serum
starve both
ARPE19
% cells with cilia
% Ki-67 positive
B
MEF
relative expression
TGFβ 0 1 3 6 0 1 3 6 0 1 3 6
Evi5l Smad7 Serpine1
ARPE19
relative expression
TGFβ 0 3 18 0 3 18 0 3 18
EVI5L SMAD7 SERPINE1
C
1 kb hg19
7,893,500 7,894,000 7,894,500 7,895,000 7,895,500 7,896,000 7,896,500
EVI5L
EVI5L Hs CTCGGGGGCGGGGCAGCGGCTCCTGTCAGCGGGTGAAATGGCAGCGGCGG
Pt
Mm GCG:::T:::::
Rn ------:::::::::T:::::::::::::::::::::::::::T:::::
Bt
Ss ---:::::T:::::::::::::::::::::::::::::::::::::
D
pre-I
α-TGIF1
relative enrichment
WT cdKO WT cdKO WT cdKO
Evi5l CNE1-5 CNE1-3
ARPE19
relative enrichment
EVI5L CDKN2B
E
A549
relative luciferase activity
TGIF1 0 0
TATA-luc pEvi5l-TATA-luc
A549
fold-induction
caTBR1 - + - +
3TP-lux pEvi5l-TATA-luc
F
ARPE19
relative luciferase activity
TGIF1 0 0
TATA-luc pEvi5l-TATA-luc

Discussion

Here we show that Tgifs directly repress expression of the *Evi5l* gene by binding a conserved Tgif consensus site in the region immediately upstream of the gene. In the absence of Tgif function, *Evi5l* is over-expressed and cilia numbers are reduced. While the effects of reduced Tgif levels on ciliogenesis are likely to be dependent on a combination of factors, we show that excess *Evi5l* expression contributes to the decreased numbers of ciliated cells.

Transcriptome profiling of whole embryos identified a large number of genes that are differentially expressed between control embryos and those lacking Tgif function. The majority (70%) of genes that were considered differentially expressed showed higher expression in the mutant embryos than in the control embryos, consistent with the function of Tgifs as transcriptional repressors. Of the four over-expressed genes with potential links to ciliogenesis analyzed here, we identified conserved Tgif consensus sites in two of them (*Evi5l* and *Hdac5*). By multiple assays, we confirmed that *Evi5l* is indeed a Tgif target gene, with Tgif1 binding to a conserved consensus site 5' to the transcriptional start site. To identify putative Tgif sites, we focused on the body of the gene and the 5kb upstream of the start site, and searched close to peaks of H3K27Ac signal from human ENCODE data. It is possible some potential sites were missed in our initial analysis, and a more comprehensive analysis may be necessary to identify both putative Tgif sites and other enriched motifs associated with these genes. In addition, a more rigorous analysis to distinguish direct targets from indirect targets may be required.

Gene Ontology analysis of the genes with altered expression in cdKO embryos compared to control revealed an enrichment for genes involved in patterning and DNA metabolism among the genes with lower expression in the cdKO. This is consistent with the overall patterning defects and reduced proliferation seen in cdKO embryos, and with decreased proliferation observed in cdKO MEFs (91,188). The most enriched categories among the genes with higher expression in the cdKO included extracellular matrix and cytoskeleton, which is perhaps consistent with the observed disorganization of the PNC and of the neuroepithelium in cdKO embryos. However, GO term analysis revealed relatively few enriched categories in these gene lists, possibly due to the fact that the cdKO embryos have multiple defects and that we isolated RNA from whole embryos, rather than an isolated tissue or single cell type. Comparing the data with gene expression analysis from *Tgif1* null MEFs also revealed a relatively small set of overlapping changes, likely in part due to the difference between whole embryo and primary cultured MEFs (which were null only for *Tgif1*), and also possibly due to the different platforms used for these analyses (RNA-seq versus expression arrays). The majority of the genes that changed in both analyses were either increased or decreased in both, as would be expected, and this has allowed us to focus on what may be a higher confidence set of potential Tgif targets.

Our previous work has identified phenotypes in cdKO embryos that could be secondary to defects in cilia. L-R asymmetry determination requires the appropriate regulation of the Nodal signaling pathway, both at the PNC and in the lateral plate mesoderm (LPM), and is also dependent on the structure of the PNC and the presence of

primary cilia. It is thought that the pit shape of the PNC combined with the concerted rotation of the motile cilia drives directional fluid flow across the PNC and initiates the left-specific expression of *Nodal* in the LPM. Mutations that prevent ciliogenesis at the PNC or that result in non-motile cilia cause L-R asymmetry defects. We have previously shown that cdKO embryos have L-R asymmetry defects, and here we show that the PNC of cdKO embryos is somewhat disorganized or misshapen, but still retains an approximate pit-like shape. However, there is a clear reduction in the number of PNC pit cells that have cilia. Since we also observed effects of Tgif loss or reduction on cilia numbers in the ventral forebrain, primary MEFs, and retinal pigment epithelial cells, it is possible that Tgifs play a general role in regulating cilia; additionally, the L-R asymmetry defects in cdKO embryos are due, at least in part, to a lack of motile PNC cilia. However, it should be noted that we observed relatively minor effects on cilia in the forebrain of cdKO embryos, suggesting that the outcome of Tgif loss of function may not always result in disruption of cilia.

Reducing the dose of Nodal by introducing a heterozygous Nodal mutation into cdKO embryos resulted in a partial rescue of the L-R defects. The bi-lateral *Pitx2* expression observed in the cdKO LPM reverted to expression only on one side, suggesting that the defect may be partly Nodal dependent. However, the sidedness of *Pitx2* expression was random, rather than left LPM specific as in the control. It, therefore, remains possible that PNC defects, such as those seen here, are present in *Nodal* heterozygous cdKO embryos such that the initial choice of left or right sided expression of Nodal and its downstream targets is not made. The lack of bi-lateral *Pitx2* might then

simply be due to reduced *Nodal* expression in the LPM, resulting in lower activation of *Pitx2*, giving expression on one side or the other. Here we show that *Evi5l* is a direct target of Tgifs and does not respond to TGFß within in the cell lines tested and we have not observed any effects of adding TGFß on cilia formation in these cell lines. This is in agreement with previous work which suggests that TGFß was not able to drive cilia disassembly (134). Thus, the defects in L-R asymmetry and PNC cilia in cdKO embryos may be at least partly Nodal independent.

Even in cdKO MEFs where we observed a significant decrease there was not a complete loss of ciliated cells. This is similar to the incomplete loss of ciliated cells seen with *EVI5L* overexpression in ARPE19 cells.

Several Tgif target genes that are involved in ciliogenesis were identified, such as *Hdac5*, *Sirt2* and *Kif19*. None of these genes were as striking as *Evi5l* in all the experimental systems used here. Given that overexpression of *EVI5L* was shown to decrease cilia numbers (140), this remains our best candidate. The cognate GAP for EVI5L has been identified as Rab23 (140), although relatively little is known about the functions of Evi5l, and it remains possible that it performs other functions than regulating Rab23 and ciliogenesis. Interestingly, Rab23 has been shown to regulate the localization of Shh pathway components to the primary cilium (139,202). We do not know whether this process is defective in our cdKO embryos, although it would be tempting to speculate that this may provide a possible explanation of the defects in *Shh* expression in the forebrain. Rab23 has also been shown to play a role in L-R patterning in both mouse and zebrafish (203), although it is not known whether this depends on Evi5l. However,

Rab23 null mouse embryos did not lack cilia at the PNC, and it appears that Rab23 may regulate Nodal signaling during L-R patterning independent of direct effects on PNC cilia. Thus it is possible that the L-R defects seen in cdKO embryos are not entirely dependent on changes in *Evi5l* expression or on Evi5l effects via Rab23. However, taken together, our data clearly suggest that Tgifs play some role in regulating ciliogenesis, and indicate that Evi5l may be one of the major mediators of this effect downstream of Tgifs. In summary, we have shown that Tgifs regulate primary cilium formation and that this function may be in part at least mediated via direct transcriptional repression of the *Evi5l* gene.

Materials and Methods

Ethics statement

All animal procedures were approved by the Animal Care and Use Committee of the University of Virginia, which is fully accredited by the AAALAC.

Mice and DNA analysis

The *loxP*-flanked *Tgif* allele (86) and *Tgif2 null* (90) alleles are as described. The *Sox2-Cre* line (118) was obtained from Jax (# 4783). All mouse lines were maintained on a mixed C57BL/6J x 129Sv/J background. The cdKO MEFs were generated from $Tgif1^{f/f};Tgif2^{-/-}$ mice with a Tamoxifen inducible Cre transgene (Jax; # 4847). Genomic DNA for PCR genotype analysis was purified from ear punch, at post-natal day 21 (P21), or yolk sac (7.0-10.0 dpc), by HotShot (183).

Cell culture and luciferase assays

Primary MEFs were isolated from 13.5 day mouse embryos, and cultured in DMEM (Invitrogen) with 10% Fetal Bovine Serum (Hyclone) as described. To generate cdKO MEFs cells were transfected using Turbofect (Fisher) according to the manufacturer's instructions. Cells were transfected with firefly luciferase reporters, a Renilla transfection control (phCMVRLuc; Promega), and the indicated constructs. After 48 hours firefly luciferase activity was assayed using firefly substrate (Biotium) and Renilla luciferase was assayed with 0.09μM coelenterazine (Biosynth), using a Berthold LB953

luminometer. Luciferase constructs were generated in a modified version of pGL3 basic (Promega), containing the TATA element from the Adenovirus major late promoter.

RNA-seq

RNA was isolated and purified using Absolutely RNA kit (Agilent), and quality checked by Bioanalyzer. Poly-A RNA-seq libraries were generated at HudsonAlpha with Illumina barcodes and sequenced (Illumina HiSeq) to a target depth of ~ 25M paired end 50bp reads per sample. This resulted in 17-21M mapped reads per sample. RNA-seq raw counts (number of reads mapping to gene regions) were normalized. Genes with less than 10 reads after normalizing by library depth were removed from analysis. Count data was then analyzed with a method based on the negative binomial distribution, with variance and mean linked by local regression, using the DESeq R/Bioconductor package (204). Adjusted P-values were calculated using the Benjamini & Hochberg False Discovery Rate. A cut-off of +/- 0.5 log2 and an adjusted P-value of < 0.0001 were considered significant. qRT-PCR verification of gene expression differences identified by RNA-seq was performed on RNA from an independent set of WT and cdKO embryos isolated at the same stage. GO Term analysis was performed using DAVID (https://david.ncifcrf.gov/) (205,206) and heat maps were generated using AutoSOME (207).

RNA analysis by qRT-PCR

RNA was isolated and purified using Absolutely RNA kit (Stratagene). cDNA was generated using Superscript III (Invitrogen), and analyzed in triplicate by real time PCR using a BioRad MyIQ cycler and Sensimix Plus SYBRgreen plus FITC mix (Bioline), with intron spanning primer pairs, selected using Primer3 (http://frodo.wi.mit.edu/). Expression was normalized to Rpl4 and Actin using the delta Ct method, and is shown as mean plus standard deviation of triplicates. For knock-down, cells were plated in 6-well plates and transfected with Dharmacon SMARTpool oligonucleotides against human *TGIF1* and *TGIF2*, or mouse *Tgif1* and *Tgif2*, using DharmaFECT reagent 1. The control pool (siGENOME Non-targeting siRNA pool #3) was used for the non-targeting control.

Histology and immunofluorescence (IF)

Embryos were fixed in 4% paraformaldehyde overnight, dehydrated through an ethanol series (70%, 90%, 95%, 100% twice; 30 minutes each and overnight for second 100% ethanol incubation), incubated in xylene twice, for 30 minutes each, transitioned into xylene/paraffin wax (1:1) at 65° for an hour and embedded in paraffin wax. Blocks were sectioned in 7μm increments. For tissue section IF, sections were dewaxed with xylene and rehydrated through an ethanol series into PBS (100%, 95%, 90%, 70%, distilled water three times, PBS; 5 minutes each). Slides were gently boiled for 10 minutes in 10% Sodium Citrate, pH6.0 for antigen retrieval, allowed to cool to room temperature for half an hour, washed twice with PBS, and then blocked in M.O.M. Mouse Ig Blocking Reagent (Vector Laboratories) for one hour at room temperature. Sections were

incubated with mouse monoclonal acetylated tubulin (1:400, Sigma T6793) and rabbit monoclonal alpha tubulin (1:400, Abcam ab52866), Alexafluor 488-labeled goat-anti-mouse (1:500, Invitrogen), Alexafluor 594-labeled goat-anti-rabbit (1:500, Invitrogen), and Hoechst 33342 (1:1000, Sigma). Images were captured using a Nikon Eclipse TS100 microscope and Nikon DS-Qi1Mc or Nikon DS-Ri1 camera and manipulated in Adobe Photoshop. For whole embryo IF, embryos were dissected at 8.0-8.5 dpc for PNC and 9.25-9.75 dpc for forebrain. Embryos were fixed in 4% paraformaldehyde for half an hour, then permeabilized in 0.3% Triton X-100 in PBS for 30 minutes and blocked for 1 hour as described (208). The forebrain was dissected by removing the head of the embryo and removing the top and sides of the forebrain vesicle without damaging the ventral forebrain lumen. Embryos were incubated in mouse monoclonal ARL13B (1:400, Abcam ab136648), rabbit polyclonal pericentrin (1:400, Abcam ab4448), rhodamine phalloidin (1:400, Invitrogen R415), Alexafluor 488-labeled goat-anti-mouse (1:500, Invitrogen), Alexafluor 594-labeled goat-anti-rabbit (1:500, Invitrogen). Images were captured using a Leica SP5 X imaging system coupled to a DMI6000 epifluorescence microscope using a white light laser and manipulated in ImageJ and Adobe Photoshop. For cilia IF, cells (ARPE19 or MEFs) were plated in chamber slides. Cells were washed for 1 minute with PHEM buffer and then fixed in 4% paraformaldehyde in PHEM for 15 minutes. Cells were permeabilized in 0.25% Triton X-100 in BPS for 20 minutes and blocked in 10% NGS, 0.25% TritonX-100 in PBS for 1 hour. Cells were incubated in mouse monoclonal acetylated tubulin (1:400, Sigma T6793), rabbit polyclonal pericentrin (1:400, Abcam ab4448) or rabbit polyclonal IFT46 (1:100, Abcam ab122422), Alexafluor 488-labeled

goat-anti-rabbit (1:500, Invitrogen), Alexafluor 594-labeled goat-anti-mouse (1:500, Invitrogen), and Hoechst 33342 (1:5000, Sigma). Images were captured using a Zeiss LSM710 Multiphoton Confocal microscope and manipulated in Adobe Photoshop. Cilia were counted using NIS-Elements BR software.

Chromatin immunoprecipitation

Chromatin immunoprecipitation was performed as previously described. Briefly, Primary MEFs or ARPE-19 cells were cross-linked with 1% formaldehyde for 20 minutes at 37°C. Following chromatin isolation, DNA was sheared by sonication to between 200bp and 1000bp in length using a Branson digital sonifier, with microtip. Immunoprecipitations were carried out using 2µl of a polyclonal Tgif1 antiserum (78), 2µl of pre-immune serum. Bound and input fractions were analyzed by qPCR on a BioRad MyIQ cycler using Sensimix Plus SYBRgreen plus FITC mix (Bioline).

Chapter Four

Overview and Future Directions

We previously developed a mouse model of HPE by conditionally deleting *Tgif1* in the epiblast in the context of a *Tgif2* null (cdKO). While cdKO embryos do not survive past approximately 11.0 dpc, they have disrupted Shh signaling, defects in L-R patterning, and HPE (91).

We have shown that in addition to defects typical to HPE cdKO embryos have disrupted epithelial morphology. H&E stained sections of the FB show disorganization and a thickened layer of surface ectoderm with inappropriate separation of the ventral lips of the cephalic folds. The apical marker aPKC is disrupted in the forebrain and regionally within the neural tube. Diffuse staining of junctional markers such as β-catenin and N-cadherin show evidence of disrupted cell junctions.

When $Gli3^{r/+}$ is added to the cdKO embryo, polarity within the forebrain remains disrupted but structure and ventral separation is partially rescued. When $Nodal^{z/+}$ is added, forebrain structure remains disrupted but polarity is restored. When these two mutations are combined, the rescue of cdKO phenotypes is more complete, providing improved epithelial polarity with better forebrain structure, aiding in appropriate Shh signaling, and restoring patterning of the forebrain.

Polarity

We currently have a very limited understanding of the polarity defects in the cdKO embryo. With more information about the type and frequency of polarity

disruptions, we would better understand the mechanism of this disruption. This knowledge would add to our understanding of Tgif as a transcriptional regulator. To start we will examine other common polarity-related markers. By analyzing the expression of polarity complexes, such as the PAR, Crumbs and Scribble complexes, we will learn if all polarized domains (apical, lateral, and basal) are completely disrupted, partially disrupted, or fully intact. This information coupled with our knowledge of how polarity is established will help us to understand where the breakdown of polarity begins.

The patchy disruption of polarity within the neural tube suggests that polarity can be established in the cdKO but is harder to maintain. This may not be the case in the forebrain as all cdKO forebrain samples heretofore examined exhibit significant disruption of cell structure. It is possible that appropriate epithelial polarization is never established. We will examine this by looking at the expression of polarity proteins within sections of the cdKO forebrain through a range of stages.

Knowing to what extent polarity is restored in the *Nodal* rescue would help us better understand the mechanism by which Nodal regulates polarity. As with further examination of polarity defects in the cdKO, knowing what aspects of polarity—be it apical, lateral, basal organization or cell junctions—are disrupted in the context of *Nodal* rescue will help clarify a mechanism for polarity disruption without Tgifs.

Polarity defects could also be examined more closely using a polarized epithelial cell model with 3D culture, such as MDCK cells. When polarized MDCK cells can form cysts with a lumen similar to that of the neural tube. Apical, lateral, and basal markers can be examined by IF within this context. The ability of these cells to form organized

cysts would likely be defective when *Tgifs* are knocked down. We will observe the ability of *Tgif* knockdown MDCK cells to form organized polarized cell layers and tease out which aspects of polarity are not functioning. We will then knockdown *Nodal* within the cells as well and see if that improves their ability to polarize in 3D culture. Once this is established, perhaps more subtle methods could be used to examine the mechanism here, such as looking at genes downstream of Nodal and how they might be inhibiting polarity.

Neural tube development

While examining the neuroepithelium within the neural tube, we observed an IT ventral to the neural tube. The IT seemed to arise out of a reorganization of cells after an initial disruption of epithelial polarity at the floor plate. Deletion of one allele of *Nodal* partially rescued this phenotype by decreasing the presence of the IT within 70% of sections in the cdKO to approximately 5% of sections in the Nodal z/+ cdKO (Figure 7).

The observed IT phenotype is distinct and unique, and understanding the process by which it comes about would be useful in understanding the process of neural tube defects. It is possible the presence of an IT is due to loss and then reestablishment of polarity. It is also possible the presence of an IT is persistent instead of transient. This would help explain why loss of Tgifs is lethal to developing embryos. To explore these possibilities, we will undertake an experiment with the mT/mG mouse strain to observe live neural tube development. The mT/mG strain expresses a membrane targeted Tomato (mT) which gives way to membrane-targeted green fluorescent protein (GFP; mG) after Cre-mediated excision (209). This makes possible live embryo visualization and cell

tracing experiments. By carefully isolating embryos at 8.0 dpc and culturing them in the appropriate conditions, we will observe their growth via confocal microscope, capturing slices every 30 μm through the depth of the neural tube every thirty minutes for 12 to 24 hours. Reconstructing these images after capturing them will allow us to analyze the developing neural tube and determine if the IT is persistent or transient and if it is preceded by a disruption in polarity that then spontaneously organizes into a tube or if it comes about by some other mechanism.

We observed the posterior neural tube to be much more disorganized than the anterior neural tube. It is known that planar cell polarity (PCP) is required for elongation along the A-P axis, including elongation of the notochord and neural tube (210,211). In addition, cells of the posterior notochord (PNC, sometimes referred to as the node) give rise to the trunk and tail notochord (212). It has been shown that Wnt signaling is required for PCP, with *Wnt5a* deletion resulting in limb truncation and shortening of the A-P axis (213). Knowing that the PNC is disorganized in cdKO embryos, it is logical that cells derived from that structure would also be disorganized and it does appear that the cdKO A-P axis is shortened compared to stage-matched control embryos. It has also been suggested that there is a relationship between Tgif function and Wnt signaling, especially in the context of Wnt-driven oncogenesis (214). With this in mind, we will test whether the increase of posterior disorganization and shortening of the A-P axis in cdKO embryos is due to decreased Wnt signaling. As Wnt5a and Wnt11 have been implicated in A-P elongation (215), we will test expression of these genes by WISH and see if their expression is decreased in the posterior neural tube as comparted to expression

in control embryos. An understanding of all signaling pathways involved in the defective neural tube will clarify the phenotype and give insight into the causes of the polarity disruption observed.

Genetic manipulation and RNA-sequencing

Nodal is a target for Tgif repression as part of the TGFβ superfamily. Decreasing *Nodal* genetically can help overcome consequences of its inappropriate overexpression. We hypothesized that *Gli3* is a direct Tgif target as it is also overexpressed in the cdKO. Several studies have focused on conserved non-coding regions of the *Gli3* gene, with the goal of identifying important regulatory elements. A large number of conserved regions have been identified and several have been characterized for transcriptional activity in chick and mouse (177–180). The *Gli3* gene itself, in both mouse and human, spans more than 250kb and has a complex expression pattern during both embryogenesis and in the adult. Several of the conserved non-coding elements within the *Gli3* have been shown to direct reporter expression in transgenic mouse embryos, specifically to brain and spinal cord, forebrain, and limbs. We scanned the majority of these elements for conserved Tgif1 consensus sites (CTGTCAA) and tested six of them by ChIP. The region to which we show Tgif1 binding (termed HCNE1) has previously been shown to direct reporter expression in chick neural tube and to be bound by homeodomain proteins of the Pbx and Meis/Prep families. In some contexts, Tgif1 and Meis family proteins have been shown to compete for binding to the same sites to either repress or activate gene expression (216,217). This raises the possibility that competition between Tgifs and other homeodomain proteins such as Meis family members may fine-tune *Gli3* expression

levels at some stages of development. However, we do not currently have any evidence to support this.

We performed transcriptome analysis of the cdKO and found 1172 genes that were increased in the cdKO as compared to the control. Due to the function of Tgif as a transcriptional corepressor, upregulated genes are good candidates for direct Tgif targets. Any genes that show differential expression in this analysis could be either direct targets of Tgifs or secondary to altered expression of primary Tgif targets. It is also possible that some of the transcriptional changes may be a more indirect response to the phenotypic alterations in the mutant embryos. Thus, definitively identifying direct targets will require analysis of Tgif binding, either genome wide or on a gene-by-gene basis. Comparing this list with our previous *Tgif1* null MEF array helped us further restrict the list of upregulated genes, providing a higher confidence set of potential Tgif targets. More genes within this high confidence list need to be validated by qPCR and then examined for functional implications. The first set of genes we validated and explored functionally were those genes associated with cilia formation and function. Misregulation of genes related to ciliogenesis was consistent with observed phenotypes within cdKO embryos, such as lack of PNC cilia and disruption of forebrain cilia.

To validate the RNA-seq, we analyzed several genes that were upregulated or downregulated in both the RNA-seq and MEF array by qPCR, both on cDNA derived from embryos and from unstarved knockout cells (MEFs and ARPE19s). While many of these gene changes were validated, some, such as changes in IFT genes, were not. IFT genes are very specialized and function only in transport along the cilium. It is possible

that IFT genes did not appear to be decreased in our tissue culture models because the cells were in various cell cycle stages, with and without cilia. To determine if expression of IFT genes is truly decreased in the absence of Tgifs, we will perform qPCR on cells that have been starved, thus providing a more homogenous sample of cells that are unlikely to be undergoing mitosis and are more likely to be ciliated.

TGIF targets

Recent work in mouse ES cells has identified a large number of potential Tgif1 binding sites across the genome (218). Comparison of these ChIP-seq peaks with our data reveals a large overlap, but without much selectivity. In this analysis, the authors predicted almost 10,000 Tgif target genes, based simply on ChIP-seq enrichment. If we rank the peaks by enrichment score and use a more stringent cut-off, we observe greater overlap among these possibly higher confidence ChIP-seq peaks and genes that have increased expression in our cdKO embryos than with genes that have lower expression in the cdKO. Among the higher confidence peaks are those that span the regions we identified in the *Evi5l* and *Hdac5* genes by scanning the ENCODE data. However, the relatively low level of similarity between these multiple datasets perhaps reinforces the idea that Tgifs may perform cell-type specific functions and that comparison of expression and binding data should be performed in the same cell type. Those Tgif motifs we found in target genes within the experiments described here were found by eye. This process resulted in data, but it is less efficient and more prone to mistake than a bioinformatics approach. To get the most out of our RNA-seq data we will use computational methods to scan for the Tgif binding motif within 5kb upstream of the start

of each upregulated gene. Those genes that do not have Tgif binding motifs will have to be considered as indirect Tgif targets.

Potential epithelial to mesenchymal transition (EMT)

Signaling to Smads from TGFß family ligands is well-known to limit proliferation in epithelial tissues (9). Similarly, induction of EMT can be driven by TGFß family signaling, so an increase in EMT-like phenotypes and decreased proliferation in the absence of Smad transcriptional corepressors is consistent with known functions for this pathway. Although it does not appear that the cdKO NE undergoes complete EMT, we did observe increased expression of *Snail2* and *Twist2* in the cdKO, consistent with the induction of EMT, and it is possible if cdKO embryos survived longer the neuroepithelium would undergo more extensive EMT. Since the cdKO forebrain becomes apoptotic by approximately 10 dpc, we are unable to examine this. Although relatively little is known about the role of TGFß family signaling in early NE development, phospho-Smad2 is present in the nuclei of neuroepithelial cells of the forebrain, hindbrain and dorsal neural tube at 8.5 dpc and 9.5 dpc, suggesting that this pathway is active (219). Thus, Tgifs may control proliferation and epithelial polarity during normal anterior neural development by limiting Nodal/TGFß activated gene expression. To test this possibility we will perform WISH and probe for *Snail2* and *Twist2* expression in control and cdKO embryos. We will then examine the embryos for regional upregulation of EMT drivers and assess the extent to which its location correlates with the location of polarity defects, especially the forebrain and neuroepithelium. Examination of these same EMT drivers in $Nodal^{z/+}$ cdKO —by qPCR

and WISH—will determine whether restoration of polarity correlates with a decrease in EMT driver expression.

EMT could also be tested and observed by the use of a Boyden chamber assay. Migratory cells, such as those that have undergone EMT, have the ability to travel toward an attractant, such as serum. Tgif knockdown cells will be placed with in a Boyden chamber as a way to assay for EMT. While we don't see basement membrane breakdown in our tissue samples in forebrain and neural tube, we do see upregulation of two EMT regulators, which might be sufficient for cell migration in this assay (220).

Evi5L and cilia

When we knock down *Tgifs* in tissue culture cells we can recapitulate the cilia defect in vitro and rescue it with *Evi5l* knockdown. We also showed that *Evi5l*, a ciliogenesis regulator, is a direct Tgif target. To confirm that *Evi5l* is expressed in regions where we see a defect, we will perform WISH and probe for *Evi5l*. Not only will this confirm the RNA-seq, but knowing the specific location of *Evi5l* expression within the embryo will give us an idea of its affect and role. For example, low *Evi5l* expression in the forebrain, even in the absence of Tgifs, would explain the intermediate cilia phenotype seen there as compared to the stark loss of cilia in the PNC. While it is known that Evi5l affects the function of the cilia-related GAP Rab23, it is also possible that Evi5l has additional, unknown functions that affect cilia. Transfection of various truncation mutants featuring the various domains of Evi5l would help to narrow down the essential functional pieces of the protein and clarify if it has any other functions within the cell.

Whole mount immunofluorescence revealed defects in both PNC and forebrain cilia, although defects in the PNC were more pronounced than those in the forebrain, including misshapen PNC pit, consistent with an inability to generate flow and specify asymmetry. It is possible that cdKO cilia defects are caused by a delay in ciliogenesis and not a complete inhibition of cilia formation. As PNC cilia are required within a fairly tight window of time (several hours), it is possible they were too far delayed to be functional, whereas forebrain cilia have more time to grow, even if they are delayed. To test the possibility of delayed ciliogenesis as opposed to absent ciliogenesis, cdKO MEFs will be grown in full media, starved to encourage ciliogenesis, fixed, and stained for cilia at 2, 4, 8, 16, and 24-hour time points. If ciliogenesis is simply delayed, we expect gradually more and more cilia as the time points progress. Of course, these cells aren't perfectly synchronized. Cilia growth will be unsynchronized, possibly confounding a result. In addition to simply counting the cells with cilia, we will treat these cells with Shh and test Shh-target genes by qPCR to determine whether the cilia present are able to assist in propagating Shh signaling. An alternate method to examine this same question would be to culture different stages of embryos in Shh as suggested above. If embryos are able to respond to Shh, they have intact cilia. We would culture embryos at several different stages and see if later stages respond better to short periods of Shh exposure.

It would seem that the restoration of Nodal signaling would not restore proper ciliogenesis even though it partially rescued polarity defects in cdKO embryos as *Evi5l* would still be overexpressed. We were unable to test this within our tissue culture models, but perhaps we could understand this better within the whole embryo. To test

whether Nodal rescue has an effect on ciliogenesis, we will look at whole *Nodal*$^{z/+}$ embryos stained with Arl13b, pericentrin, and phalloidin. Presumably phalloidin staining will show improved epithelial structure, but if the percent of ciliated cells is similar to that seen in the cdKO, this experiment will show ciliogenesis to be independent of Nodal in this model.

Although we have focused on *Evi5l* as a target for Tgifs, it is still possible that other Tgif target genes may play a role in the effects of Tgif loss of function on cilia numbers. Possibilities include *Sirt2*, *Hdac5* and *Kif19*, although we did not observe such clearly reproducible effects on expression of these genes in the different systems analyzed here. It is also possible that disruption of other cellular processes in the absence of Tgifs contributes indirectly to the effects on ciliated cells. Nonetheless, we should test these additional potential targets for their effects on cilia in the absence of Tgifs. *Hdac5*, a tubulin deacetylase, is overexpressed in the cdKO. To test whether *Hdac5* overexpression is affecting ciliogenesis in the absence of Tgifs, we will treat cells, either cdKO MEFs or *TGIF* knockdown ARPE19s, with an Hdac5-specific inhibitor. If Hdac5 is also involved in the cilia defects seen in cdKOs, inhibitor treatment will rescue the cilia defect.

Having achieved a rescue of the cilia defects in cdKO tissue culture cells, the next step is to attempt rescue in the embryo. We will develop an *Evi5l* knockout mutation in mice. Combined with a cdKO background we will then perform IF on embryonic forebrain and PNC to see if cilia structure has been restored. We will also examine *Evi5l* knockout mice for possible rescue of L-R defects. If the *Evi5l* rescue is combined with

the Nodal rescue, there might even be seen a partial HPE rescue and restoration of Shh signaling to combat the excess Gli3 present in cdKO embryos.

Polycystic kidney disease (PKD) is a disease in which defects in appropriate signaling through cilia leads to the formation of kidney cysts. PKD can be associated with HPE (221,222). Knowing that mutations in Tgif are associated with both HPE and cilia defects, we will explore the extent to which HPE patients with TGIF mutations also have cilia-related problems. To uncover this information HPE patients with TGIF mutations will be assayed for cilia-related disorders (such as PKD and L-R defects), as well as assayed for expression of cilia-related genes such as *Evi5l*. Additionally, we will search through sequencing datasets from patients with known ciliopathies of unknown origin for mutations in Tgif. If Tgif is found to be involved in this way, this correlation will provide an additional marker to screen in diagnosing ciliopathies.

With the *Nodal*$^{z/+}$ cdKO, embryos are able to survive long enough to develop full HPE. At 18.5 dpc *Nodal*$^{z/+}$ cdKO embryos have cyclopia and proboscis. *Nodal* heterozygosity rescues the proliferation and cell organization defects seen in cdKO embryos but not the anterior DV patterning defects. In cdKOs where *Nodal* heterozygosity allows survival to late embryogenesis, we observe a classic HPE phenotype caused by the excess *Gli3* expression observed early in development. Thus it is possible that Tgif mutations cause HPE, not by disrupting Nodal signaling, but rather by increasing *Gli3* expression and disrupting Shh signaling. The introduction of a *Gli3* mutation into cdKO embryos did improve forebrain DV patterning, but was insufficient to fully rescue the phenotype. The lack of complete rescue could simply be due to an

insufficient amount of Gli3 for normal development, or it could imply some contribution of other pathways. Embryos that were heterozygous for both *Nodal* and *Gli3* (*Nodal*$^{z/+}$; *Gli3*$^{r/+}$*)* appeared to have further improved ventral patterning, although they also had severe dorsal defects. This combined rescue may, therefore, suggest that reducing Nodal can improve DV patterning, or possibly the effects of reducing *Gli3* are more apparent when overall NE integrity is improved.

Now that we have an HPE model that approaches live birth (*Nodal*$^{z/+}$ cdKO), we can examine other organ systems with epithelial and ciliated cells. We expect epithelial defects to be mostly absent, but cilia will also still be absent. Cilia are important in the brain and kidneys and lungs in a functioning postnatal mouse. If 18.5 dpc *Nodal*$^{z/+}$ cdKO embryos are too delicate or too difficult to obtain, these same organ systems can be examined for cilia defects in 3-allele *Tgif* mutants (*Tgif1*$^{-/-}$; *Tgif2*$^{+/-}$ or vice versa). Specifically we will examine these mice for PKD or other kidney defects, and functional cilia within the brain ventricles. Mutations in *Tgif1* have been associated with Otitis Media or inflammation of the middle ear (223). This association has been attributed to excess TGFβ signaling, but knowing Tgifs regulate ciliogenesis provides an additional possibility. Otitis Media is associated with motile cilia dysfunction and it is possible that mutations in Tgif lead to chronic Otitis Media and hearing loss in *Tgif* null mice due to defective ciliary function as opposed to excess TGFbeta signaling (224,225). Examination of the cilia within the middle ear will be performed on *Tgif1* null or 3-allele *Tgif* mutants to clarify the cause of Otitis Media in the absence of Tgif.

The realization that excess *Gli3* and *Nodal* both play independent roles in the cdKO led us to develop the model in Figure 10. While we know excess Gli3 causes HPE in cdKO embryos, there are several possible mechanisms to explain why Shh signaling is lacking. Mutations that affect ciliogenesis can result in phenotypes, including HPE and polydactyly, similar to those seen in *Shh* mutants. This raises the possibility that the HPE and lower forebrain *Shh* expression seen in cdKO embryos may be due to defects in ciliogenesis. Our analysis of the ventricular surface of the ventral forebrain suggests that there is indeed disruption of the organization of the neuroepithelial surface, with larger, less regular apical surfaces of the cells. However, the majority of cells have a primary cilium, and although we did observe a mild reduction in the number of cilia, disrupted ciliogenesis did not appear to be the major phenotype. In the forebrain, it is possible that the combination of NE disorganization and a reduction in ciliated cells results in lower *Shh* expression, or that altered *Shh* expression is independent of any function of Tgifs in regulating ciliogenesis.

Nodal and Gli3 Signaling

The HPE observed at 18.5 dpc in $Nodal^{z/+}$ cdKO embryos argues against a direct role for excess Nodal signaling causing HPE. Several previous studies have suggested that mutations that reduce the activity of the Nodal/Smad pathway can cause HPE (226). This has seemed somewhat at odds with the HPE observed in patients with heterozygous *TGIF1* mutations and in our cdKO embryos. Loss of Tgifs would be expected to increase Smad2 transcriptional output in response to Nodal. With loss-of-function mutations in *NODAL* associated with HPE, it seems both increase of NODAL function and decrease of

NODAL function are associated with HPE. A model in which loss of either an activator (NODAL ligand) or a repressor (TGIF1) has the same phenotype requires speculation about a specific window of pathway activity, above or below which the same phenotype is generated. It is possible that these two types of mutations (*Tgif* or *Nodal*/*Smad*) cause apparently similar phenotypes but have mechanistic differences in how they cause the phenotype. In our previous analysis, we observed primarily anterior truncations but no HPE in *Smad2*$^{r/+}$*; Nodal*$^{z/+}$ embryos. While these truncations can appear similar to the proboscis-like phenotype seen with HPE, the tissue is clearly distinct, with most of the presumptive forebrain tissue being absent. Evidence from human studies does suggest that reduced Nodal signaling can contribute to HPE (176). While mutations in the *NODAL*, *FOXH1* and *TDGF1* genes have all been found in human HPE patients, it should be noted that these mutations are quite rare in HPE and are more generally associated with other congenital defects (175,227). Evidence from model organisms also supports a role for NODAL signaling in the pathogenesis of HPE. For example, mutations in the zebrafish *tdgf1* gene (also known as *oep* or *cripto*) result in fish with a single central eye (228). Recent work in chick using chemical inhibition of SHH and Nodal signaling suggests that combining partial inhibition of both pathways could increase the frequency of HPE-like phenotypes over that seen with the same level of single inhibitor treatment (174,229). One possibility is that reduced Nodal pathway activity can contribute to HPE, dependent on genetic interactions with other predisposing factors, such as reduced Shh signaling. The partial penetrance and variable severity of most HPE mutations fit with such a model.

Our analysis here is consistent with a model in which reduced Nodal signaling in *Nodal*$^{z/+}$ cdKO embryos allows embryos with severe HPE to survive to late gestation, when they would otherwise fail to do so. On its own, loss of Tgif function causes HPE, but these embryos do not survive beyond mid-gestation. If the embryo is also heterozygous for *Nodal,* this can rescue the more severe defects that result in mid-gestational death. The result of this "rescue" yields some embryos surviving to late embryogenesis (essentially to birth, given that E18.5 embryos are very likely to be born). These compound mutants have a classic HPE phenotype such that the presence of HPE here correlates with a loss of function mutation in an activating component of the Nodal pathway. Clearly, this does not have to be the case for all, or any, *TGIF1* mutations in humans with HPE. However, it does raise the possibility that mutations in genes such as *TDGF1* may not directly cause HPE, but rather uncover a pre-existing defect by allowing the embryo to survive to a later stage of development.

At this point, it will be interesting to see what happens to *Nodal*$^{z/+}$; *Gli3*$^{r/+}$ cdKO embryos at later stages of development. It is possible that such a high degree of genetic modification would be detrimental to development, but considering what we've learned about the roles these genes play in rescues to this point, it will be interesting to see if embryos still have proboscis and cyclopia at 18.5 dpc with decreased *Gli3* and *Nodal* expression

Excess Gli3, due to lack of Tgif direct repression, can inhibit Shh expression. Lack of cilia, also a consequence of loss of Tgifs, can also interfere with Shh signaling. It would be informative to determine which scenario has more weight in this system. By

culturing live embryos in Shh for approximately 24 hours starting around 8.0 dpc and then examining them by WISH, we will learn if additional Shh ligand is sufficient to activate downstream Shh signaling and restore expression of downstream targets such as *Gli1* and *Ptch1*. We will also examine the effect of additional Shh on *Gli3* levels. Repeating these experiments within the full range of rescue mutants (*Nodal*$^{z/+}$ cdKO, *Gli3*$^{r/+}$ cdKO, and *Nodal*$^{z/+}$; *Gli3*$^{r/+}$ cdKO) will give us a more complete understanding of the Shh signaling defects in the absence of Tgifs, especially in the forebrain.

Conclusions

Holoprosencephaly is a common and devastating developmental disorder. Its cause is not well understood and only a small fraction of incidences are associated with known genetic mutations. Even when a genetic association is found, the severity of HPE is unpredictable, ranging from incompatible with life to phenotypically normal. With such a complex etiology it is important to study and understand those causes that are known.

With this in mind, the Wotton Lab developed a mouse model of HPE with the deletion of *Tgifs*. Using this model we have found insight into the mechanism of Tgifs within the developing embryo and the roles they might play in diseases such as HPE and other ciliopathies. The knowledge that Tgifs directly regulate ciliogenesis and thereby assist in maintaining appropriate Sonic Hedgehog signaling clarifies the association of *TGIF* mutations with HPE in humans while also suggesting recommending examination of *TGIF* in ciliopathies of unknown genetic origin.

Supplementary Table 1. Gene list for cilia

Ahi1	Dync2h1	Kat2a	Kif5c	Sirt7
Alms1	Dync2li1	Kif11	Kif6	Tbc1d30
Atat1	Dynlt1a	Kif12	Kif7	Tbc1d7
Aurka	Dynlt1b	Kif13a	Kif9	Tmem67
Bbs1	Efcab7	Kif13b	Kifap3	Traf3ip1
Bbs10	Elp3	Kif14	Kifap3	Ttc21b
Bbs12	Evc	Kif15	Kifc1	Ttc26
Bbs2	Evc2	Kif16b	Kifc2	Ttc30b
Bbs4	Evi5l	Kif17	Kifc3	Ttl
Bbs5	Gsk3b	Kif18a	Kifc5b	Ttll1
Bbs7	Hdac1	Kif18b	Mks1	Ttll10
Bbs9	Hdac10	Kif19a	Nedd9	Ttll11
Cc2d2a	Hdac11	Kif19a	Nek1	Ttll12
Ccp110	Hdac2	Kif1a	Nek2	Ttll3
Ccsap	Hdac3	Kif1b	Nek3	Ttll4
Cep110	Hdac4	Kif1c	Nek4	Ttll5
Cep120	Hdac5	Kif20a	Nek6	Ttll7
Cep135	Hdac6	Kif20b	Nek7	Ttll9
Cep152	Hdac7	Kif21a	Nek8	Vhl
Cep164	Hdac8	Kif21b	Nek9	Wdr19
Cep170	Hdac9	Kif22	Nphp1	Wdr34
Cep192	Hyls1	Kif23	Nphp3	Wdr35
Cep250	Ift122	Kif24	Nphp4	
Cep290	Ift140	Kif26a	Ofd1	
Cep350	Ift172	Kif26b	Poc1a	
Cep55	Ift20	Kif27	Poc1b	
Cep57	Ift27	Kif2a	Poc5	
Cep57l1	Ift43	Kif2c	Rab17	
Cep63	Ift46	Kif3a	Rab23	
Cep68	Ift52	Kif3a	Rab8a	
Cep70	Ift57	Kif3b	Rpgrip1l	
Cep72	Ift74	Kif3b	Sirt1	
Cep76	Ift80	Kif3c	Sirt2	
Cep78	Ift81	Kif3c	Sirt3	
Cep97	Ift88	Kif4	Sirt4	
Cluap1	Inpp5e	Kif5a	Sirt5	
Dido1	Iqce	Kif5b	Sirt6	

Bibliography

1. Whitman M. Nodal Signaling in Early Vertebrate Embryos. Dev Cell. 2001 Nov;1(5):605–617.
2. Kishigami S, Mishina Y. BMP signaling and early embryonic patterning. Cytokine Growth Factor Rev. 2005 Jun;16(3):265–278.
3. Rahman MS, Akhtar N, Jamil HM, Banik RS, Asaduzzaman SM. TGF-β/BMP signaling and other molecular events: regulation of osteoblastogenesis and bone formation. Bone Res. 2015 Apr 14;3:15005.
4. Savage-Dunn C. TGF-beta signaling. WormBook. 2005 Sep 9;1–12.
5. Haddow A. Molecular repair, wound healing, and carcinogenesis: tumor production a possible overhealing? Adv Cancer Res. 1972;16:181–234.
6. Derynck R, Akhurst RJ, Balmain A. TGF-beta signaling in tumor suppression and cancer progression. Nat Genet. 2001 Oct;29(2):117–129.
7. Siegel PM, Massagué J. Cytostatic and apoptotic actions of TGF-beta in homeostasis and cancer. Nat Rev Cancer. 2003 Nov;3(11):807–821.
8. Waite KA, Eng C. From developmental disorder to heritable cancer: it's all in the BMP/TGF-beta family. Nat Rev Genet. 2003 Oct 1;4(10):763–773.
9. Massagué J, Blain SW, Lo RS. TGFβ Signaling in Growth Control, Cancer, and Heritable Disorders. Cell. 2000 Oct;103(2):295–309.
10. Massagué J. TGF-beta signal transduction. Annu Rev Biochem. 1998;67:753–791.
11. Urist MR. Bone: formation by autoinduction. Science. 1965 Nov 12;150(3698):893–899.
12. Little SC, Mullins MC. Extracellular modulation of BMP activity in patterning the dorsoventral axis. Birth Defects Res C Embryo Today. 2006 Sep;78(3):224–242.
13. Little SC, Mullins MC. Bone morphogenetic protein heterodimers assemble heteromeric type I receptor complexes to pattern the dorsoventral axis. Nat Cell Biol. 2009 May;11(5):637–643.
14. Baker JC, Beddington RS, Harland RM. Wnt signaling in Xenopus embryos inhibits bmp4 expression and activates neural development. Genes Dev. 1999 Dec 1;13(23):3149–3159.
15. Kodach LL, Wiercinska E, de Miranda NF, Bleuming SA, Musler AR, Peppelenbosch MP, et al. The bone morphogenetic protein pathway is inactivated in the majority of sporadic colorectal cancers. Gastroenterology. 2008 May;134(5):1332–1341.
16. Hardwick JC, Kodach LL, Offerhaus GJ, van den Brink GR. Bone morphogenetic protein signalling in colorectal cancer. Nat Rev Cancer. 2008 Oct 1;8(10):806–812.
17. Dudley AT, Lyons KM, Robertson EJ. A requirement for bone morphogenetic protein-7 during development of the mammalian kidney and eye. Genes Dev. 1995 Nov 15;9(22):2795–2807.

18. Luo G, Hofmann C, Bronckers AL, Sohocki M, Bradley A, Karsenty G. BMP-7 is an inducer of nephrogenesis, and is also required for eye development and skeletal patterning. Genes Dev. 1995 Nov 15;9(22):2808–2820.
19. Roberts AB, Anzano MA, Lamb LC, Smith JM, Sporn MB. New class of transforming growth factors potentiated by epidermal growth factor: isolation from non-neoplastic tissues. Proc Natl Acad Sci U S A. 1981 Sep;78(9):5339–5343.
20. Anzano MA, Roberts AB, Meyers CA, Komoriya A, Lamb LC, Smith JM, et al. Synergistic interaction of two classes of transforming growth factors from murine sarcoma cells. Cancer Res. 1982 Nov 1;42(11):4776–4778.
21. Sporn MB, Roberts AB, Shull JH, Smith JM, Ward JM, Sodek J. Polypeptide transforming growth factors isolated from bovine sources and used for wound healing in vivo. Science. 1983 Mar 18;219(4590):1329–1331.
22. Roberts AB, Sporn MB, Assoian RK, Smith JM, Roche NS, Wakefield LM, et al. Transforming growth factor type beta: rapid induction of fibrosis and angiogenesis in vivo and stimulation of collagen formation in vitro. Proc Natl Acad Sci U S A. 1986 Jun;83(12):4167–4171.
23. Tucker RF, Shipley GD, Moses HL, Holley RW. Growth inhibitor from BSC-1 cells closely related to platelet type beta transforming growth factor. Science. 1984 Nov 9;226(4675):705–707.
24. Peinado H, Quintanilla M, Cano A. Transforming growth factor beta-1 induces snail transcription factor in epithelial cell lines: mechanisms for epithelial mesenchymal transitions. J Biol Chem. 2003 Jun 6;278(23):21113–21123.
25. Savagner P, Yamada KM, Thiery JP. The zinc-finger protein slug causes desmosome dissociation, an initial and necessary step for growth factor-induced epithelial-mesenchymal transition. J Cell Biol. 1997 Jun 16;137(6):1403–1419.
26. Romano LA, Runyan RB. Slug is an essential target of TGFbeta2 signaling in the developing chicken heart. Dev Biol. 2000 Jul 1;223(1):91–102.
27. Hajra KM, Chen DY, Fearon ER. The SLUG zinc-finger protein represses E-cadherin in breast cancer. Cancer Res. 2002 Mar 15;62(6):1613–1618.
28. Loeys BL, Schwarze U, Holm T, Callewaert BL, Thomas GH, Pannu H, et al. Aneurysm syndromes caused by mutations in the TGF-beta receptor. N Engl J Med. 2006 Aug 24;355(8):788–798.
29. LeMaire SA, Pannu H, Tran-Fadulu V, Carter SA, Coselli JS, Milewicz DM. Severe aortic and arterial aneurysms associated with a TGFBR2 mutation. Nat Clin Pract Cardiovasc Med. 2007 Mar;4(3):167–171.
30. Loeys BL, Chen J, Neptune ER, Judge DP, Podowski M, Holm T, et al. A syndrome of altered cardiovascular, craniofacial, neurocognitive and skeletal development caused by mutations in TGFBR1 or TGFBR2. Nat Genet. 2005 Mar;37(3):275–281.
31. Kainulainen K, Karttunen L, Puhakka L, Sakai L, Peltonen L. Mutations in the fibrillin gene responsible for dominant ectopia lentis and neonatal Marfan syndrome. Nat Genet. 1994 Jan 1;6(1):64–69.

32. Dietz HC, Loeys B, Carta L, Ramirez F. Recent progress towards a molecular understanding of Marfan syndrome. Am J Med Genet C Semin Med Genet. 2005 Nov 15;139C(1):4–9.
33. Mathews LS, Vale WW. Expression cloning of an activin receptor, a predicted transmembrane serine kinase. Cell. 1991 Jun 14;65(6):973–982.
34. Franzén P, ten Dijke P, Ichijo H, Yamashita H, Schulz P, Heldin CH, et al. Cloning of a TGF beta type I receptor that forms a heteromeric complex with the TGF beta type II receptor. Cell. 1993 Nov 19;75(4):681–692.
35. Wrana JL, Attisano L, Cárcamo J, Zentella A, Doody J, Laiho M, et al. TGFβ signals through a heteromeric protein kinase receptor complex. Cell. 1992 Dec;71(6):1003–1014.
36. Wotton D, Massagué J. Smad transcriptional corepressors in TGF beta family signaling. Curr Top Microbiol Immunol. 2001;254:145–164.
37. Xu L, Chen YG, Massagué J. The nuclear import function of Smad2 is masked by SARA and unmasked by TGFbeta-dependent phosphorylation. Nat Cell Biol. 2000 Aug 1;2(8):559–562.
38. Tsukazaki T, Chiang TA, Davison AF, Attisano L, Wrana JL. SARA, a FYVE Domain Protein that Recruits Smad2 to the TGFβ Receptor. Cell. 1998 Dec;95(6):779–791.
39. Lo RS, Massagué J. Ubiquitin-dependent degradation of TGF-beta-activated smad2. Nat Cell Biol. 1999 Dec;1(8):472–478.
40. Hayashi H, Abdollah S, Qiu Y, Cai J, Xu Y, Grinnell BW, et al. The MAD-Related Protein Smad7 Associates with the TGFβ Receptor and Functions as an Antagonist of TGFβ Signaling. Cell. 1997 Jun;89(7):1165–1173.
41. Yan X, Liu Z, Chen Y. Regulation of TGF-beta signaling by Smad7. Acta Biochim Biophys Sin (Shanghai). 2009 Apr;41(4):263–272.
42. Seo SR, Lallemand F, Ferrand N, Pessah M, L'Hoste S, Camonis J, et al. The novel E3 ubiquitin ligase Tiul1 associates with TGIF to target Smad2 for degradation. EMBO J. 2004 Oct 1;23(19):3780–3792.
43. Sun L, Wu G, Willson JK, Zborowska E, Yang J, Rajkarunanayake I, et al. Expression of transforming growth factor beta type II receptor leads to reduced malignancy in human breast cancer MCF-7 cells. J Biol Chem. 1994 Oct 21;269(42):26449–26455.
44. Kim S-J, Im Y-H, Markowitz SD, Bang Y-J. Molecular mechanisms of inactivation of TGF-β receptors during carcinogenesis. Cytokine Growth Factor Rev. 2000 Apr;11(1-2):159–168.
45. Böttinger EP, Jakubczak JL, Haines DC, Bagnall K, Wakefield LM. Transgenic mice overexpressing a dominant-negative mutant type II transforming growth factor beta receptor show enhanced tumorigenesis in the mammary gland and lung in response to the carcinogen 7,12-dimethylbenz-[a]-anthracene. Cancer Res. 1997 Dec 15;57(24):5564–5570.
46. Wang J, Sun L, Myeroff L, Wang X, Gentry LE, Yang J, et al. Demonstration that mutation of the type II transforming growth factor beta receptor inactivates its

tumor suppressor activity in replication error-positive colon carcinoma cells. J Biol Chem. 1995 Sep 15;270(37):22044–22049.
47. Massagué J. TGFbeta in Cancer. Cell. 2008 Jul 25;134(2):215–230.
48. Thomas DA, Massagué J. TGF-beta directly targets cytotoxic T cell functions during tumor evasion of immune surveillance. Cancer Cell. 2005 Nov;8(5):369–380.
49. Shull MM, Ormsby I, Kier AB, Pawlowski S, Diebold RJ, Yin M, et al. Targeted disruption of the mouse transforming growth factor-beta 1 gene results in multifocal inflammatory disease. Nature. 1992 Oct 22;359(6397):693–699.
50. Kulkarni AB, Huh CG, Becker D, Geiser A, Lyght M, Flanders KC, et al. Transforming growth factor beta 1 null mutation in mice causes excessive inflammatory response and early death. Proc Natl Acad Sci U S A. 1993 Jan 15;90(2):770–774.
51. Diebold RJ, Eis MJ, Yin M, Ormsby I, Boivin GP, Darrow BJ, et al. Early-onset multifocal inflammation in the transforming growth factor beta 1-null mouse is lymphocyte mediated. Proc Natl Acad Sci U S A. 1995 Dec 19;92(26):12215–12219.
52. Sanford LP, Ormsby I, Gittenberger-de Groot AC, Sariola H, Friedman R, Boivin GP, et al. TGFbeta2 knockout mice have multiple developmental defects that are non-overlapping with other TGFbeta knockout phenotypes. Development. 1997 Jul 1;124(13):2659–2670.
53. Proetzel G, Pawlowski SA, Wiles MV, Yin M, Boivin GP, Howles PN, et al. Transforming growth factor-beta 3 is required for secondary palate fusion. Nat Genet. 1995 Dec 1;11(4):409–414.
54. Zhou X, Sasaki H, Lowe L, Hogan BL, Kuehn MR. Nodal is a novel TGF-beta-like gene expressed in the mouse node during gastrulation. Nature. 1993 Feb 11;361(6412):543–547.
55. Conlon FL, Lyons KM, Takaesu N, Barth KS, Kispert A, Herrmann B, et al. A primary requirement for nodal in the formation and maintenance of the primitive streak in the mouse. Development. 1994 Jul;120(7):1919–1928.
56. Collignon J, Varlet I, Robertson EJ. Relationship between asymmetric nodal expression and the direction of embryonic turning. Nature. 1996 May 9;381(6578):155–158.
57. Levin M, Johnson RL, Stern CD, Kuehn M, Tabin C. A molecular pathway determining left-right asymmetry in chick embryogenesis. Cell. 1995 Sep 8;82(5):803–814.
58. Lowe LA, Supp DM, Sampath K, Yokoyama T, Wright CV, Potter SS, et al. Conserved left-right asymmetry of nodal expression and alterations in murine situs inversus. Nature. 1996 May 9;381(6578):158–161.
59. Piccolo S, Agius E, Leyns L, Bhattacharyya S, Grunz H, Bouwmeester T, et al. The head inducer Cerberus is a multifunctional antagonist of Nodal, BMP and Wnt signals. Nature. 1999 Feb 25;397(6721):707–710.

60. Perea-Gomez A, Vella FD, Shawlot W, Oulad-Abdelghani M, Chazaud C, Meno C, et al. Nodal antagonists in the anterior visceral endoderm prevent the formation of multiple primitive streaks. Dev Cell. 2002 Nov 1;3(5):745–756.
61. Saijoh Y, Adachi H, Sakuma R, Yeo CY, Yashiro K, Watanabe M, et al. Left-right asymmetric expression of lefty2 and nodal is induced by a signaling pathway that includes the transcription factor FAST2. Mol Cell. 2000 Jan;5(1):35–47.
62. Yamamoto M, Mine N, Mochida K, Sakai Y, Saijoh Y, Meno C, et al. Nodal signaling induces the midline barrier by activating Nodal expression in the lateral plate. Development. 2003 May 1;130(9):1795–1804.
63. Meno C, Saijoh Y, Fujii H, Ikeda M, Yokoyama T, Yokoyama M, et al. Left-right asymmetric expression of the TGF beta-family member lefty in mouse embryos. Nature. 1996 May 9;381(6578):151–155.
64. Meno C, Ito Y, Saijoh Y, Matsuda Y, Tashiro K, Kuhara S, et al. Two closely-related left-right asymmetrically expressed genes,lefty-1 andlefty-2 : their distinct expression domains, chromosomal linkage and direct neuralizing activity inXenopus embryos. Genes Cells. 1997 Aug;2(8):513–524.
65. Bianco C, Adkins HB, Wechselberger C, Seno M, Normanno N, De Luca A, et al. Cripto-1 activates nodal- and ALK4-dependent and -independent signaling pathways in mammary epithelial Cells. Mol Cell Biol. 2002 Apr;22(8):2586–2597.
66. Yan YT, Liu JJ, Luo Y, E C, Haltiwanger RS, Abate-Shen C, et al. Dual roles of Cripto as a ligand and coreceptor in the nodal signaling pathway. Mol Cell Biol. 2002 Jul;22(13):4439–4449.
67. Yeo C, Whitman M. Nodal signals to Smads through Cripto-dependent and Cripto-independent mechanisms. Mol Cell. 2001 May;7(5):949–957.
68. Brennan J, Norris DP, Robertson EJ. Nodal activity in the node governs left-right asymmetry. Genes Dev. 2002 Sep 15;16(18):2339–2344.
69. Nonaka S, Tanaka Y, Okada Y, Takeda S, Harada A, Kanai Y, et al. Randomization of left-right asymmetry due to loss of nodal cilia generating leftward flow of extraembryonic fluid in mice lacking KIF3B motor protein. Cell. 1998 Dec 11;95(6):829–837.
70. Nonaka S, Shiratori H, Saijoh Y, Hamada H. Determination of left-right patterning of the mouse embryo by artificial nodal flow. Nature. 2002 Jul 4;418(6893):96–99.
71. Saijoh Y, Oki S, Ohishi S, Hamada H. Left–right patterning of the mouse lateral plate requires nodal produced in the node. Dev Biol. 2003 Apr;256(1):161–173.
72. Varlet I, Collignon J, Robertson EJ. nodal expression in the primitive endoderm is required for specification of the anterior axis during mouse gastrulation. Development. 1997 Mar;124(5):1033–1044.
73. Reissmann E, Jörnvall H, Blokzijl A, Andersson O, Chang C, Minchiotti G, et al. The orphan receptor ALK7 and the Activin receptor ALK4 mediate signaling by Nodal proteins during vertebrate development. Genes Dev. 2001 Aug 1;15(15):2010–2022.

74. Lowe LA, Yamada S, Kuehn MR. Genetic dissection of nodal function in patterning the mouse embryo. Development. 2001 May 1;128(10):1831–1843.
75. Bertolino E, Reimund B, Wildt-Perinic D, Clerc RG. A novel homeobox protein which recognizes a TGT core and functionally interferes with a retinoid-responsive motif. J Biol Chem. 1995 Dec 29;270(52):31178–31188.
76. Bertolino E, Wildt S, Richards G, Clerc RG. Expression of a novel murine homeobox gene in the developing cerebellar external granular layer during its proliferation. Dev Dyn [Internet]. 1996 Apr 1; Available from: http://onlinelibrary.wiley.com/store/10.1002/(SICI)1097-0177(199604)205:4%3C410::AID-AJA5%3E3.0.CO;2-L/asset/5_ftp.pdf?v=1&t=iixf1li9&s=3c8e5fa887183db53977e0ac371876dea5a857d3
77. Bürglin TR. Analysis of TALE superclass homeobox genes (MEIS, PBC, KNOX, Iroquois, TGIF) reveals a novel domain conserved between plants and animals. Nucleic Acids Res. 1997 Nov 1;25(21):4173–4180.
78. Wotton D, Lo RS, Lee S, Massagué J. A Smad transcriptional corepressor. Cell. 1999 Apr 2;97(1):29–39.
79. Melhuish TA, Wotton D. The interaction of the carboxyl terminus-binding protein with the Smad corepressor TGIF is disrupted by a holoprosencephaly mutation in TGIF. J Biol Chem. 2000 Dec 15;275(50):39762–39766.
80. Wotton D, Knoepfler PS, Laherty CD, Eisenman RN, Massagué J. The Smad transcriptional corepressor TGIF recruits mSin3. Cell Growth Differ. 2001 Sep;12(9):457–463.
81. Wotton D, Lo RS, Swaby LA, Massagué J. Multiple modes of repression by the Smad transcriptional corepressor TGIF. J Biol Chem. 1999 Dec 24;274(52):37105–37110.
82. Melhuish TA, Gallo CM, Wotton D. TGIF2 interacts with histone deacetylase 1 and represses transcription. J Biol Chem. 2001 Aug 24;276(34):32109–32114.
83. Zhang MZ, Ferrigno O, Wang Z, Ohnishi M, Prunier C, Levy L, et al. TGIF governs a feed-forward network that empowers Wnt signaling to drive mammary tumorigenesis. Cancer Cell. 2015 Apr 13;27(4):547–560.
84. Gripp KW, Wotton D, Edwards MC, Roessler E, Ades L, Meinecke P, et al. Mutations in TGIF cause holoprosencephaly and link NODAL signalling to human neural axis determination. Nat Genet. 2000 Jun;25(2):205–208.
85. El-Jaick KB, Powers SE, Bartholin L, Myers KR, Hahn J, Orioli IM, et al. Functional analysis of mutations in TGIF associated with holoprosencephaly. Mol Genet Metab. 2007 Jan;90(1):97–111.
86. Shen J, Walsh CA. Targeted disruption of Tgif, the mouse ortholog of a human holoprosencephaly gene, does not result in holoprosencephaly in mice. Mol Cell Biol. 2005 May;25(9):3639–3647.
87. Bartholin L, Powers SE, Melhuish TA, Lasse S, Weinstein M, Wotton D. TGIF inhibits retinoid signaling. Mol Cell Biol. 2006 Feb;26(3):990–1001.
88. Jin JZ, Gu S, McKinney P, Ding J. Expression and functional analysis of Tgif during mouse midline development. Dev Dyn. 2006 Feb;235(2):547–553.

89. Bartholin L, Melhuish TA, Powers SE, Goddard-Léon S, Treilleux I, Sutherland AE, et al. Maternal Tgif is required for vascularization of the embryonic placenta. Dev Biol. 2008 Jul 15;319(2):285–297.
90. Powers SE, Taniguchi K, Yen W, Melhuish TA, Shen J, Walsh CA, et al. Tgif1 and Tgif2 regulate Nodal signaling and are required for gastrulation. Development. 2010 Jan;137(2):249–259.
91. Taniguchi K, Anderson AE, Sutherland AE, Wotton D. Loss of Tgif function causes holoprosencephaly by disrupting the SHH signaling pathway. PLoS Genet. 2012 Feb 23;8(2):e1002524.
92. Demyer W, Zeman W. Alobar holoprosencephaly (arhinencephaly) with median cleft lip and palate: clinical, electroencephalographic and nosologic considerations. Confin Neurol. 1963;23:1–36.
93. Demyer W, Zeman W, Palmer CG. The face predicts the brain: diagnostic significance of median facial anomalies for holoprosencephaly (arhinencephaly). Pediatrics. 1964 Aug;34:256–263.
94. Barkovich AJ, Quint DJ. Middle interhemispheric fusion: an unusual variant of holoprosencephaly. AJNR Am J Neuroradiol. 1993 Apr 1;14(2):431–440.
95. Simon EM, Hevner RF, Pinter JD, Clegg NJ, Delgado M, Kinsman SL, et al. The middle interhemispheric variant of holoprosencephaly. AJNR Am J Neuroradiol. 2002 Jan 1;23(1):151–156.
96. Matsunaga E, Shiota K. Holoprosencephaly in human embryos: epidemiologic studies of 150 cases. Teratology. 1977 Dec;16(3):261–272.
97. Orioli IM, Castilla EE. Epidemiology of holoprosencephaly: Prevalence and risk factors. Am J Med Genet C Semin Med Genet. 2010 Feb 15;154C(1):13–21.
98. Wallis DE, Muenke M. Molecular mechanisms of holoprosencephaly. Mol Genet Metab. 1999 Oct;68(2):126–138.
99. Nanni L, Ming JE, Bocian M, Steinhaus K, Bianchi DW, Die-Smulders C, et al. The mutational spectrum of the sonic hedgehog gene in holoprosencephaly: SHH mutations cause a significant proportion of autosomal dominant holoprosencephaly. Hum Mol Genet. 1999 Dec;8(13):2479–2488.
100. Johnson CY, Rasmussen SA. Non-genetic risk factors for holoprosencephaly. Am J Med Genet C Semin Med Genet. 2010 Feb 15;154C(1):73–85.
101. Miller EA, Rasmussen SA, Siega-Riz AM, Frías JL, Honein MA, National Birth Defects Prevention Study. Risk factors for non-syndromic holoprosencephaly in the National Birth Defects Prevention Study. Am J Med Genet C Semin Med Genet. 2010 Feb 15;154C(1):62–72.
102. Ming JE, Muenke M. Multiple hits during early embryonic development: digenic diseases and holoprosencephaly. Am J Hum Genet. 2002 Nov;71(5):1017–1032.
103. Nüsslein-Volhard C, Wieschaus E. Mutations affecting segment number and polarity in Drosophila. Nature. 1980 Oct 30;287(5785):795–801.
104. Ingham PW, McMahon AP. Hedgehog signaling in animal development: paradigms and principles. Genes Dev. 2001 Dec 1;15(23):3059–3087.

105. Echelard Y, Epstein DJ, St-Jacques B, Shen L, Mohler J, McMahon JA, et al. Sonic hedgehog, a member of a family of putative signaling molecules, is implicated in the regulation of CNS polarity. Cell. 1993 Dec 31;75(7):1417–1430.
106. Lee JJ, Ekker SC, von Kessler DP, Porter JA, Sun BI, Beachy PA. Autoproteolysis in hedgehog protein biogenesis. Science. 1994 Dec 2;266(5190):1528–1537.
107. Porter JA, Young KE, Beachy PA. Cholesterol modification of hedgehog signaling proteins in animal development. Science. 1996 Oct 11;274(5285):255–259.
108. Burke R, Nellen D, Bellotto M, Hafen E, Senti KA, Dickson BJ, et al. Dispatched, a novel sterol-sensing domain protein dedicated to the release of cholesterol-modified hedgehog from signaling cells. Cell. 1999 Dec 23;99(7):803–815.
109. Chen Y, Struhl G. Dual roles for patched in sequestering and transducing Hedgehog. Cell. 1996 Nov 1;87(3):553–563.
110. Chuang PT, McMahon AP. Vertebrate Hedgehog signalling modulated by induction of a Hedgehog-binding protein. Nature. 1999 Feb 18;397(6720):617–621.
111. Marigo V, Johnson RL, Vortkamp A, Tabin CJ. Sonic hedgehog differentially regulates expression of GLI and GLI3 during limb development. Dev Biol. 1996 Nov 25;180(1):273–283.
112. Ruiz i Altaba A. Combinatorial Gli gene function in floor plate and neuronal inductions by Sonic hedgehog. Development. 1998 Jun 1;125(12):2203–2212.
113. Briscoe J, Pierani A, Jessell TM, Ericson J. A homeodomain protein code specifies progenitor cell identity and neuronal fate in the ventral neural tube. Cell. 2000 May 12;101(4):435–445.
114. Hayhurst M, McConnell SK. Mouse models of holoprosencephaly. Curr Opin Neurol. 2003 Apr;16(2):135–141.
115. Chiang C, Litingtung Y, Lee E, Young KE, Corden JL, Westphal H, et al. Cyclopia and defective axial patterning in mice lacking Sonic hedgehog gene function. Nature. 1996 Oct 3;383(6599):407–413.
116. Zhang XM, Ramalho-Santos M, McMahon AP. Smoothened mutants reveal redundant roles for Shh and Ihh signaling including regulation of L/R asymmetry by the mouse node. Cell. 2001 Jun 15;105(6):781–792.
117. Nagai T, Aruga J, Minowa O, Sugimoto T, Ohno Y, Noda T, et al. Zic2 regulates the kinetics of neurulation. Proc Natl Acad Sci U S A. 2000 Feb 15;97(4):1618–1623.
118. Hayashi S, Lewis P, Pevny L, McMahon AP. Efficient gene modulation in mouse epiblast using a Sox2Cre transgenic mouse strain. Mech Dev. 2002 Dec;119 Suppl 1:S97–S101.
119. Schier AF. Nodal signaling in vertebrate development. Annu Rev Cell Dev Biol. 2003;19:589–621.
120. Eggenschwiler JT, Anderson KV. Cilia and developmental signaling. Annu Rev Cell Dev Biol. 2007 Jan 1;23:345–373.

121. Goetz SC, Anderson KV. The primary cilium: a signalling centre during vertebrate development. Nat Rev Genet. 2010 May;11(5):331–344.
122. Ishikawa H, Marshall WF. Ciliogenesis: building the cell's antenna. Nat Rev Mol Cell Biol. 2011 Apr;12(4):222–234.
123. Nonaka S, Yoshiba S, Watanabe D, Ikeuchi S, Goto T, Marshall WF, et al. De novo formation of left-right asymmetry by posterior tilt of nodal cilia. PLoS Biol. 2005 Aug;3(8):e268.
124. Okada Y, Takeda S, Tanaka Y, Izpisúa Belmonte JC, Hirokawa N. Mechanism of nodal flow: a conserved symmetry breaking event in left-right axis determination. Cell. 2005 May 20;121(4):633–644.
125. Levin M. Left-right asymmetry in embryonic development: a comprehensive review. Mech Dev. 2005 Jan;122(1):3–25.
126. Casey B. Left–right axis malformations in man and mouse. Curr Opin Genet Dev. 2000 Jun 1;10(3):257–261.
127. Afzelius BA. Genetics and pulmonary medicine. 6. Immotile cilia syndrome: past, present, and prospects for the future. Thorax. 1998 Oct 1;53(10):894–897.
128. Meno C, Shimono A, Saijoh Y, Yashiro K, Mochida K, Ohishi S, et al. lefty-1 is required for left-right determination as a regulator of lefty-2 and nodal. Cell. 1998 Aug 7;94(3):287–297.
129. Garcia-Gonzalo FR, Reiter JF. Scoring a backstage pass: mechanisms of ciliogenesis and ciliary access. J Cell Biol. 2012 Jun 11;197(6):697–709.
130. Scholey JM. Intraflagellar transport. Annu Rev Cell Dev Biol. 2003;19:423–443.
131. Huangfu D, Liu A, Rakeman AS, Murcia NS, Niswander L, Anderson KV. Hedgehog signalling in the mouse requires intraflagellar transport proteins. Nature. 2003 Nov 6;426(6962):83–87.
132. Haycraft CJ, Banizs B, Aydin-Son Y, Zhang Q, Michaud EJ, Yoder BK. Gli2 and Gli3 localize to cilia and require the intraflagellar transport protein polaris for processing and function. PLoS Genet. 2005 Oct 28;1(4):e53.
133. Parker JD, Hilton LK, Diener DR, Rasi MQ, Mahjoub MR, Rosenbaum JL, et al. Centrioles are freed from cilia by severing prior to mitosis. Cytoskeleton (Hoboken). 2010 Jul 1;67(7):425–430.
134. Pugacheva EN, Jablonski SA, Hartman TR, Henske EP, Golemis EA. HEF1-dependent Aurora A activation induces disassembly of the primary cilium. Cell. 2007 Jun 29;129(7):1351–1363.
135. The biology of cilia and flagella (Book, 1962) [University of Virginia Libraries]. [cited 2015 Dec 22]. Available from: http://uva.worldcat.org/title/biology-of-cilia-and-flagella/oclc/636774408
136. Ishikawa H, Kubo A, Tsukita S, Tsukita S. Odf2-deficient mother centrioles lack distal/subdistal appendages and the ability to generate primary cilia. Nat Cell Biol. 2005 May;7(5):517–524.
137. Lütcke A, Jansson S, Parton RG, Chavrier P, Valencia A, Huber LA, et al. Rab17, a novel small GTPase, is specific for epithelial cells and is induced during cell polarization. J Cell Biol. 1993 May;121(3):553–564.

138. Zacchi P, Stenmark H, Parton RG, Orioli D, Lim F, Giner A, et al. Rab17 regulates membrane trafficking through apical recycling endosomes in polarized epithelial cells. J Cell Biol. 1998 Mar 9;140(5):1039–1053.
139. Boehlke C, Bashkurov M, Buescher A, Krick T, John AK, Nitschke R, et al. Differential role of Rab proteins in ciliary trafficking: Rab23 regulates smoothened levels. J Cell Sci. 2010 May 1;123(Pt 9):1460–1467.
140. Yoshimura S, Egerer J, Fuchs E, Haas AK, Barr FA. Functional dissection of Rab GTPases involved in primary cilium formation. J Cell Biol. 2007 Jul 30;178(3):363–369.
141. Rodriguez-Boulan E, Kreitzer G, Müsch A. Organization of vesicular trafficking in epithelia. Nat Rev Mol Cell Biol. 2005 Mar;6(3):233–247.
142. Sawyer JM, Harrell JR, Shemer G, Sullivan-Brown J, Roh-Johnson M, Goldstein B. Apical constriction: a cell shape change that can drive morphogenesis. Dev Biol. 2010 May 1;341(1):5–19.
143. Cereijido M, Contreras RG, Shoshani L. Cell adhesion, polarity, and epithelia in the dawn of metazoans. Physiol Rev. 2004 Oct 1;84(4):1229–1262.
144. Lim J, Thiery JP. Epithelial-mesenchymal transitions: insights from development. Development. 2012 Oct 1;139(19):3471–3486.
145. Ozdamar B, Bose R, Barrios-Rodiles M, Wang HR, Zhang Y, Wrana JL. Regulation of the polarity protein Par6 by TGFbeta receptors controls epithelial cell plasticity. Science. 2005 Mar 11;307(5715):1603–1609.
146. Lechler T, Fuchs E. Asymmetric cell divisions promote stratification and differentiation of mammalian skin. Nature. 2005 Sep 8;437(7056):275–280.
147. Sauer ME, Walker BE. Radioautographic study of interkinetic nuclear migration in the neural tube. Proc Soc Exp Biol Med. 1959 Jul;101(3):557–560.
148. Sauer FC. The interkinetic migration of embryonic epithelial nuclei. J Morphol. 1936 Dec;60(1):1–11.
149. Goldstein B, Macara IG. The PAR proteins: fundamental players in animal cell polarization. Dev Cell. 2007 Nov;13(5):609–622.
150. Assémat E, Bazellières E, Pallesi-Pocachard E, Le Bivic A, Massey-Harroche D. Polarity complex proteins. Biochim Biophys Acta. 2008 Mar;1778(3):614–630.
151. Tepass U. The apical polarity protein network in Drosophila epithelial cells: regulation of polarity, junctions, morphogenesis, cell growth, and survival. Annu Rev Cell Dev Biol. 2012 Aug 6;28:655–685.
152. Kemphues KJ, Priess JR, Morton DG, Cheng NS. Identification of genes required for cytoplasmic localization in early C. elegans embryos. Cell. 1988 Feb 12;52(3):311–320.
153. Yamanaka T, Horikoshi Y, Suzuki A, Sugiyama Y, Kitamura K, Maniwa R, et al. PAR-6 regulates aPKC activity in a novel way and mediates cell-cell contact-induced formation of the epithelial junctional complex. Genes Cells. 2001 Aug 1;6(8):721–731.
154. Graybill C, Wee B, Atwood SX, Prehoda KE. Partitioning-defective protein 6 (Par-6) activates atypical protein kinase C (aPKC) by pseudosubstrate displacement. J Biol Chem. 2012 Jun 15;287(25):21003–21011.

155. Benton R, St Johnston D. Drosophila PAR-1 and 14-3-3 inhibit Bazooka/PAR-3 to establish complementary cortical domains in polarized cells. Cell. 2003 Dec 12;115(6):691–704.
156. Jaulin F, Xue X, Rodriguez-Boulan E, Kreitzer G. Polarization-dependent selective transport to the apical membrane by KIF5B in MDCK cells. Dev Cell. 2007 Oct 1;13(4):511–522.
157. Fan S, Hurd TW, Liu CJ, Straight SW, Weimbs T, Hurd EA, et al. Polarity proteins control ciliogenesis via kinesin motor interactions. Curr Biol. 2004 Aug 24;14(16):1451–1461.
158. Lock JG, Stow JL. Rab11 in recycling endosomes regulates the sorting and basolateral transport of E-cadherin. Mol Biol Cell. 2005 Apr;16(4):1744–1755.
159. McCaffrey LM, Macara IG. Epithelial organization, cell polarity and tumorigenesis. Trends Cell Biol. 2011 Dec;21(12):727–735.
160. Moreno-Bueno G, Portillo F, Cano A. Transcriptional regulation of cell polarity in EMT and cancer. Oncogene. 2008 Nov 24;27(55):6958–6969.
161. Thiery JP. Epithelial-mesenchymal transitions in development and pathologies. Curr Opin Cell Biol. 2003 Dec;15(6):740–746.
162. Jeanes A, Gottardi CJ, Yap AS. Cadherins and cancer: how does cadherin dysfunction promote tumor progression? Oncogene. 2008 Nov 24;27(55):6920–6929.
163. Peinado H, Portillo F, Cano A. Transcriptional regulation of cadherins during development and carcinogenesis. Int J Dev Biol. 2004;48(5-6):365–375.
164. Roessler E, Belloni E, Gaudenz K, Vargas F, Scherer SW, Tsui LC, et al. Mutations in the C-terminal domain of Sonic Hedgehog cause holoprosencephaly. Hum Mol Genet. 1997 Oct 1;6(11):1847–1853.
165. Roessler E, Belloni E, Gaudenz K, Jay P, Berta P, Scherer SW, et al. Mutations in the human Sonic Hedgehog gene cause holoprosencephaly. Nat Genet. 1996 Nov;14(3):357–360.
166. Hooper JE, Scott MP. The Drosophila patched gene encodes a putative membrane protein required for segmental patterning. Cell. 1989 Nov 17;59(4):751–765.
167. Ingham PW, Taylor AM, Nakano Y. Role of the Drosophila patched gene in positional signalling. Nature. 1991 Sep 12;353(6340):184–187.
168. Van den Heuvel M, Ingham PW. smoothened encodes a receptor-like serpentine protein required for hedgehog signalling. Nature. 1996 Aug 8;382(6591):547–551.
169. Alcedo J, Ayzenzon M, Von Ohlen T, Noll M, Hooper JE. The Drosophila smoothened gene encodes a seven-pass membrane protein, a putative receptor for the hedgehog signal. Cell. 1996 Jul 26;86(2):221–232.
170. Aoto K, Nishimura T, Eto K, Motoyama J. Mouse GLI3 regulates Fgf8 expression and apoptosis in the developing neural tube, face, and limb bud. Dev Biol. 2002 Nov 15;251(2):320–332.
171. Fuccillo M, Joyner AL, Fishell G. Morphogen to mitogen: the multiple roles of hedgehog signalling in vertebrate neural development. Nat Rev Neurosci. 2006 Oct;7(10):772–783.

172. Tole S, Ragsdale CW, Grove EA. Dorsoventral patterning of the telencephalon is disrupted in the mouse mutant extra-toes(J). Dev Biol. 2000 Jan 15;217(2):254–265.
173. Blaess S, Stephen D, Joyner AL. Gli3 coordinates three-dimensional patterning and growth of the tectum and cerebellum by integrating Shh and Fgf8 signaling. Development. 2008 Jun 1;135(12):2093–2103.
174. Mercier S, David V, Ratié L, Gicquel I, Odent S, Dupé V. NODAL and SHH dose-dependent double inhibition promotes an HPE-like phenotype in chick embryos. Dis Model Mech. 2013 Mar;6(2):537–543.
175. Roessler E, Ouspenskaia MV, Karkera JD, Vélez JI, Kantipong A, Lacbawan F, et al. Reduced NODAL signaling strength via mutation of several pathway members including FOXH1 is linked to human heart defects and holoprosencephaly. Am J Hum Genet. 2008 Jul;83(1):18–29.
176. Roessler E, Pei W, Ouspenskaia MV, Karkera JD, Veléz JI, Banerjee-Basu S, et al. Cumulative ligand activity of NODAL mutations and modifiers are linked to human heart defects and holoprosencephaly. Mol Genet Metab. 2009 Oct;98(1-2):225–234.
177. Paparidis Z, Abbasi AA, Malik S, Goode DK, Callaway H, Elgar G, et al. Ultraconserved non-coding sequence element controls a subset of spatiotemporal GLI3 expression. Dev Growth Differ. 2007 Aug;49(6):543–553.
178. Abbasi AA, Paparidis Z, Malik S, Goode DK, Callaway H, Elgar G, et al. Human GLI3 intragenic conserved non-coding sequences are tissue-specific enhancers. PLoS ONE. 2007 Apr 11;2(4):e366.
179. Abbasi AA, Paparidis Z, Malik S, Bangs F, Schmidt A, Koch S, et al. Human intronic enhancers control distinct sub-domains of Gli3 expression during mouse CNS and limb development. BMC Dev Biol. 2010 Apr 28;10:44.
180. Coy S, Caamaño JH, Carvajal J, Cleary ML, Borycki AG. A novel Gli3 enhancer controls the Gli3 spatiotemporal expression pattern through a TALE homeodomain protein binding site. Mol Cell Biol. 2011 Apr;31(7):1432–1443.
181. Rallu M, Machold R, Gaiano N, Corbin JG, McMahon AP, Fishell G. Dorsoventral patterning is established in the telencephalon of mutants lacking both Gli3 and Hedgehog signaling. Development. 2002 Nov 1;129(21):4963–4974.
182. Hayashi S, Lewis P, Pevny L, McMahon AP. Efficient gene modulation in mouse epiblast using a Sox2Cre transgenic mouse strain. Gene Expr Patterns. 2002 Nov;2(1-2):93–97.
183. Truett GE, Heeger P, Mynatt RL, Truett AA, Walker JA, Warman ML. Preparation of PCR-quality mouse genomic DNA with hot sodium hydroxide and tris (HotSHOT). BioTechniques. 2000 Jul;29(1):52, 54.
184. Wilkinson DG. In situ hybridization: a practical approach. [Internet]. 1998. Available from: http://www.cabdirect.org/abstracts/19991603522.html;jsessionid=7F1FC8258BBF1EF1BA0B54EDF64F6FD6
185. Melhuish TA, Chung DD, Bjerke GA, Wotton D. Tgif1 represses apolipoprotein gene expression in liver. J Cell Biochem. 2010 Oct 1;111(2):380–390.

186. Bjerke GA, Hyman-Walsh C, Wotton D. Cooperative transcriptional activation by Klf4, Meis2, and Pbx1. Mol Cell Biol. 2011 Sep;31(18):3723–3733.
187. Hyman CA, Bartholin L, Newfeld SJ, Wotton D. Drosophila TGIF proteins are transcriptional activators. Mol Cell Biol. 2003 Dec;23(24):9262–9274.
188. Zerlanko BJ, Bartholin L, Melhuish TA, Wotton D. Premature senescence and increased TGFβ signaling in the absence of Tgif1. PLoS ONE. 2012 Apr 13;7(4):e35460.
189. Melhuish TA, Wotton D. The Tgif2 gene contains a retained intron within the coding sequence. BMC Mol Biol. 2006 Jan 25;7:2.
190. Seo SR, Ferrand N, Faresse N, Prunier C, Abécassis L, Pessah M, et al. Nuclear retention of the tumor suppressor cPML by the homeodomain protein TGIF restricts TGF-beta signaling. Mol Cell. 2006 Aug 1;23(4):547–559.
191. Geng X, Oliver G. Pathogenesis of holoprosencephaly. J Clin Invest. 2009 Jun 1;119(6):1403–1413.
192. Mar L, Hoodless PA. Embryonic fibroblasts from mice lacking Tgif were defective in cell cycling. Mol Cell Biol. 2006 Jun 1;26(11):4302–4310.
193. Corbit KC, Aanstad P, Singla V, Norman AR, Stainier DY, Reiter JF. Vertebrate Smoothened functions at the primary cilium. Nature. 2005 Oct 13;437(7061):1018–1021.
194. Rohatgi R, Milenkovic L, Scott MP. Patched1 regulates hedgehog signaling at the primary cilium. Science. 2007 Jul 20;317(5836):372–376.
195. Shiratori H, Hamada H. The left-right axis in the mouse: from origin to morphology. Development. 2006 Jun;133(11):2095–2104.
196. Vandenberg LN, Levin M. A unified model for left-right asymmetry? Comparison and synthesis of molecular models of embryonic laterality. Dev Biol. 2013 Jul 1;379(1):1–15.
197. Cho Y, Cavalli V. HDAC5 is a novel injury-regulated tubulin deacetylase controlling axon regeneration. EMBO J. 2012 Jul 18;31(14):3063–3078.
198. Hubbert C, Guardiola A, Shao R, Kawaguchi Y, Ito A, Nixon A, et al. HDAC6 is a microtubule-associated deacetylase. Nature. 2002 May 23;417(6887):455–458.
199. North BJ, Marshall BL, Borra MT, Denu JM, Verdin E. The human Sir2 ortholog, SIRT2, is an NAD+-dependent tubulin deacetylase. Mol Cell. 2003 Feb 1;11(2):437–444.
200. Sung CH, Leroux MR. The roles of evolutionarily conserved functional modules in cilia-related trafficking. Nat Cell Biol. 2013 Dec;15(12):1387–1397.
201. Niwa S, Nakajima K, Miki H, Minato Y, Wang D, Hirokawa N. KIF19A is a microtubule-depolymerizing kinesin for ciliary length control. Dev Cell. 2012 Dec 11;23(6):1167–1175.
202. Eggenschwiler JT, Bulgakov OV, Qin J, Li T, Anderson KV. Mouse Rab23 regulates hedgehog signaling from smoothened to Gli proteins. Dev Biol. 2006 Feb 1;290(1):1–12.
203. Fuller K, O'Connell JT, Gordon J, Mauti O, Eggenschwiler J. Rab23 regulates Nodal signaling in vertebrate left-right patterning independently of the Hedgehog pathway. Dev Biol. 2014 Jul 15;391(2):182–195.

204. Anders S, Huber W. Differential expression analysis for sequence count data. Genome Biol. 2010 Oct 27;11(10):R106.
205. Huang DAW, Sherman BT, Lempicki RA. Systematic and integrative analysis of large gene lists using DAVID bioinformatics resources. Nat Protoc. 2009;4(1):44–57.
206. Huang DAW, Sherman BT, Lempicki RA. Bioinformatics enrichment tools: paths toward the comprehensive functional analysis of large gene lists. Nucleic Acids Res. 2009 Jan;37(1):1–13.
207. Newman AM, Cooper JB. AutoSOME: a clustering method for identifying gene expression modules without prior knowledge of cluster number. BMC Bioinformatics. 2010 Mar 4;11:117.
208. Devenport D, Fuchs E. Planar polarization in embryonic epidermis orchestrates global asymmetric morphogenesis of hair follicles. Nat Cell Biol. 2008 Nov;10(11):1257–1268.
209. Muzumdar MD, Tasic B, Miyamichi K, Li L, Luo L. A global double-fluorescent Cre reporter mouse. Genesis. 2007 Sep;45(9):593–605.
210. Ybot-Gonzalez P, Savery D, Gerrelli D, Signore M, Mitchell CE, Faux CH, et al. Convergent extension, planar-cell-polarity signalling and initiation of mouse neural tube closure. Development. 2007 Feb;134(4):789–799.
211. Keller R. Shaping the vertebrate body plan by polarized embryonic cell movements. Science. 2002 Dec 6;298(5600):1950–1954.
212. Sausedo RA, Schoenwolf GC. Quantitative analyses of cell behaviors underlying notochord formation and extension in mouse embryos. Anat Rec. 1994 May;239(1):103–112.
213. Yamaguchi TP, Bradley A, McMahon AP, Jones S. A Wnt5a pathway underlies outgrowth of multiple structures in the vertebrate embryo. Development. 1999 Mar 1;126(6):1211–1223.
214. Razzaque MS, Atfi A. TGIF function in oncogenic Wnt signaling. Biochim Biophys Acta. 2015 Oct 31;
215. Andre P, Song H, Kim W, Kispert A, Yang Y. Wnt5a and Wnt11 regulate mammalian anterior-posterior axis elongation. Development. 2015 Apr 15;142(8):1516–1527.
216. Yang Y, Hwang CK, D'Souza UM, Lee SH, Junn E, Mouradian MM. Three-amino acid extension loop homeodomain proteins Meis2 and TGIF differentially regulate transcription. J Biol Chem. 2000 Jul 7;275(27):20734–20741.
217. Pramfalk C, Melhuish TA, Wotton D, Jiang ZY, Eriksson M, Parini P. TG-interacting factor 1 acts as a transcriptional repressor of sterol O-acyltransferase 2. J Lipid Res. 2014 Apr;55(4):709–717.
218. Lee BK, Shen W, Lee J, Rhee C, Chung H, Kim KY, et al. Tgif1 Counterbalances the Activity of Core Pluripotency Factors in Mouse Embryonic Stem Cells. Cell Rep. 2015 Oct 6;13(1):52–60.
219. De Sousa Lopes SM, Carvalho RL, van den Driesche S, Goumans MJ, ten Dijke P, Mummery CL. Distribution of phosphorylated Smad2 identifies target tissues of

TGF beta ligands in mouse development. Gene Expr Patterns. 2003 Jun;3(3):355–360.
220. Fan F, Samuel S, Evans KW, Lu J, Xia L, Zhou Y, et al. Overexpression of snail induces epithelial-mesenchymal transition and a cancer stem cell-like phenotype in human colorectal cancer cells. Cancer Med. 2012 Aug;1(1):5–16.
221. Koplay M, Onbas O, Alper F, Borekci B. Prenatal MRI findings of polycystic kidney disease associated with holoprosencephaly. Korean J Radiol. 2009 Jun;10(3):307–309.
222. Yoder BK. Role of primary cilia in the pathogenesis of polycystic kidney disease. J Am Soc Nephrol. 2007 May;18(5):1381–1388.
223. Tateossian H, Morse S, Parker A, Mburu P, Warr N, Acevedo-Arozena A, et al. Otitis media in the Tgif knockout mouse implicates TGFβ signalling in chronic middle ear inflammatory disease. Hum Mol Genet. 2013 Jul 1;22(13):2553–2565.
224. Jahrsdoerfer R, Feldman PS, Rubel EW, Guerrant JL, Eggleston PA, Selden RF. Otitis media and the immotile cilia syndrome. Laryngoscope. 1979 May;89(5 Pt 1):769–778.
225. Mata M, Milian L, Armengot M, Carda C. Gene mutations in primary ciliary dyskinesia related to otitis media. Curr Allergy Asthma Rep. 2014 Mar;14(3):420.
226. Nomura M, Li E. Smad2 role in mesoderm formation, left-right patterning and craniofacial development. Nature. 1998 Jun 25;393(6687):786–790.
227. De la Cruz JM, Bamford RN, Burdine RD, Roessler E, Barkovich AJ, Donnai D, et al. A loss-of-function mutation in the CFC domain of TDGF1 is associated with human forebrain defects. Hum Genet. 2002 May 1;110(5):422–428.
228. Zhang J, Talbot WS, Schier AF. Positional cloning identifies zebrafish one-eyed pinhead as a permissive EGF-related ligand required during gastrulation. Cell. 1998 Jan 23;92(2):241–251.
229. Hu D, Helms JA. The role of sonic hedgehog in normal and abnormal craniofacial morphogenesis. Development. 1999 Nov;126(21):4873–4884.